

**The role of KDM6A in the clonal evolution
of acute myeloid leukemia**

Dissertation der Fakultät für Biologie
der Ludwig-Maximilians-Universität München

vorgelegt von

SOPHIE MARIA STIEF

Geboren in München

20. Dezember 2018

**The role of KDM6A in the clonal evolution
of acute myeloid leukemia**

Dissertation der Fakultät für Biologie
der Ludwig-Maximilians-Universität München

vorgelegt von

SOPHIE MARIA STIEF

Geboren in München

Erstgutachter: Prof. Dr. Heinrich Leonhardt

Zweitgutachter: Prof. Dr. Bettina Kempkes

Tag der Abgabe: 20.12.2018

Tag der mündlichen Prüfung: 22.07.2019

Eidesstaatliche Erklärung

Ich versichere hiermit an Eides statt, dass die vorgelegte Dissertation von mir selbstständig und ohne unerlaubte Hilfe angefertigt ist.

Erklärung

Hiermit erkläre ich, dass die Dissertation nicht ganz oder in wesentlichen Teilen einer anderen Prüfungskommission vorgelegt worden ist.

Hiermit erkläre ich, dass ich mich anderweitig einer Doktorprüfung ohne Erfolg nicht unterzogen habe.

München, den 20.12.2018

Sophie Stief

Table of Contents

1	Introduction	1
1.1	Acute myeloid leukemia.....	1
1.1.1	Pathogenesis	2
1.1.2	Therapy	6
1.1.3	Tumor evolution at relapse	7
1.1.4	Mechanisms of therapy resistance.....	9
1.2	Epigenetic regulation	13
1.2.1	Chromatin structure and histone modifications	13
1.2.2	Histone methylation and demethylation.....	15
1.2.3	The histone H3K27 demethylase KDM6A	17
1.2.3.1	KDM6A during embryonic development, hematopoiesis, and differentiation	18
1.2.3.2	Human diseases associated with the deregulation of KDM6A.....	20
1.3	Aims of this work	21
2	Materials and Methods.....	22
2.1	Materials.....	22
2.1.1	Reagents and chemicals.....	22
2.1.2	Chemotherapeutic and targeted agents	24
2.1.3	Buffers and solutions	24
2.1.4	Kits.....	25
2.1.5	Antibodies	26
2.1.6	Oligonucleotides	26
2.1.7	Plasmids.....	28
2.1.8	Cell lines and patient-derived xenograft AML cells	29
2.1.9	Genomic DNA	30
2.1.10	Patient samples.....	30
2.1.11	Laboratory equipment and consumables	31
2.1.12	Software and Programs.....	33
2.2	Methods.....	34
2.2.1	Molecular biology methods.....	34
2.2.1.1	Chemical Transformation of recombinant bacteria	34
2.2.1.2	Preparation of plasmid DNA.....	34
2.2.1.4	Restriction digestion.....	34
2.2.1.5	Electrophoretic DNA separation	35
2.2.1.6	DNA purification.....	35
2.2.1.7	DNA cloning.....	35
2.2.1.8	Mutagenesis	36
2.2.1.9	Sequencing	37
2.2.1.9.1	Sanger sequencing.....	37
2.2.1.9.2	Targeted sequencing.....	37
2.2.1.10	Extraction of genomic DNA	37
2.2.1.11	Multiplex Ligation-dependent Probe Amplification (MLPA) analysis.....	37
2.2.1.12	Numerical aberrations	38
2.2.1.13	RNA isolation	38
2.2.1.14	cDNA synthesis.....	38
2.2.1.15	Quantitative real-time PCR	39
2.2.1.16	RNA Sequencing	39
2.2.1.16.1	Library preparation and sequencing.....	39
2.2.1.16.2	Data Processing	40
2.2.2	Cell biology methods.....	40

2.2.2.1	Cell culture cultivation and handling.....	40
2.2.2.2	Cell thawing and freezing.....	41
2.2.2.3	Mycoplasma testing.....	42
2.2.2.4	Transient transfection	42
2.2.2.5	Stable transfection with lentivirus	43
2.2.2.6	CRISPR/Cas9-mediated gene editing	43
2.2.2.7	MG132 treatment	44
2.2.2.8	Proliferation assay and cell counting.....	44
2.2.2.9	Competitive growth assay	44
2.2.2.10	In vivo therapy trial.....	45
2.2.3	Protein biochemistry methods	45
2.2.3.1	Preparation of cell lysates.....	45
2.2.3.2	Determination of protein concentration by Bradford Protein Assay	46
2.2.3.3	SDS-Polyacrylamide gel electrophoresis	46
2.2.3.4	Western Blot	47
2.2.3.6	Statistical analysis.....	48
3	Results	49
3.1	Investigation of KDM6A during AML progression	49
3.1.1	Analysis of <i>KDM6A</i> mutations in AML patients at diagnosis.....	49
3.1.2	Gain of <i>KDM6A</i> mutations in AML patients at relapse.....	49
3.1.3	Proteasomal degradation of <i>KDM6A</i> mutants in HEK293T cells	52
3.1.4	<i>KDM6A</i> mutation independent protein expression at diagnosis and relapse	53
3.1.5	Status of <i>KDM6A</i> in PDX relapsed AML cells	55
3.2	KDM6A in AML cell lines	58
3.2.1	Mutation and expression analysis of <i>KDM6A</i> in AML cell lines.....	58
3.2.2	Global H3K27 methylation in <i>KDM6A</i> WT and mutant AML cell lines	60
3.2.3	Analysis of H3K27 modifiers in AML cell lines.....	61
3.3	Investigation of the role of KDM6A in chemotherapy resistance	63
3.3.1	shRNA mediated knockdown of <i>KDM6A</i> in K562 cells	63
3.3.1.1	Generation of stable <i>KDM6A</i> knockdown cells.....	63
3.3.1.2	Effect of <i>KDM6A</i> knockdown on chemotherapy sensitivity	64
3.3.1.3	Selective growth advantage of <i>KDM6A</i> KD cells.....	66
3.3.2	CRISPR/Cas9-mediated knockout of <i>KDM6A</i> in K562 cells.....	67
3.3.2.1	Generation of <i>KDM6A</i> knockout single cell clones	67
3.3.2.2	Effect of <i>KDM6A</i> loss in K562 cells on chemotherapy sensitivity	69
3.3.3	CRISPR/Cas9-mediated knockout of <i>KDM6A</i> in MM-1 cells.....	70
3.3.3.1	Generation of <i>KDM6A</i> KO MM-1 single cell clones.....	71
3.3.3.2	Effect of <i>KDM6A</i> loss in MM-1 cells on chemotherapy sensitivity	72
3.4	Identification of KDM6A target genes with different KD/KO approaches	73
3.4.1	siRNA-mediated silencing of <i>KDM6A</i>	73
3.4.2	shRNA-mediated knockdown of <i>KDM6A</i>	75
3.4.3	CRISPR/Cas9-mediated knockout of <i>KDM6A</i>	76
3.4.4	Overlap of <i>KDM6A</i> target genes between different silencing approaches	78
4	Discussion	81
4.1	Inactivation of <i>KDM6A</i> during the clonal evolution of AML.....	81
4.2	Deletions of <i>KDM6A</i> facilitate an altered epigenetic phenotype in AML cell lines	85
4.3	Inactivation of <i>KDM6A</i> confers drug resistance in AML	87
4.4	Identification of key <i>KDM6A</i> target genes involved in mediating drug resistance.....	89
5	Summary	93
6	Zusammenfassung	95
7	References.....	97

8 Annex.....	109
8.1 Supplementary Figures.....	109
8.2 Supplementary Table.....	111
8.3 Abbreviations.....	114
8.4 Table of Figures.....	119
8.5 Table of Supplementary Figures	120
8.6 Table of Tables	120
8.7 Publications	121
8.8 Acknowledgment.....	122

1 Introduction

1.1 Acute myeloid leukemia

From the earliest times, scientists and physicians have speculated about the origin and nature of cancer, but it was not until the second half of the twentieth century that profound insights into its genetics and treatment, beyond surgical interventions, were gained¹. Scientific advances including the discovery and application of anti-cancer drugs as well as a deeper understanding of genetics first emerged in leukemia and related blood cell cancers. Important variables for the success story of leukemia research were a solid foundation of basic biology for the corresponding normal tissue and good tissue accessibility¹. Blood cell related cancers including leukemia and other hematological malignancies account for only 7 to 9% compared to all other cancer types².

Leukemia is defined as a hematopoietic malignancy of white blood cells initiated by a few abnormal leukemic stem cells (LSC) or more committed progenitors. With time, these immature blood cells, also known as blast cells, accumulate and crowd out normal hematopoietic cells in the bone marrow and blood. Blood cells are mainly composed of lymphoid (B cells, T cells, and natural killer cells) and myeloid-erythroid cells (erythrocytes, granulocytes, megakaryocytes/thrombocytes, monocytes/macrophages, and mast cells). Based on the affected cell type, leukemias are classified into two main categories, lymphoid and myeloid, which are each further subdivided into acute and chronic forms. In chronic leukemia, the abnormal cells are more mature and there is usually no need for immediate treatment as the disease progresses slowly. In contrast, immediate medical care is required for acute leukemias due to a fast increase of immature blood cells resulting in an aggressive crowd out of normal blood cells. If left untreated, acute leukemias can progress quickly and become fatal within weeks or few months.

The most common form of acute leukemia in adults is acute myeloid leukemia (AML), which is characterized by rapid clonal expansion of undifferentiated myeloid precursor cells in the bone marrow and blood with possible spread to other tissues like liver and spleen. About 18,376 new diagnoses of AML are estimated to occur per year in Europe with a median age of 68 and a slightly higher prevalence in men compared to women^{3,4}. Patients with AML have a one-year relative survival rate of only 37%, which decreases to 19% after five years³. Generally, survival rates decrease with increasing age as young

patients in the age group of 0-14 have a 5-year survival rate of 67% compared to only 5% in patients older than 65 years³.

1.1.1 Pathogenesis

AML is a group of heterogeneous subentities with substantial differences in cytogenetic and mutational profiles that profoundly influence treatment response and patient outcome⁵⁻⁷. Based on morphology and cytochemistry, AML was initially divided into 8 subtypes (M₀-M₇) according to the French-American-British (FAB) classification system⁸. In 2002, the World Health Organization (WHO) introduced the *WHO Classification of Tumours of Haematopoietic and Lymphoid Tissues* classification system incorporating morphology, biologic, and genetic information⁹, which was updated in 2008 and 2016^{10,11}. The 2016 revision was necessary due to major advances in technology like whole genome sequencing (WGS), whole exome sequencing (WES), and gene expression analysis, which resulted in the identification of numerous new molecular genetic lesions as prognostic and predictive markers¹¹. One of the most important prognostic marker for the rate of complete remission (CR), second CR after first disease recurrence (relapse), overall survival (OS), and disease-free survival (DFS) is the karyotype^{5,12-16}. For instance, cytogenetic abnormalities like inversion inv(16) are associated with a favorable prognosis whereas adverse outcome is observed among patients with chromosome 5q deletions^{12,14,17}. However, about 45-50% of AML patients lack these prognostic chromosomal aberrations and are termed cytogenetically normal (CN) AML.^{6,7} CN-AML is classified into the intermediate-risk group and patients outcome is strongly influenced by the mutational status¹⁸.

With an average number of 13 to 15 coding mutations per case of which only 2-5 are recurrently mutated in AML^{19,20}, the mutational burden in AML is relatively low compared to other adult tumor types including breast, ovarian, colorectal and lung squamous cancer¹⁹. According to their roles in pathogenesis, a two-class gene classification model has initially been proposed⁷. Mutations in genes that lead to activated signal transduction and confer a proliferative advantage are considered as class I mutations (e.g. *FLT3*-ITD and *NRAS*). The class II gene mutations are associated with transcription regulation leading to impaired hematopoietic cell

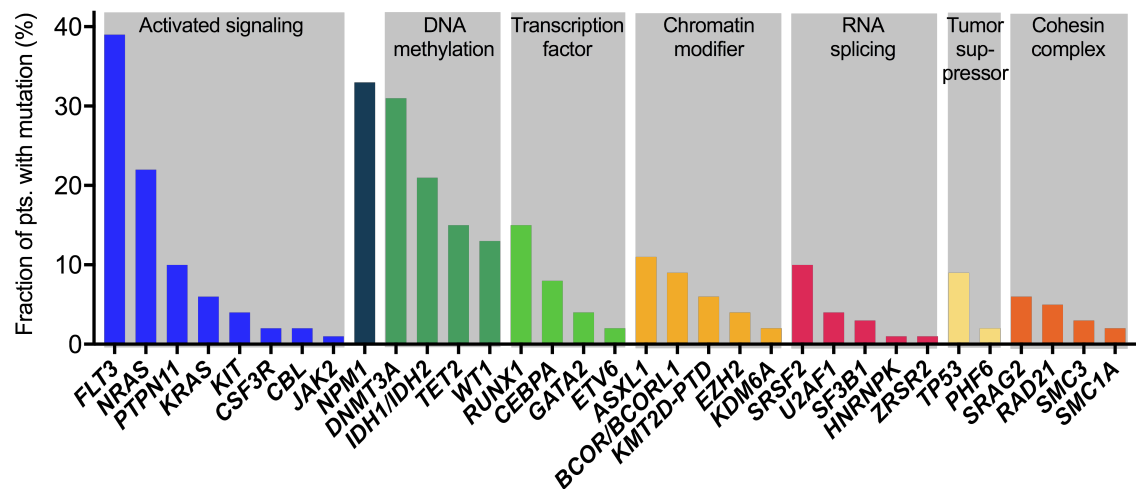


Figure 1 Overview of recurrently mutated genes in AML. Histogram showing the frequency of driver gene mutations detected in >1% of patients in a cohort of 664 AML patients. Genes are clustered according to their respective functional groups. Data was obtained from Metzeler *et al.*²¹.

differentiation (e.g. *NPM1*). The recent identification of recurrent mutations in a large number of genes encoding epigenetic regulators like DNA (*DNMT3A*, *TET2*, *IDH1/2*) and chromatin (*KMT2D*, *EZH2*) modifiers has led to the proposal of a third category of gene mutations^{6,22–30}. Epigenetic deregulation appears to be one of the major driver of AML^{31,32}. Evolutionary studies as well as evidence from mouse models suggest that cooperation of two or more lesions is required to generate AML^{20,33–35}. For instance, compared to single-mutant controls, combination of *NPM1* mutation and *FLT3*-ITD is rapidly and universally leukemogenic in knock-in mice with the possibility that additional mutations are rapidly acquired³⁵.

The most recurrently mutated genes in AML are the fms-like tyrosine kinase *FLT3* (28–39%), nucleophosmin *NPM1* (27–33%), and DNA methyltransferase *DNMT3A* (20–31%)^{19,21,36} (Figure 1). Although with less frequency, several other mutations in genes belonging to functional groups like RNA splicing, transcription factor, cohesion complex or chromatin modifiers have been found to occur in AML (Figure 1). Among these genes, mutations in *CEBPA*, *NPM1*, and *FLT3* are routinely used as prognostic markers, as reflected in the European LeukemiaNet (ELN) recommendations³⁷. The prognostic importance is less clear for some other recurrently mutated genes and can be influenced by the karyotype, type of mutation, patients age, and co-occurring mutations¹¹. In many cases, co-occurring alterations have an effect on CR rates, DFS, relapse-free survival (RFS) and OS. For instance, AML patients with a *NPM1* mutation who lack *FLT3*-ITD

have a significantly better outcome than patients with a *NPM1* mutation and a *FLT3*-ITD^{11,38,39}. The proportion of mutations within the tumor population can be estimated by the variant allele frequency (VAF), which refers to the frequency of sequencing reads of the mutated allele compared to the wild type (WT) allele. Advances in technology including greater sequencing depth have allowed to detect mutations in minor cell subpopulations (subclones) of the bulk tumor, to estimate the size of subclones, and to map clonal evolution of AML.

Peter Nowell was the first to describe cancer as an evolutionary process through the sequential selection of increasingly abnormal cells, which initially originate from a single cell, or at most a very few cells (Figure 2a)⁴⁰. By means of intraclonal competition and ecological bottlenecks like insufficient resources within the tissue microenvironment or anti-cancer therapy, alterations that provide the most selective growth advantage will be selected⁴⁰. Unless a mutation confers self-renewal ability on a later progenitor, mutations occurring in non-self-renewing cells will be lost due to a limited lifespan. Mutations in AML blasts but also in normal, self-renewing hematopoietic stem cells (HSC) of healthy individuals accumulate gradually with age²⁰, and age-related clonal hematopoiesis is a common condition in about 10% of healthy individuals older than 70 years of age⁴¹. Although associated with an increased risk of hematologic malignancies and cardiovascular disease, people with clonal hematopoiesis can live for many years without developing hematologic cancers⁴¹. Moreover, clinically silent clonal hematopoiesis appears to be far more common in healthy middle-aged adults than previously thought but progression to hematologic malignancies is exceptionally rare⁴². As clonal hematopoiesis shares many mutations with AML, this suggests that some mutations in AML are random background mutations that first occurred in HSCs^{20,43}. Years before developing AML, the occurrence of mutations in certain genes including spliceosome genes, *IDH1/2*, *TP53*, *DNMT3A*, and *TET2* appears to increase the risk of developing AML⁴⁴. As *DNMT3A* and *TET2* mutations were also common in individuals that did not develop AML, a higher risk of AML was only associated with these genes if high VAF and high number of variants were detected⁴⁴. At some point an initiating mutation (e.g. *DNMT3A*, *TET2*, *IDH1/2*) is acquired in addition to preexisting mutations in the HSCs^{20,43,45,46}. These so called pre-leukemic (preL)-HSCs are capable of increased proliferation or self-renewal, but retain normal characteristics of multi-lineage differentiation³⁶.

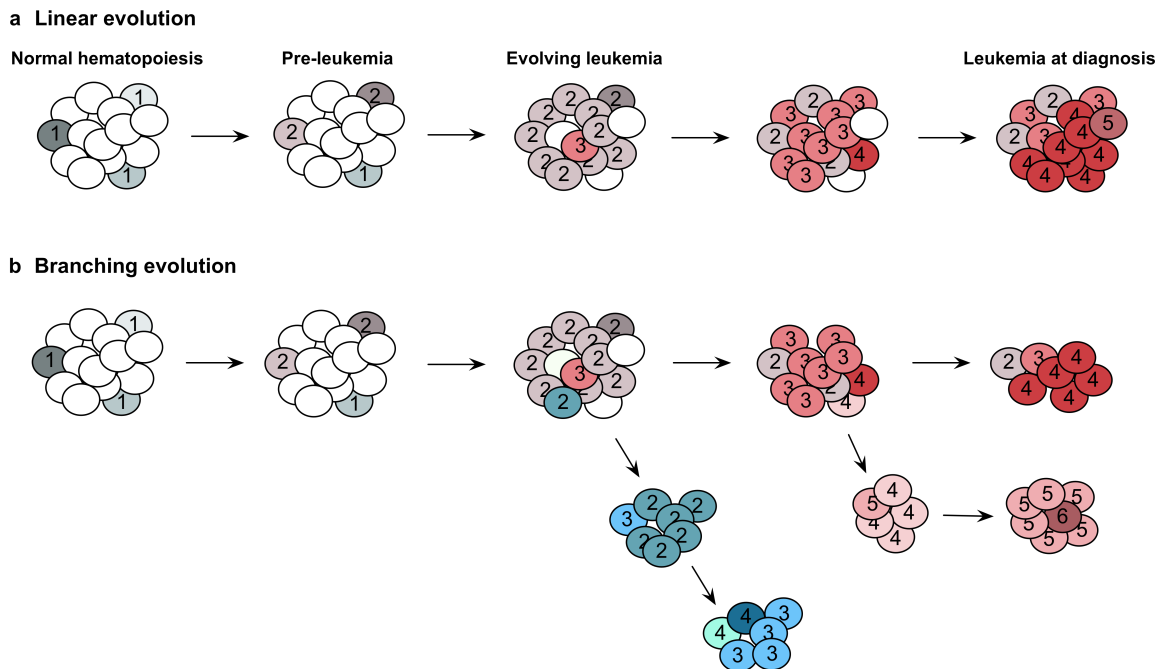


Figure 2 Process of clonal evolution with linear and branching architecture. Evolutionary process with linear (a) or variable nonlinear, branching dynamic (b). During normal hematopoiesis, mutations accumulate with age. At some point an initiating mutation occurs resulting in the pre-leukemic clone. **a**, Pre-leukemic clone evolves by acquiring additional mutations and overwhelms earlier clones carrying only some of the mutations. The dominant clone at diagnosis carries all mutations that emerged during the evolutionary process. **b**, Originating from the pre-leukemic clone, various mutations can emerge and create divergent mutational pathways. Of note, small subclones might fall below the detection limit leading to an underestimated branching complexity. Numerals indicate the number of mutations in cells. Cells carrying identical mutations are represented in the same color. Adapted from Grove et al.⁴⁷.

A portion of the preL-HSC population might acquire additional cooperating mutations (e.g. *NPM1*, *FLT3*) at a later time point contributing to disease progression or relapse^{20,36,47}. Interestingly, ancestral preL-HSCs that carry *DNMT3A* mutations were shown to exhibit competitive repopulation advantage over non-mutated HSC in xenograft assays, survive induction therapy and persist in the bone marrow at complete remission⁴⁶. Although with less frequency, persisting mutations at remission also occur in certain other genes like *NPM1*, *TET2*, *IDH2*, *ASXL1*, *RUNX1*, and *SRSF* and contribute to a higher relapse risk^{48,49}.

Clonal architecture appears to be a dynamic process with great variation between individual AML patients. A study by Anderson *et al.*⁵⁰ revealed that the evolutionary process has either a linear dynamic with sequentially dominant clones, as originally

proposed by Nowell's model, or a nonlinear dynamic with a variable branching architecture (Figure 2). It is likely that many cancers evolve with a complex, nonlinear dynamic. Serial transplantations of primary acute lymphoblastic leukemia (ALL) cells into immunodeficient mice showed patterns of variable competitive subclonal regeneration, which reflected the diversity of genetically distinct subclones identified in the original diagnostic sample⁵⁰. Genetic and clonal heterogeneity within individual patients with consistent patterns of clonal regeneration after transplantation into NSG mice was also observed in AML⁵¹.

1.1.2 Therapy

For several decades, the general therapeutic strategy in patients with AML remained largely unchanged and the "3+7" regimen is still employed as the standard of care for induction therapy. The "3+7" regimen combines 7 days of continuous-infusion cytarabine (AraC; 100-200mg/m²) and 3 days of an intravenous anthracycline like daunorubicin (DNR; 60 mg/m²), idarubicin (10-12 mg/m²), or the anthracenedione mitoxantrone (10-12 mg/m²)^{17,52}. Different combination of drugs and intensification of dose or duration were intensively investigated⁵³⁻⁵⁶ and promising results were reported for certain subgroups. For instance, intensification of the dose of DNR from standard- to high-dose improved the outcome in AML patients (<60 years of age) with mutations in *DNMT3A*, *NPM1* or with *MLL* translocations⁵⁷. The addition of a third drug, e.g. 6-Thioguanine (6-TG), was applied (TAD schedule) although there is no evidence of benefit compared to the "3+7" schedule⁵².

A morphologic complete remission which is indicated by less than 5% blasts in the bone marrow and a regeneration of peripheral counts⁵⁸, is achieved in 60 to 85% of young adults (≤ 60 years) and 40 to 60% of elderly patients (≥ 60 years) undergoing standard induction therapy¹⁷. To achieve a complete remission, two cycles of induction therapy are applied with the exception for elderly patients that might just receive one cycle. In first remission, a key strategic decision is whether to apply chemotherapy or undertake allogeneic hematopoietic-cell transplantation (allo-HCT), which is guided by cytogenetics, certain established genetic markers, and additional patient-related factors. Although transplantation-related mortality is still an issue, the benefit of transplantation in terms of reduced relapse rate usually outweighs the transplantation-associated risks in patients with a high risk of relapse³⁶. An exception to this approach might be made for patients who

present with favorable mutations at diagnosis. The recommended postremission therapy for these patients is to receive repetitive cycles (2-4) of an intermediate-dose cytarabine-based regimen¹⁷.

A major complication in the treatment of AML is disease recurrence, which requires a blast rise above 5% after achieving CR and occurs in most patients within 2 to 3 years from diagnosis. The risk of relapse is influenced by the degree of detectable residual leukemia after CR and the biologic characteristics of the AML¹⁷. Once the disease reoccurs, certain factors such as older age, poor general health status, adverse genetics, prior allo-HCT, and a short duration of remission (under 6 months) are generally associated with an inferior outcome¹⁷.

In recent years, new drugs in the area of targeted therapy including the *FLT3* inhibitor midostaurin and an anti-CD33 antibody-drug conjugate gemtuzumab ozogamycin have been approved for the treatment of AML. An exciting and promising therapeutic area is the development of new epigenetic therapies. The FDA has recently approved the *IDH2* inhibitor enasidenib⁵⁹ and the *IDH1* inhibitor ivosidenib⁶⁰ for the treatment of relapsed or refractory AML with an *IDH2* or *IDH1* mutation, respectively. The clinical development of several other inhibitors against epigenetic regulators is under way. Due to the heterogeneity of AML, knowledge of the full mutational inventory, which might be gained by access to panel-based or whole next-generation-sequencing (NGS) in the diagnostic work-up, may help to facilitate assessment of treatment response in the future.

1.1.3 Tumor evolution at relapse

Although the majority of patients with AML undergoing induction therapy achieve complete remission, a large number of them will relapse, often with resistant disease and poor response to subsequent therapy. Therefore, it is essential to understand the factors that contribute to the recurrence of disease. Anti-cancer therapy can interfere with the composition of the heterogeneous AML population by altering the relative competitiveness of different subpopulations^{50,61}. By comparing the genomic sequence of 8 patients with AML at diagnosis and at the time of relapse by deep sequencing, Ding *et al.*⁶¹ identified two major patterns of tumor evolution at relapse in AML. These include one in which the dominant clone in the primary tumor evolved into the relapse clone by gaining relapse-specific mutations, and another one in which a minor subclone within the founding clone survived and evolved to become the dominant clone at relapse by acquiring

additional mutations (Figure 3)⁶¹. Additionally, DNA damage caused by cytotoxic chemotherapy seems to have a substantial effect on the spectrum of acquired mutations observed at relapse.

Two mechanisms of overcoming the cytotoxic effects of chemotherapy are possible, either a subpopulation is already intrinsically drug-resistant (primary resistance) or surviving cells acquire additional mutations under the selective pressure of therapy resulting in a drug-resistant phenotype (acquired resistance). Often the relapse appears rather quickly, suggesting that a primary resistance plays a dominant role⁶². In therapy-related AML (t-AML), where AML typically develops 1-5 years following exposure to chemo-, radiation-, or immunosuppressive therapy, clones carrying a *TP53* mutation are often selectively enriched⁶³. Contrary to the assumption that cytotoxic therapy induces *TP53* mutations, findings from a recent study suggest that rare hematopoietic stem and progenitor cells (HSPCs) harboring age-related *TP53* mutations are resistant to chemotherapy, expand under the selective pressure of chemotherapy, and acquire additional mutations (Figure 3)⁶⁴. Similar results were reported in childhood ALL, where

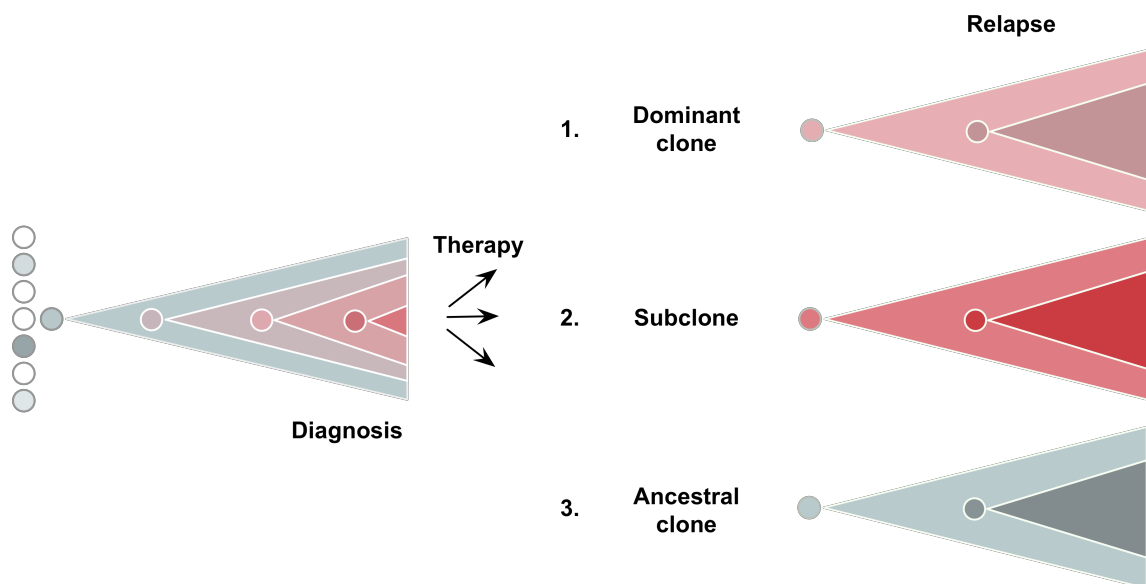


Figure 3 Patterns of tumor evolution at relapse in AML. Possible patterns of clonal evolution at relapse that originate from the hypothetical, diagnostic tumor sample after chemotherapy are shown. 1, dominant clone in the primary tumor evolved into the relapse clone by gaining relapse-specific mutations; 2, subclone within the founding clone evolved to become the dominant clone at relapse by acquiring additional; 3, relapse of an ancestrally related clone. For simplicity, a linear evolutionary pattern is shown. Adapted from Ding *et al.*⁶¹ and Grimwade *et al.*³⁶.

selection and outgrowth of preexisting, drug-resistant subclones was the major mechanism of relapse and a shorter time to relapse correlated with a higher quantity of the relapsing clone at diagnosis⁶⁵.

Taken together, these findings by Ding *et al.*⁶¹ and others^{45,65,66} reveal that incomplete eradication of the leukemic clone rather than the emergence of genetically unrelated, novel clones underlies relapse and persistence. A more efficient therapy to target and eradicate such clones might improve outcome in AML patients.

1.1.4 Mechanisms of therapy resistance

So far, most likely only a fraction of the mechanisms responsible for drug resistance has been discovered. Most of the mechanisms affecting the response to chemotherapy include either reduction in the amount of active agents inside target cells or a decrease in effectiveness of these compounds on target mechanisms like upregulation of anti-apoptotic genes or changes in microenvironment⁶⁷ (Figure 4). One of the most investigated mechanisms of drug resistance is the multidrug-resistance (MDR) phenotype, which involves the upregulation of the drug efflux transmembrane ATPase P-glycoprotein (Pgp; encoded by the *MDR1* gene)⁶⁸. Upregulation of Pgp appears to be a direct consequence of the exposure to cytotoxic drugs, including DNR and AraC, which, interestingly, is not a Pgp substrate^{68,69}. In AML, Pgp was shown not only to function as a drug efflux pump, but also to affect the apoptotic threshold and actively exert a pro-survival effect⁷⁰. Several studies have linked increased expression of Pgp with treatment failure and shorter survival^{71–77}, whereas others do not^{78,79} and its contribution to treatment failure remains debatable. Other transmembrane proteins belonging to the ABC transporter family such as multi-drug resistance-associated protein 1 (MRP1)⁶², 7 (MRP7)⁸⁰, and 8 (MRP8)⁸¹ might also contribute to resistance.

The main transporter for the cellular uptake of the hydrophilic drug AraC which is an analogue of the nucleoside cytidine, is the human equilibrative nucleoside transporter 1 (ENT1), also known as SLC29A1 (Figure 5). It is responsible for 80% of AraC influx and low ENT1 expression in AML blasts was linked with AraC resistance *ex vivo*^{82,83} and correlates with a shorter disease-free and overall survival in AML patients⁸⁴.

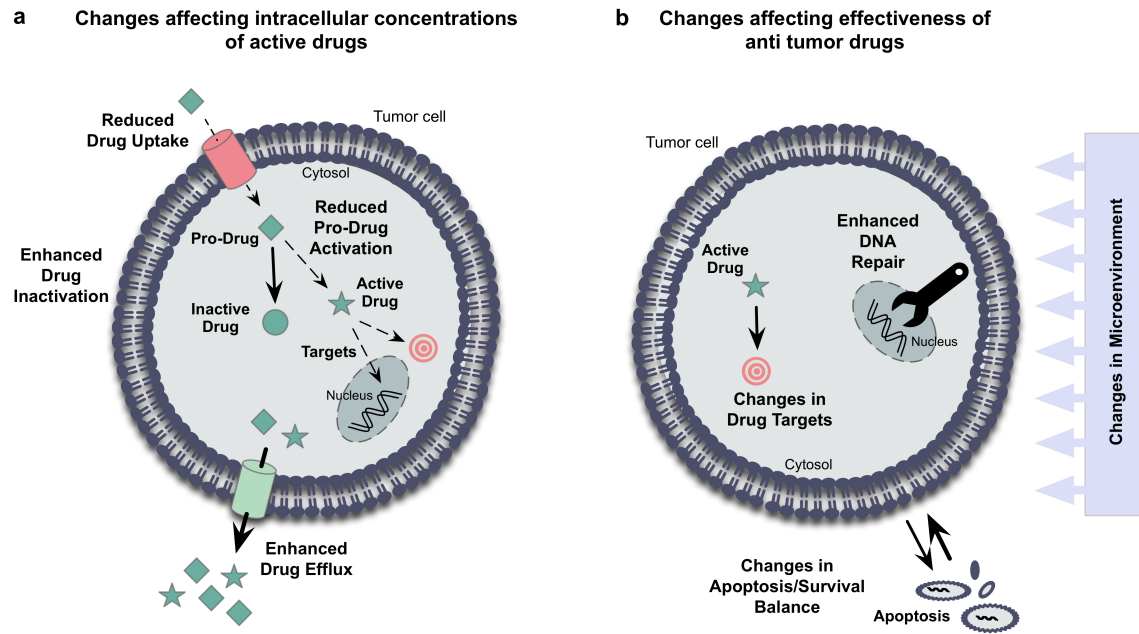


Figure 4 Schematic representation of common mechanisms of resistance to chemotherapeutic agents. a,b, Various mechanisms account for chemoresistance in tumor cells including reduction of either active drugs inside target cells (a) or the effectiveness of drugs on target mechanisms (b). **a,** The amount of active drugs that reach their intracellular targets can be reduced by different mechanisms like decreased intracellular uptake or enhanced efflux, reduced activation of pro-drugs or an increased drug inactivation. **b,** The effectiveness of anticancer drugs can be affected as well and these mechanisms include enhanced DNA damage repair, decreased activity of pro-apoptotic factors, increased activity of anti-apoptotic factors, changes in microenvironment, and functional or expressional changes of the molecular targets. Adapted from Marin *et al.*⁶⁷.

Once the deoxycytidine analogue is in the cytoplasm, it needs to be converted to its active, 5'-triphosphate derivative (Ara-CTP) by three different kinases (Figure 5). During DNA synthesis, Ara-CTP is incorporated into DNA in place of deoxycytidine triphosphate (dCTP), which leads to reducing chain elongation, block in DNA synthesis and initiation of apoptosis^{85,86}. Low levels of deoxycytidine kinase (DCK) which is believed to be the key rate-limiting activating enzyme by phosphorylating AraC to AraC monophosphate (Ara-CMP), were reported to correlate with low AraC sensitivity^{87,88} and to predict shorter DFS^{83,89}. The intracellular concentration of Ara-CTP can also be influenced by the action of inactivating enzymes including 5'-nucleotidase (NT5C2), cytidine deaminase (CDA), and deoxycytidylate deaminase (DCTD)⁸⁵. For example in AML patients treated with AraC, high levels of the inactivating enzyme NT5C2 were reported to predict shorter DFS⁹⁰. Recently, the dNTP triphosphohydrolase SAMHD1 was shown to reduce the

amount of active AraC derivatives by hydrolyzing Ara-CTP and thereby facilitating increased resistance to AraC treatment^{91,92}. Other reported mechanisms of resistance are cytarabine metabolic pathway polyphorphisms⁹⁴⁻⁹⁶. Mutations or differential expression in genes important for DNA synthesis or apoptosis might also contribute to an inferior response to AraC therapy.

Contrary to AraC, mitoxantrone and anthracyclines including DNR and idarubicin exert their cytotoxic effect by inhibiting the activity of nuclear DNA topoisomerase II, which leads to DNA damage and initiation of apoptosis (Figure 5). DNA topoisomerase II alters

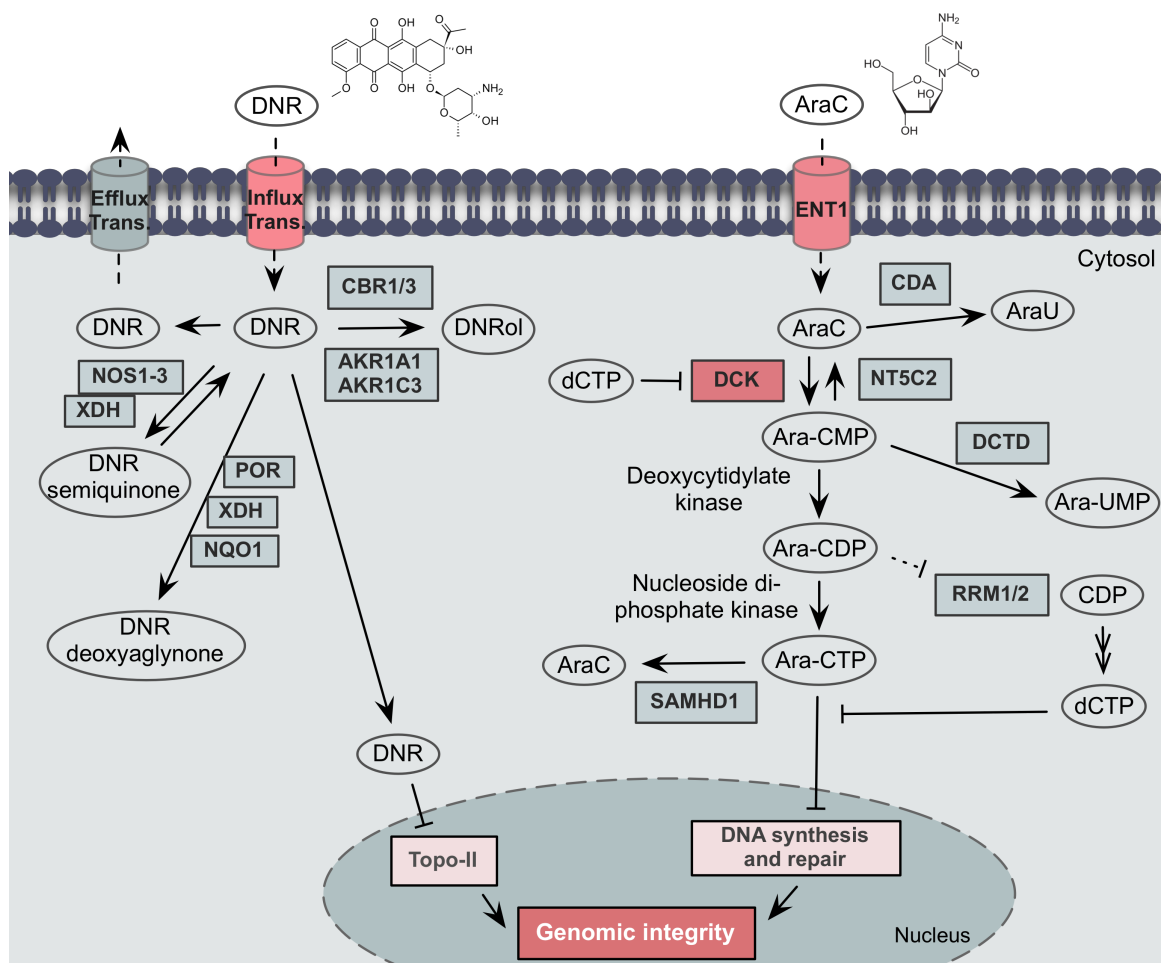


Figure 5 Metabolic pathway of DNR and AraC. Key candidate genes involved in the metabolic activation of AraC and the metabolism of DNR are shown. AraC: cytarabine; CDA: cytidine deaminase; CDP: cytidine diphosphate; dCTP: deoxycytidine triphosphate; DCK: deoxycytidine kinase; DCTD: Deoxycytidylate deaminase; DNR: daunorubicin; ENT1: equilibrative nucleoside transporter 1; NT5C2: 5' nucleotidase; Topo-II: topoisomerase II. Adapted from McLornan *et al.*⁸⁶, J. Lamba *et al.*⁸⁵, and Megias-Vericat *et al.*⁹³.

the topological state of DNA by generating a transient double-stranded break and passing an intact helix through this break thereby relaxing supercoiled DNA during replication and transcription⁹⁷. Alterations in anthracyclines metabolizing enzymes (Figure 5) including influx (SLC22A16, SLC28A3, SLCO1B1) and efflux (Pgp, ABCC1-3, ABCG2) transporters, detoxification through hydroxylation by carbonyl (CBR1, CBR3) and aldo-keto reductases (AKR1A1, AKR1C3), deglycosylation, and semiquinone formation might all influence the efficacy of anthracyclines⁹³.

Although misregulation of cell intrinsic factors plays a major role in resistance, extrinsic factors such as the microenvironment also contribute to the biology of resistance in AML blasts⁹⁸⁻¹⁰². Future studies are required to validate and confirm drug resistant candidate genes, which preferably should be identified in patient samples and not only by generating resistant cell line models. Eventually, a panel of resistant-associated genes might then be used as a diagnostic tool to identify patients with an altered drug response even before treatment.

1.2 Epigenetic regulation

Epigenetic is defined as heritable but biochemically reversible changes of a given expression state without inducing alteration in the DNA sequence^{103,104}. Epigenetic mechanisms involve DNA methylation, post-translational histone modifications, nucleosome remodeling, histone variants and non-coding RNAs. These mechanisms control cell type-specific patterns of gene expression and are therefore essential for establishing and maintaining cell identity and function.

1.2.1 Chromatin structure and histone modifications

Eukaryotes package their genomic DNA into repeating units of nucleosomes to form chromatin fibers¹⁰⁵ (Figure 6). The basic unit of chromatin is the nucleosome, which occurs every 200 ± 40 base pairs (bp) throughout all eukaryotic genomes^{105,106}. One nucleosome core consists of 146-147 bp of DNA wrapped around a histone octamer that is composed of two copies of each of the histone pairs H3-H4 and H2A-H2B^{107,108}. To establish higher-order chromatin compaction, the repeating nucleosome cores are stabilized by the linker histone H1, which binds to DNA between the nucleosome cores^{109,110}. By determining DNA accessibility, the nucleosome plays an important role in the regulation of transcription. Thus, modification of histone proteins can have great implications on the transcriptional regulation. Histone proteins, especially their 20-35 amino acid long N-terminal “tail” domains that protrude from the surface of the nucleosome, can interact with other proteins and are subject to a variety of post-translational modifications¹¹¹. These modifications involve acetylation and methylation of lysine and arginine residues, phosphorylation of serine and threonine residues, sumoylation, ubiquitination and crotonylation of lysine residues, and ADP ribosylation. The net level of modifications is regulated by a balance between “writer” (histone acetyltransferases and methyltransferases), “eraser” (histone deacetylases and demethylases) and “reader” (e.g. PHD- and bromodomain-containing proteins) enzymes. For instance, lysine acetylation by histone acetyltransferases (HATs) is thought to loosen the interaction between histones and the negatively charged DNA backbone by neutralizing the positive charge on lysine. Thereby it promotes an open, transcriptionally active chromatin state where transcription factors can more efficiently bind to DNA. As histone lysine and arginine methylation does not profoundly affect the charge on individual lysine and arginine residues, it most likely influences the binding of chromatin-

associated proteins. For example, methylation of the histone 3 lysine 27 (H3K27) is essential for the binding of the polycomb repressive complex 1 (PCR1) and subsequent ubiquitination of H2A¹¹². The motif of adjacent amino acids of posttranscriptional modified residues can also play a role in histone-binding specificity. HAT GCN5, for instance, requires a specific consensus motif, G-K14-X-P, to acetylate lysine 14 on histone 3¹¹³. HMTs like the H3K9 HMT G9a and GLP can also recruit DNA methyltransferases to histone modifications. By independently inducing both H3K9 and DNA methylation, G9a/GLP suppresses transcription in embryonic stem cells^{114,115}.

In addition to the canonical histones, histone variants such as H3.3, CENP-A, H2A.Z, and H2A.X modulate chromatin dynamics. Whereas multiple gene copies of canonical histones exist through the genome to meet the high demand of histone protein required for genome duplication, histones variant genes lie outside the histone gene cluster¹¹⁶.

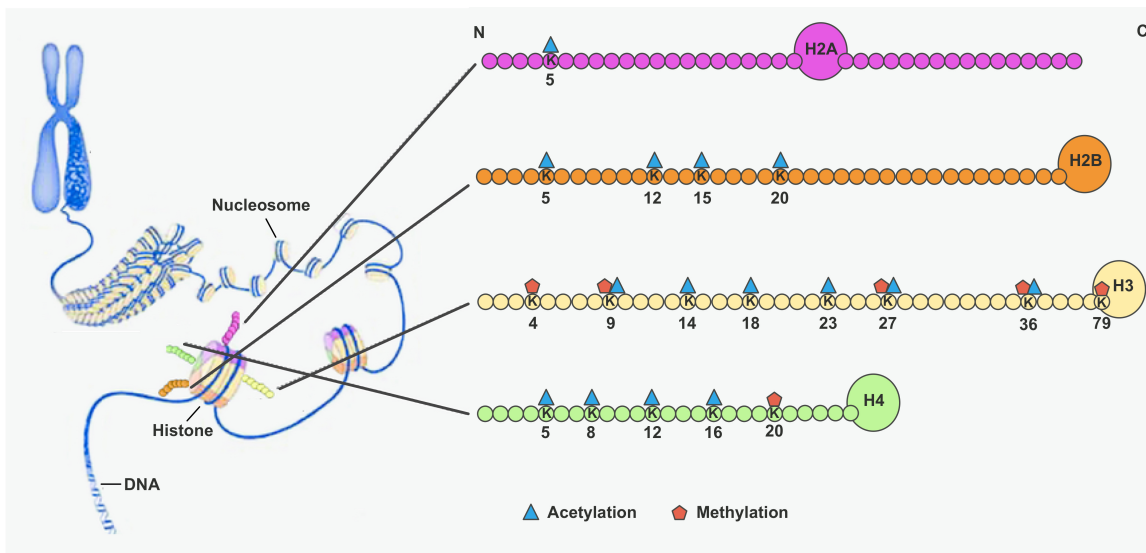


Figure 6 Chromatin organization and histone modifications at N-terminal histone tails. Eukaryotic DNA is packaged into repeating units of nucleosomes to form chromatin fibers, which are then compacted into higher ordered structures to form chromosomes. One nucleosome core consists of DNA wrapped around a histone octamer that is composed of two copies of each of the histone pairs H3-H4 and H2A-H2B. In addition to their globular domains, these histone proteins have N-terminal peptides, so called “tails”, that protrude from the surface of the nucleosome. H2A also has a C-terminal tail with similar regulatory features. Certain amino acid residues on histone tails are frequently post-translationally modified. All known mammalian acetylation (blue triangle) and methylation (red pentagon) modifications on histone lysine (K) residues are displayed. The above depictions of chromatin structure and histone tails are only schematic and are not meant to reflect the exact size. Adapted from Bagot *et al.*¹¹⁷.

Subtle differences in the amino acid sequence between H3 and H3.3 facilitate recognition by variant-specific chaperone proteins and post-translational modifications of variant-specific sites. Variant H3.3 which was found to be enriched at enhancers, impairs higher-ordered chromatin folding and promotes gene activation¹¹⁸.

It is now clear that histones and its associated modifying enzymes are remarkable diverse and highly dynamic components of the machinery responsible for regulating gene transcription. Recent discoveries of mutations targeting these components in cancer and other diseases have further revealed a crucial role in pathological processes.

1.2.2 Histone methylation and demethylation

Histone methylation is an important biological process through which the expression state of many genes is controlled. Lysine residues can be mono-, di- or trimethylated and depending on the site and methylation state, transcription is either activated or repressed. Generally, actively transcribed regions are marked with high levels of H3K27me1, H3K9me1, H4K20me1, H3K36me3, H3K4me3 and H2BK5me1¹¹⁹. In contrast, trimethylation of H3K9 and H3K27 is correlated with gene silencing. Opposing histone marks co-exist at certain genomic domains and these domains are referred to as “bivalent” domains. Bivalent genes are transcriptionally repressed, but hold in a poised state, enabling them to be rapidly activated upon stimulation. Activating H3K4me3 and repressive H3K27me3 marks are commonly found within developmental gene promoters of embryonic stem (ES) cells, like the *Homeotic (HOX)* locus^{120,121}. Global histone lysine methylation patterns are maintained by two enzyme families, lysine methyltransferases (KMTs) and demethylases (KDMs). The human KMT protein family is a group of 52 known KMTs, which have a catalytic SET domain except for the H3K79-specific KMT DOT1L. KMT enzymes utilize S-adenosyl-L-methionine (SAM) as the methyl donor and are highly specific for the histone residue and the degree of methylation. KMTs are multi-domain proteins and have been found to operate as multisubunit protein complexes^{112,122}. The Polycomb repressive complex 2 (PRC2) is responsible for the deposition of H3K27me3 marks by catalyzing the mono-, di- and trimethylation of H3K27¹²³. Mammalian PRC2 can be further classified into two distinct complexes, PRC2.1 and PRC2.2¹²⁴, which both comprise the methyltransferase EZ homolog 2 (EZH2) as a catalytic subunit. Besides EZH2, human PRC2.2 complex contains the subunits SUZ12, AEBP2, RpAp48, and EED¹²⁵. SUZ12 and EED are essential for the methyltransferase

activity of EZH2¹²⁶. PRC2 complex was found to have essential roles in developmental processes, X inactivation and carcinogenesis^{127–130}. In pediatric glioblastomas, researchers discovered that global H3K27me3 marks are reduced because of a point mutation (H3K27M) in the histone 3 variant H3.3, which inhibits the enzymatic activity of PRC2^{131–133}.

Demethylation of histone lysines was first experimentally confirmed in 2004 when Shi *et al.* discovered that H3K4 demethylation was mediated by a KDM called LSD1¹³⁴. To date, two functional enzymatic families have been identified to possess lysine demethylase activity^{112,122}. These two KDM families differ from each other in terms of catalytic domain organization and type of demethylase mechanism. KDM1A (LSD1) and KDM1B (LSD2) belong to the family of amine oxidases that utilize flavin adenine dinucleotide (FAD) as a cofactor to catalyze demethylation of only mono- and di-methylated lysine residues. These amine oxidases cannot remove trimethyl lysine residues because they require a protonatable lysine ϵ -amine group¹³⁵. The Jumonji C (JmjC) domain-containing KDM family members catalyze oxidative demethylation of all three methylation states with the cofactors iron and α -ketoglutarate¹³⁵. Similar to KMTs, KDMs are mostly selective for a specific lysine residue and the degree of methylation. In addition, it has recently emerged that KDMs also have many activities that are distinct from histone demethylation¹³⁶. Demethylation of non-histone proteins like transcription factors, chromatin-associated proteins, or proteins involved in signal transduction appears to regulate the abundance, stability or activity of non-histone substrates^{137–140}. Furthermore, demethylase-independent functions can be facilitated through protein-protein interaction domains as part of large multiprotein complexes or through chromatin-binding domains¹²². Dysregulation of these epigenetic regulatory processes have major implications in the development of many diseases, especially cancer. Lysine demethylases are often found to be deregulated in cancer^{141–145}. Overexpression of LSD1, for instance, was reported to contribute to carcinogenesis in a variety of cancer types including colorectal, bladder and lung carcinomas¹⁴⁶. In addition, changes in intracellular levels of cofactors required for KDM reactions can effect histone demethylation. Low concentrations of the cofactor α -ketoglutarate and thus inhibition of KDMs were observed in certain AML and glioblastomas cases with *IDH1* or *IDH2* mutations¹⁴⁷. Mutated IDH1 and IDH2 convert α -ketoglutarate to 2-hydroxyglutarate causing a “hypermethylator” phenotype¹²².

1.2.3 The histone H3K27 demethylase KDM6A

In 2007, KDM6A (UTX; ubiquitously transcribed tetratricopeptide repeat, X chromosome) was discovered by several research groups as a histone demethylase that specifically targets di- and tri-methyl groups on lysine 27 of histone 3, a mark important for transcriptional repression^{148–151}. The ubiquitously expressed KDM6A belongs to the family of JmjC domain-containing proteins and consists of 1401 amino acids (Figure 7). In contrast to the KDM6 family member KDM6B (JMJD3), it contains 6 protein interaction-mediating tetratricopeptide repeat (TPR) domains, which are believed to mediate protein-protein interactions. The human *KDM6A* and mice *Kdm6a* genes are both located on chromosome X and sequence alignment between the cDNA of the mouse and human genes revealed that the two genes are 95% identical¹⁵². KDM6A is one of the few genes known to escape X chromosome inactivation in both mice and humans^{152,153}. Thus, KDM6A is expressed at higher levels in females than in males^{48,153,154}.

The third member of the KDM6 family is *KDM6C* (*UTY*; Figure 7). *UTY* is a homologue of KDM6A with 83% sequence homology in humans, which is encoded on the Y chromosome¹⁵². The Y-linked homolog in males, which has a substitution of critical amino acids within the JmjC domain compared to KDM6A¹⁵⁵, was reported to have reduced demethylase activity *in vitro*¹⁵⁵ but appears to have no demethylase activity *in vivo*¹⁵⁶.

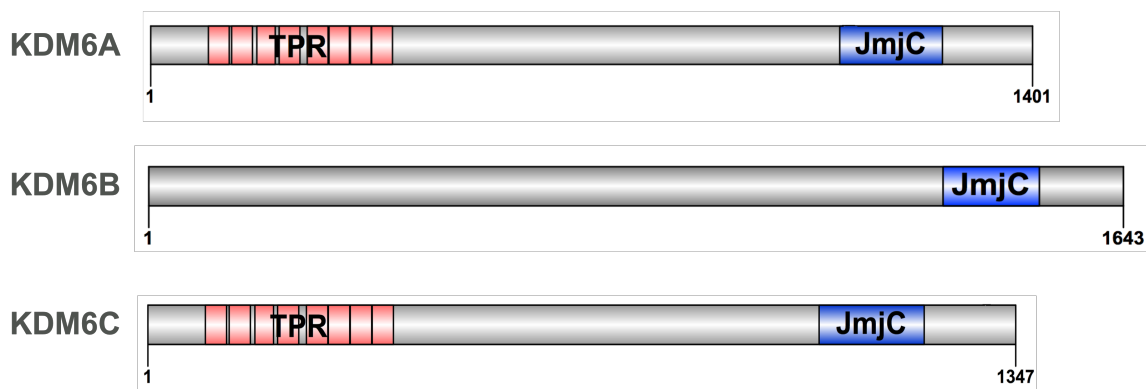


Figure 7 Schematic overview of the KDM6 protein family. Protein structures of KDM6A (UTX; NP_066963.2), KDM6B (JMJD3; NP_001335645.1) and KDM6C (UTY; NP_009056.3) are illustrated using IBS software¹⁵⁷. Amino acid positions are indicated below the graphs. TPR, tetratricopeptide repeat; JmjC, Jumonji C.

The H3K37 methylation status is mainly regulated by methyltransferase complex PRC2 and the H3K27me_{2/3} demethylases KDM6A and KDM6B. KDM6A also associates with KMT2D (MLL2/MLL4) or KMT2C (MLL3) in the COMPASS (Complex of Proteins-Associated with Set1)-like multi-protein complex responsible for H3K4 methylation (Figure 8)^{158,159}. KMT2D methylates specific promoter regions, but also enhancer regions which can then be further activated by H3K27 acetyltransferases CBP/p300^{160–162}. By removing the H3K27me₃ mark, KDM6A appears to facilitate a stable interaction between H3 and members of the COMPASS complex, WDR5 and RbBP5, necessary for H3K4 methylation¹⁶³. Furthermore, the protein stability of KDM6A depends on KMT2D in ES cells¹⁶⁴.

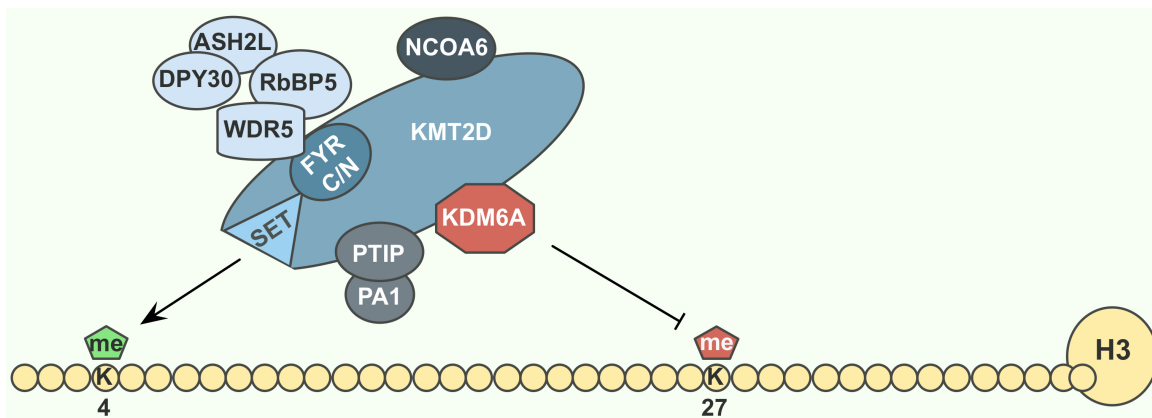


Figure 8 The KMT2D protein complex. KDM6A is a member of the KMT2D (MLL2/MLL4) multi-protein complex. KMT2D associates with NCOA6, PA1, PTIP, WDR5, RbBP5, ASH2L, DPY30, and KDM6A in one complex. KMT2D harbors a SET domain, which is responsible for H3K4 methyltransferase activity. KDM6A is a H3K27me_{2/me3} demethylase. H3K4 methylation and H3K27 demethylation is associated with transcriptionally active genes. Adapted from Froimchuk *et al.*¹⁵⁸.

1.2.3.1 KDM6A during embryonic development, hematopoiesis, and differentiation

KDM6A is broadly expressed and is essential in a wide array of functions. During murine embryonic development, KDM6A functions are critical for cardiovascular development and neural tube closure. Homozygous knockout (KO) of *KDM6A* in females is mid-gestational embryonic lethal with severe defects in the development of mesoderm-derived cardiac, posterior notochord, and hematopoietic tissues^{156,165–168}. In comparison to *KDM6A* hemizygous males, *KDM6A* homozygous females demonstrated a significantly more severe embryonic phenotype suggesting a functional redundancy of KDM6A and

UTY during embryonic development^{156,166,167}. Whereas some of these studies propose that H3K27 demethylation is non-essential for embryonic viability¹⁵⁶ and ES cell differentiation into mesoderm¹⁶⁷, other researchers conclude a demethylase activity-dependent as well as -independent role for KDM6A in the activation of cardiac-specific genes^{165,166}. For example, KDM6A was demonstrated to recruit the Brg1-containing chromatin remodeling SWI/SNF complex to the cardiac specific genes independent of its demethylase activity¹⁶⁵.

KDM6A is highly expressed in HSPCs, with lower expression in lineage-dedicated precursors and is a key factor for hematopoiesis¹⁶⁷⁻¹⁶⁹. Homozygous deletion in female adult mice resulted in myelodysplasia with reduced hemoglobin levels, anemia, and enlarged spleen¹⁶⁸. KDM6A is also involved in the regulation of stem cell migration since loss of KDM6A in HSPCs promoted a strong reduction in cell migration capability¹⁶⁸. In a study by Zheng *et al.*¹⁷⁰, loss of KDM6A in mice causes a chronic myelomonocytic leukemia (CMML)-like disease by increasing hematopoietic stem cell self-renewal and differentiation.

During retinoic acid-induced differentiation of teratocarcinoma NT2/D1 and ES cells, KDM6A was found to participate in the transcriptional activation of *HOX* genes by reducing H3K27me3 levels at the promoters of these genes¹⁴⁸. In primary human fibroblasts, in which *HOX* genes are differentially expressed, KDM6A was reported to be enriched around the transcription start sites of *HOX* genes and H3K27me3 levels at *HOX* promoters increased upon silencing of KDM6A¹⁵¹. KDM6A is also essential during early embryogenesis in *Drosophila* to prevent PRC2 mediated repression of *HOX* genes necessary for differentiation¹⁷¹. During myogenesis, KDM6A is targeted to regions upstream of the transcriptional start site of muscle-specific genes to mediate removal of H3K27me3 marks by a two-step mechanism¹⁷². After H3K27me3 demethylation near certain promoters, KDM6A appears to move across the coding regions with the RNA Polymerase II to facilitate demethylation¹⁷².

KDM6A also plays an important role in cell fate regulation via Retinoblastoma (RB)-dependent pathways¹⁷³. Depletion of KDM6A provides cells with an immediate proliferative advantage by preventing the expression of RB-binding proteins, important for cell cycle arrest¹⁷³.

1.2.3.2 Human diseases associated with the deregulation of KDM6A

Deletions or mutations in the *KDM6A* gene were identified in a variety of human diseases. In recent years, *KDM6A* mutations have been found in a rare genetic disease called Kabuki syndrome (KS) that causes developmental delay and congenital anomalies^{174–177}. Another, more frequently occurring, genetic cause of KS are heterozygous, nonsense and frameshift mutations in the *KMT2D* gene^{177–180}. To date, a few cases with both KS and cancer have been reported, but whether KS predisposes individuals to cancer remains uncertain^{181,182}.

In 2009, *KDM6A* was the first described histone demethylase to be targeted by somatic inactivating mutations and deletions in human cancer¹⁴⁵. Since then, several research groups have reported inactivating *KDM6A* mutations and deletions in a wide array of cancer types^{183–191} including leukemia^{153,192–195}. In urothelial bladder cancer, it is the second most altered cancer-associated gene, after *TP53*¹⁸⁶. In most cases, inactivating mutations and deletions were identified suggesting a tumor suppressor function for *KDM6A*. For instance, reduced expression or mutations/deletions of *KDM6A* correlate with poor overall survival in patients with CN-AML⁴⁸ or myeloma¹⁹¹, respectively.

Although *KDM6A* is a recurrent mutational target in a broad range of cancer types, the regulatory mechanisms of its tumor suppressor function seem to be diverse and specific for each tumor type. In *KDM6A* mutated urothelial bladder carcinoma, loss of the *KDM6A* demethylase-activity seems to create an EZH2 dependency in cell proliferation making these cells vulnerable to EZH2 inhibition¹⁸⁹. A similar conclusion may be drawn from a study in T-cell ALL (T-ALL), in which T-ALL driven by *KDM6A* inactivation showed sensitivity to pharmacologic H3K27me3 inhibition¹⁵³. In contrast, the tumor suppressor role of *KDM6A* in a subset of pancreatic cancer is largely independent of its catalytic function and *KDM6A* loss resulted in a deregulation of the COMPASS-like complex and aberrant activation of super-enhancers¹⁹⁶.

A recent study shed light on *KDM6A*'s role during myeloid leukemogenesis. In a mouse model, *KDM6A* was shown to prevent myeloid leukemogenesis through noncatalytic repression of pro-oncogenic ETS and maintenance of tumor-suppressive GATA transcriptional programs¹⁹⁷. During the evolution to AML, the demethylase function of *KDM6A* appears to be redundant for tumor suppression and *KDM6A* operates by interacting with KMT2C/D-containing COMPASS complex and certain chromatin remodeling factors like SMARCA4, important for chromatin accessibility¹⁹⁷. The Y-linked homolog UTY facilitates *KDM6A*-similar noncatalytic functions during myeloid

leukemogenesis and can rescue KDM6A-deficient preleukemic phenotypes¹⁹⁷. Depending on whether the demethylase activity is essential for pathogenesis, there appears to be a gender bias towards males (in T-ALL¹⁵³) or females (in pancreatic cancer¹⁹⁶ and myeloid leukemogenesis¹⁹⁷).

1.3 Aims of this work

Although recent studies have reported a crucial role for the histone H3K27me3 demethylase KDM6A in the development of cancer, its functions during clonal evolution of AML from diagnosis to relapse are still unresolved. Relapse of AML occurs in the majority of patients and drug resistance is likely to play an essential role in its development. It was the aim of this project to characterize the clonal evolution dynamics of KDM6A during AML progression and to investigate if KDM6A loss facilitates resistance to drugs that are commonly used in the induction therapy for AML. For this purpose, different silencing approaches including siRNA, shRNA and CRISPR/Cas9-mediated gene editing were used to generate transient and stable KDM6A knockdown/knockout models in human myeloid leukemia cell lines. Furthermore, genomewide RNA expression analysis was performed to identify potential KDM6A target genes involved in chemotherapy resistance.

2 Materials and Methods

2.1 Materials

2.1.1 Reagents and chemicals

Table 1 List of used reagents and chemicals.

Reagent	Supplier	Product number
1 kb DNA ladder	Promega (Madison, WI, USA)	G571A
2-Mercaptoethanol	Sigma-Aldrich (St. Louis, MO, USA)	M3148
2-Propanol	AppliChem (Darmstadt, Germany)	A3928
Acetic acid	Sigma-Aldrich (St. Louis, MO, USA)	A6283
Agarose	Carl Roth (Karlsruhe, Germany)	2267.5
Albumin Fraction V (pH 7.0) (BSA)	AppliChem (Darmstadt, Germany)	A1391
Ammonium persulfate (APS)	Carl Roth (Karlsruhe, Germany)	9592.3
Ampicillin sodium salt	Sigma-Aldrich (St. Louis, MO, USA)	A0166
Aprotinin	Sigma-Aldrich (St. Louis, MO, USA)	10820
Bio-Rad Protein Assay Dye R.	Bio-Rad (Hercules, CA, USA)	5000006
Bromophenol blue	Sigma-Aldrich (St. Louis, MO, USA)	B8026
Calcium Chloride 2-hydrate	AppliChem (Darmstadt, Germany)	A4689
CutSmart Buffer	New England Biolabs (Frankfurt, Germany)	B7204S
Coulter Clenz Cleaning Agent	Beckman Coulter (Krefeld, Germany)	8546929
Coulter Isoton II Diluent	Beckman Coulter (Krefeld, Germany)	8546719
DNase I	Roche (Basel, CH)	4536282001
DAPI	Sigma-Aldrich (St. Louis, MO, USA)	D9542
DEPC-treated water	Thermo Fisher Scientific (Waltham, MA, USA)	11531575
DH5alpha competent bacteria	Thermo Fisher Scientific (Waltham, MA, USA)	18265017
Dimethyl Sulfoxide (DMSO)	Sigma-Aldrich (St. Louis, MO, USA)	D2438
Dulbecco's MEM (DMEM), high glucose, Gibco™	Thermo Fisher Scientific (Waltham, MA, USA)	31966021
EcoRI	New England Biolabs (Frankfurt, Germany)	R0101S
EcoRI-HF	New England Biolabs (Frankfurt, Germany)	R3101S
EDTA	Sigma-Aldrich (St. Louis, MO, USA)	ED-500G
Ethanol	Merck Millipore (Darmstadt, Germany)	64-17-5
Fast Digest BpiI	Thermo Fisher Scientific (Waltham, MA, USA)	FD1014
Fast Digest HpyF10VI	Thermo Fisher Scientific (Waltham, MA, USA)	FD1734
Fetal Bovine Serum (FBS)	PAN-Biotech (Aidenbach, Germany) ^[1] _{SEP}	P40-37500
Gel Loading Dye Purple 6x	New England Biolabs (Frankfurt, Germany)	B7025S
Glycerol	AppliChem (Darmstadt, Germany)	A4443.1000
Glycine	Sigma-Aldrich (St. Louis, MO, USA)	G8898
HBS 2x	Sigma-Aldrich (St. Louis, MO, USA)	51558
HEPES	AppliChem (Darmstadt, Germany)	A3724.0500
Kanamycin Sulfate	Sigma-Aldrich (St. Louis, MO, USA)	K1377
Kaliumchlorid KCl	AppliChem (Darmstadt, Germany)	A2939
LB-Agar (Lennox)	Carl Roth (Karlsruhe, Germany)	X964.1
LB-Medium (Lennox)	Carl Roth (Karlsruhe, Germany)	X965.1

Materials and Methods

L-Glutamine	Sigma-Aldrich (St. Louis, MO, USA)	G7513
Lipofectamine 3000	Thermo Fisher Scientific (Waltham, MA, USA)	L3000001
Magnesium Chloride 6-hydrate	AppliChem (Darmstadt, Germany)	A4425
Maxima H Minus Reverse Transcriptase	Thermo Fisher Scientific (Waltham, MA, USA)	EP0751
Methanol	Carl Roth (Karlsruhe, Germany)	8388.5
Milk powder blotting grade	Carl Roth (Karlsruhe, Germany)	T145.1
MyTaq Polymerase	Bioline (London, UK)	BIO-21105
NEBuffer™ 2.1	New England Biolabs (Frankfurt, Germany)	B7201S
NEBuffer™ 3.1	New England Biolabs (Frankfurt, Germany)	B7203S
NEBuffer™ 4	New England Biolabs (Frankfurt, Germany)	B7204S
Non-essential amino acids 10x	Biochrom (Berlin, Germany)	K0293
NP40 Substitute	AppliChem (Darmstadt, Germany)	A1694
Opti-MEM® I Reduced Serum Medium, Gibco™	Thermo Fisher Scientific (Waltham, MA, USA)	11058021
PageRuler™ Prestained Protein Ladder	Thermo Fisher Scientific (Waltham, MA, USA)	26616
PBS Dulbecco w/o Mg ²⁺ , Ca ²⁺	PAN-Biotech (Aidenbach, Germany)	P04-36500
Penicillin-Streptomycin, Gibco™	Thermo Fisher Scientific (Waltham, MA, USA)	15140122
peqGold Protein Marker VI	Peqlab (Erlangen, Germany)	27-2310P
Phenylmethylsulfonyl fluoride (PMSF) solution	Sigma-Aldrich (St. Louis, MO, USA)	93482
Pierce ECL Plus Western Blotting Substrate	Thermo Fisher Scientific (Waltham, MA, USA)	32106
Polybrene	Sigma-Aldrich (St. Louis, MO, USA)	H9268
Propidium iodide (PI)	Sigma-Aldrich (St. Louis, MO, USA)	P4170
Proteinase K	New England Biolabs (Frankfurt, Germany)	P8107S
Quick-Load Purple 50bp DNA ladder	New England Biolabs (Frankfurt, Germany)	N0556S
Recombinant Human FLT3 (rhFLT3) Ligand	R&D Systems (Minneapolis, MN, USA)	PRD308
Recombinant Human IL3 (rhIL3) protein	R&D Systems (Minneapolis, MN, USA)	203-IL
Recombinant Human Thrombopoietin (rhTPO) protein	R&D Systems (Minneapolis, MN, USA)	288-TP
Recombinant Human SCF (rhSCF) protein	R&D Systems (Minneapolis, MN, USA)	255-SC
Restore™ PLUS Western Blot Stripping Buffer	Thermo Fisher Scientific (Waltham, MA, USA)	46430
RNase AWAY	Carl Roth (Karlsruhe, Germany)	3865.1
Rotiphorese gel 30	Carl Roth (Karlsruhe, Germany)	3029.1
RPMI 1640 + Glutamax, Gibco	Invitrogen (Darmstadt, Germany)	61870-044
Sodium chloride NaCl	Carl Roth (Karlsruhe, Germany)	3957.1
Sodium dodecyl sulfate (SDS)	Sigma-Aldrich (St. Louis, MO, USA)	L4509
Sodium fluoride NaF	Sigma-Aldrich (St. Louis, MO, USA)	201154
Sodium Orthovanadate	Sigma-Aldrich (St. Louis, MO, USA)	S-6508
Sodium pyrophosphate decahydrate	Sigma-Aldrich (St. Louis, MO, USA)	221368
Sodium pyruvate 100mM	Biochrom (Berlin, Germany)	L0473
S.O.C. Medium	Invitrogen (Darmstadt, Germany)	15544-034
StemPro-34 SFM Media	Thermo Fisher Scientific (Waltham, MA, USA)	10639011
SYBR™ Safe DNA gel stain	Invitrogen (Darmstadt, Germany)	S33102
T4 DNA Ligase	Promega (Madison, WI, USA)	M1801

TAE Buffer 10x	In-house	-
TBE Buffer 10x	Invitrogen (Darmstadt, Germany)	15581-028
TBS Buffer 10x	In-house	T03290
Tetramethylethylenediamine (TEMED)	Sigma-Aldrich (St. Louis, MO, USA)	T9281
Tris-(hydroxymethyl)-aminomethane (TRIS)	Carl Roth (Karlsruhe, Germany)	AE15.2
Triton X-100	Sigma-Aldrich (St. Louis, MO, USA)	X100
Trypan Blue	Sigma-Aldrich (St. Louis, MO, USA)	T8154
Trypsin-EDTA (0.05%), phenol red	Thermo Fisher Scientific (Waltham, MA, USA)	25300054
Tween20	Sigma-Aldrich (St. Louis, MO, USA)	P1379
XhoI	New England Biolabs (Frankfurt, Germany)	R0146S

2.1.2 Chemotherapeutic and targeted agents

Stock solutions of cytarabine (Selleck Chemicals, Houston, TX, USA) at 20 mM, 6-thioguanine (Sigma-Aldrich, St. Louis, MO, USA) at 20 mM, and MG132 (Calbiochem, Merck, Darmstadt, Germany) at 50 mM were prepared by dissolving the drugs in sterile DMSO under sterile conditions. Daunorubicin was prepared at the in-house clinical pharmacy at 3.2 mM in sterile deionized water. To avoid repetitive freeze-thaw cycles, stock solutions were stored in aliquots at -80°C. Stock solutions were diluted with media to the required concentrations before each experiment.

2.1.3 Buffers and solutions

Table 2 List of used buffers.

Name	Composition
Agarose gels 0.8-1.5%	0.8-1.5% agarose in 1x TAE or TBE buffer with SYBR™ Safe (1:10 000)
Electrophoresis buffer 10x	5 L: 151.4 g Tris (pH 8.3), 720.7 g Glycine, 50 g SDS, ad Aqua dest.
KCM 5x	13 mL: 5 mL 3M KCl, 4,5 ml 1M CaCl ₂ , 7.5 ml 1M MgCl ₂ , ad Aqua dest.
Lämmli buffer 4x	10mL: 1.33 mL 1.5M Tris-HCl (pH 6.8), 0.8 g SDS, 4 mL Glycerol, 0.4 mL 14.3M 2-Mercaptoethanol, 146 mg EDTA, 8 mg Bromophenol blue
LB Agar	32 g in 1 L Aqua dest., autoclaved* ¹
LB _{Ampicillin/Kanamycin} plates	Plates containing 20 mL LB Agar with 100 µg/mL Ampicillin or 25 µg/mL Kanamycin
Luria Broth Base	25 g in 1 L Aqua dest., autoclaved* ¹
Lysis buffer WCL* ²	0.5 L: 25 mL 1 M Hepes (pH 7.5), 15 mL 5M NaCl, 2,5 mL 200 mM EGTA, 100 mL Glycerol 50%, 5 mL TritonX-100, 2.1 g NaF, 2.23 g Na ₄ P ₂ O ₇ ·10H ₂ O

Materials and Methods

Lysis buffer SC	50 mM TRIS/HCl (pH 7.5), 10 mM CaCl ₂ , 1.7 μM SDS, 50 μg/mL Proteinase K),
TAE buffer	5 L: 242.3 g Tris, 57.1 mL acetic acid 100%, 18.61 g EDTA 2Na x 2H ₂ O
TBS 10x	5 L: 12.11 g Tris (pH 8.0), 87.66 g NaCl, add Aqua dest.
TBST	TBS 1x with 0.1% Tween20
Transfer blotting solution	5 L: 15 g Tris, 71 g Glycine, 790 g Methanol, add Aqua dest.
Tris-HCl 1.5M pH 6.8	5 L: 908.55 g Tris (pH 6.8), add Aqua dest.
Tris-HCl 1.5M pH 8.8	5 L: 908.55 g Tris (pH 8.8), add Aqua dest.

*¹ Autoclave sterilization of media was performed at 120°C and 2 bar for 20 min.

*² The following inhibitors were added before use: 5 mM PMSF, 25 μg/mL Aprotinin, 50 μg/mL Sodium Orthovanadate.

2.1.4 Kits

Table 3 List of used kits.

Kit	Supplier	Product number
BigDye™ Terminator v1.1 Cycle Sequencing Kit	Thermo Fisher Scientific (Waltham, MA, USA)	4337450
Cell Line Nucleofector™ Kit V	Lonza (Basel, CH)	VVCA-1003
EndoFree Plasmid Maxi Kit	Qiagen (Hilden, Germany)	12362
EpiQuik Total Histone Extraction Kit	Epigentek (Farmingdale, NY, USA)	OP-0006-100
Gentra Puregene Kit	Qiagen (Hilden, Germany)	158389
In-Fusion® HD Cloning Plus	Takara Bio (Saint-Germain-en-Laye, France)	638909
KAPA Hifi 2x ready mix	Kapa Biosystems (Wilmington, MA, USA)	KK2601
Mouse Cell Depletion Kit	Miltenyi Biotec (Bergisch Gladbach, Germany)	130-104-694
MycoAlert® Mycoplasma Detection Kit	Lonza (Basel, CH)	LT07-218
Nextera XT DNA Library Preparation Kit	Illumina (San Diego, CA, USA)	FC-131-1024
QIAamp DNA Blood Mini Kit	Qiagen (Hilden, Germany)	51104
QIAquick Gel Extraction Kit	Qiagen (Hilden, Germany)	28106
QIAquick PCR Purification Kit	Qiagen (Hilden, Germany)	28104
QIAprep Spin Miniprep Kit	Qiagen (Hilden, Germany)	27104
Qproteome Nuclear Protein Kit	Qiagen (Hilden, Germany)	37582
QuantiTect SYBR Green PCR Kit	Qiagen (Hilden, Germany)	204141
QuickChange II XL Site-Directed Mutagenesis	Stratagene (La Jolla, CA, USA)	200521
RNase-Free DNase Kit	Qiagen (Hilden, Germany)	79254
RNeasy Mini Kit	Qiagen (Hilden, Germany)	74104
SALSA MLPA KDM6A probe mix ^[1] _{SEP}	MRC Holland (Amsterdam, Netherlands)	P445
SuperScript™ IV First-Strand Synthesis System	Thermo Fisher Scientific (Waltham, MA, USA)	18091050

2.1.5 Antibodies

Respective primary and secondary antibodies (Table 4) were used for western blot analysis.

Table 4 List of used primary and secondary antibodies.

Antibody	Supplier	Product number	Dilution
Anti- β -Actin (AC-15)	Sigma-Aldrich (St. Louis, MO, USA)	A5441	1:20000
Anti- α -Tubulin mouse	Sigma-Aldrich (St. Louis, MO, USA)	T6199	1:20000
Anti-HA-Tag (6E2)	Cell Signaling Technology (Danvers, MA, USA)	2367	1:1000
Anti-Histone H3	Abcam (Cambridge, UK)	ab1791	1:5000
Anti-KDM6A/UTX (3A2)*	Abcam (Cambridge, UK)	ab91231	1:1000
Anti-KDM6A/UTX (D3Q11)	Cell Signaling Technology (Danvers, MA, USA)	33510	1:3000
Anti-monomethyl-Histone H3 Lys27 (H3K27me1)	Merck (Darmstadt, Germany)	07-448	1:400
Anti-dimethyl-Histone H3 Lys27 (H3K27me2)	Merck (Darmstadt, Germany)	07-452	1:750
Anti-trimethyl-Histone H3 Lys27 (H3K27me3)	Merck (Darmstadt, Germany)	07-449	1:600
Anti-trimethyl-Histone H3 Lys27 (H3K27me3)	Cell Signaling Technology (Danvers, MA, USA)	9733	1:1000
Anti-Mouse IgG-HRP, goat	Santa Cruz Biotechnology (Dallas, TX, USA)	sc-2005	1:10000
Anti-Mouse IgG κ BP-HRP	Santa Cruz Biotechnology (Dallas, TX, USA)	sc-516102	1:10000
Anti-Rabbit IgG-HRP, goat	Sigma-Aldrich (St. Louis, MO, USA)	A0545	1:10000

* was used at the beginning of this work. Immunoblots shown in this work were generated with #33510.

2.1.6 Oligonucleotides

Table 5 List of used primers.

Name	Sequence (5' to 3')	Application
AML393_FOR	CACGGATGAGGAAATTGACTCC	PCR
AML393_REV	GGCATCTGTGTACATCTAGATTGTTCTTAG	PCR
AML393-Sanger_FOR	CAGGCCTGCTGAGCATTG	Sequencing
AML393-Sanger_REV	GAAACCAACAGTGGAGAGGG	Sequencing
EZH2_FOR2	CCCTGACCTCTGTCTTACTTGTGGA	qRT-PCR
EZH2_REV2	ACGTCAGATGGTGCCAGCAATA	qRT-PCR
GAPDH_FOR	AATGAAGGGGTCATTGATGG	qRT-PCR
GAPDH_REV	AAGGTGAAGGTCGGAGTCAA	qRT-PCR

Materials and Methods

HA-KDM6A_REV	CTCCCTCTCCTCGGCTGT	Sequencing
InFus-pcDNA6-KDM6A_FOR	CAGTGTGGTGGAAATCCGACGGATCAATTCACC ATGGCATAC	Cloning: KDM6A in pcDNA6 vector
InFus-pcDNA6-KDM6A_REV	GCCCTCTAGACTCGAGCCCTTTCAAGATGAGGC GGATGGT	Cloning: KDM6A in pcDNA6 vector
KDM6A_FOR_1	CCAGAGGAAATATCATTCTGCAA	Sequencing
KDM6A_FOR_2	ATGCTGTGTCACATCCTCCA	Sequencing
KDM6A_FOR_3	ACCCTGCCTAGCAATTCAGT	Sequencing
KDM6A_FOR_4	CACCTCCAAGACCACCATCT	Sequencing
KDM6A_FOR_5	TCAGTTAACATAAAATATTGGCCCAG	Sequencing
KDM6A_REV_1	GCATCCAACCTAACTGTTGTAAGA	Sequencing
KDM6A_KO_FOR	GGGGTTAGCCTAGATGCTGTTC	Screening
KDM6A_KO_REV	ATTGGCAATAATCTGCCCAAACA	Screening
KDM6A_V1113Sfs38_FOR	CTGCTTTTGTGCGTGTCTCTATCAGCAGGAAAT CT	Site-directed mutagenesis
KDM6A_V1113Sfs38_REV	AGATTTCTGCTGATAGAGACACGCACAAAAG CAG	Site-directed mutagenesis
KDM6A_L1103R_FOR	GTTGCAGCTACATGAGCGGACTAA ACT TCCTGCTT	Site-directed mutagenesis
KDM6A_L1103R_REV	AAGCAGGAAGTT TAGTCCGCTCATGTAGCTGCAAC	Site-directed mutagenesis
KDM6A E1325X_FOR	TATATGGCATGGGCGGACAAAATAAGAACCAG CTCA	Site-directed mutagenesis
KDM6A E1325X_REV	TGAGCTGGTTCTTATTTTGTCCGCCCATGCCATA TA	Site-directed mutagenesis
KDM6A H1146A_FOR	CAGGGAGCAGAACACCAGGTGCTCAGGAAAAT A ACAACT T	Site-directed mutagenesis
KDM6A H1146A_REV	AAGTTGTTATTTTCTGAGCACCTGGTGTCTGC TCCCTG	Site-directed mutagenesis
KDM6A_FOR	TACAGGCTCAGTTGTGTAACCT	qRT-PCR
KDM6A_REV	CTGCGGGAATTGGTAGGCTC	qRT-PCR
KDM6B_FOR	GGAGGCCACACGCTGCTAC	qRT-PCR
KDM6B_REV	GCCAGTATGAAAGTTCCAGAGCTG	qRT-PCR
P5NEXTPT5	AATGATACGGCGACCACCGAGATCTACACTCTT TCCCTACACGACGCTCTTCCG*A*T*C*T*	RNA-Seq
pU6_FOR	GAGGGCCTATTTCCCATGATTC	Sequencing Cas9
UTY_FOR	TTAGCCTGACAGTCGAGGAAA	qRT-PCR
UTY_REV	GTAGGGTCTTCGTTCTGGCG	qRT-PCR

Table 6 List of used siRNA's, shRNA's and gRNA.

Name	Sequence (5' to 3')	Origin
gRNA <i>KDM6A</i>	GGTATGCAGATAATGCTGAA	This work
Stealth siRNA <i>KDM6A</i> HS111232	GCAAAUGUCCAGUGUAGGUUUA	Thermo Fisher Scientific (Waltham, MA, USA)
Stealth siRNA negative ctrl, low GC	NA	Thermo Fisher Scientific (Waltham, MA, USA)
shRNA <i>KDM6A</i> #3	TACTTGAATAGCACCTCCGA	I. Jeremias, Helmholtz Zentrum München
shRNA <i>KDM6A</i> #4	TTAATGGCATCCTGAGGCTG	I. Jeremias, Helmholtz Zentrum München
shRNA <i>KDM6A</i> #7	TTTATCAATAGACTGCCTGTA	I. Jeremias, Helmholtz Zentrum München
shRNA <i>Renilla</i> , control	TAGATAAGCATTATAATTCCT	I. Jeremias, Helmholtz Zentrum München
shRNA <i>eGFP</i> , control	CAGCCACAACGTCTATATCAT	I. Jeremias, Helmholtz Zentrum München

NA, not available.

2.1.7 Plasmids

Table 7 List of used plasmids.

Name	Application	Origin
pCDH-EF1 α -MCS-T2A-copGFP (CD521A-1)	Lentivirus expression	System Biosciences (Palo Alto, CA, USA)
pcDNA6/V5-His A	Expression vector	Thermo Fisher Scientific (Waltham, MA, USA)
pcDNA6 HA <i>KDM6A</i>	HA <i>KDM6A</i> expression	This work
pcDNA6 HA <i>KDM6A</i> H1146A	HA <i>KDM6A</i> H1146A expression	This work
pcDNA6 HA <i>KDM6A</i> L1103R	HA <i>KDM6A</i> L1103R expression	This work
pcDNA6 HA <i>KDM6A</i> V1113Sfs*38	HA <i>KDM6A</i> V1113Sfs*38 expression	This work
pcDNA6 HA <i>KDM6A</i> E1325X	HA <i>KDM6A</i> E1325X expression	This work
pCMV-HA-UTX	Cloning of HA <i>KDM6A</i>	Kristian Helin; Addgene plasmid #24168
pSpCas9(BB)-2A-GFP (PX458)	Cas9-eGFP and backbone for gRNA expression	Feng Zhang; Addgene plasmid #48138
pSpCas9(BB)-2A-GFP-gRNA- <i>KDM6A</i>	Cas9-eGFP and gRNA <i>KDM6A</i> expression	This work
TRMPVIR	Extraction of dsRED-miR30 fragment	Scott Lowe; Addgene plasmid #27994

2.1.8 Cell lines and patient-derived xenograft AML cells

Human cancer cell lines and patient-derived xenograft (PDX) AML cells used for the experiments are shown in Table 8 and 9, respectively. As indicated in Table 8, certain cell lines were not cultured, but their genomic DNA (gDNA) was obtained from the German Collection of ^[1]_{SEP}Microorganisms and Cell Cultures (DSMZ, Braunschweig, Germany).

Table 8 List of used cell lines. All cell lines were obtained from the DSMZ.

Name	Cell Type	Gender	gDNA/culture
AP-1060	AML	male	gDNA
Eol-1	AML	male	culture
F-36P	AML	male	gDNA
FKH-1	AML	male	gDNA
GF-D8	AML	male	gDNA
HEK293T	embryonic kidney	female	culture
HL-60	AML	female	culture
HNT-34	AML	female	gDNA
HT-93	AML	male	gDNA
K562	CML in blast crisis	female	culture
Kasumi-1	AML	male	culture
Kasumi-3	AML	male	gDNA
KG-1a	AML	male	gDNA
M-07e	acute megakaryoblastic leukemia	female	gDNA
ME-1	AML	male	gDNA
MEGAL	acute megakaryoblastic leukemia	n.s.	gDNA
MKPL-1	acute megakaryoblastic leukemia	male	gDNA
MONO-MAC-1 (MM-1)	acute monocytic leukemia	male	culture
MONO-MAC-6 (MM-6)	acute monocytic leukemia	male	culture
Molm-13	AML	male	culture
Molm14 (sister Molm-13)	AML	male	gDNA
Molm16	AML	female	gDNA
MUTZ-2	AML	male	gDNA
MUTZ-3	acute myelomonocytic leukemia	male	gDNA
MV4-11	acute monocytic leukemia	male	culture
NB-4	acute promyelocytic leukemia	female	culture
OCI-AML1	AML	female	gDNA
OCI-AML3	AML	male	culture
OCI-AML4	AML	female	gDNA
OCI-AML5	AML	male	culture
OCI-AML6	sAML	female	gDNA
OCI-M1	AML	NA	gDNA
PLB-985	AML	female	gDNA

SKM-1	AML	male	gDNA
SKNO-1	AML	male	gDNA
TF-1	erythroleukemia	male	gDNA
THP-1	acute monocytic leukemia	male	culture
U-937	histiocytic lymphoma	male	culture
UCSD-AML1	AML	female	gDNA
UOC-M1	AML	male	gDNA
UT-7	AML	male	gDNA
YNH-1	AML	male	gDNA

NA, not available.

Table 9 List of used PDX AML cells. PDX AML cells were a gift from I. Jeremias (Helmholtz Zentrum München)⁵¹. All samples were established from patients with AML.

Sample	Disease stage	Sex	Cytogenetics	<i>NPM1</i>	<i>FLT3</i>	ELN
AML-372	Relapse	M	Complex, including -17	WT	WT	Adv
AML-393	Relapse after SCT	F	46,XX,ins(10;11)(p12;q23q23)	WT	WT	Adv
AML-407	Relapse after SCT	F	47,XX,t(4;8)(p15;q22),+12	WT	WT	Adv
AML-415	Relapse	F	Normal	Mut	ITD	Int I
AML-491	Relapse	F	Aberrant	WT	WT	Adv
AML-538	Relapse	F	Normal	WT	WT	Int I
AML-573	Relapse	F	NA	NA	ITD	Int I
AML-579	Relapse	M	Normal	Mut	ITD	Int I

SCT, stem cell transplantation; *NPM1*, nucleophosmin-1; WT, wild type; Mut, mutated; *FLT3*, Fms-related tyrosine kinase 3; ITD, internal tandem duplication; ELN, European LeukemiaNet classification system; Int I, intermediate I; Adv, adverse; F, female; M, male; NA, not available; ND, not determined.

2.1.9 Genomic DNA

The following human gDNA was used as control samples for MLPA analysis: female G1521 (Promega, Madison, WI, USA), female D1234999-G02, and male D1234999-G01 (Biochain, Newark, CA, USA).

2.1.10 Patient samples

The analysis was based on samples from AML patients from the AMLCG-99 trial (NCT00266136), AMLCG-2008 trial (NCT01382147), and the Department of Medicine III, University Hospital, LMU. The institutional review boards of the participating centers

approved the studies and informed consent for scientific use of sample material was received from all study participants in accordance with the Declaration of Helsinki. Diagnostic and relapse samples had at least 50% blasts by morphology.

2.1.11 Laboratory equipment and consumables

Table 10 List of used equipment.

Device	Supplier
ABI Prism 3500 XL Genetic Analyzer	Applied Biosystems (Foster City, CA, USA)
Amaxa Nucleofactor II device	Lonza (Basel, CH)
Analytical balance ABJ 220-4NM	Kern & Sohn (Balingen-Frommern, Germany)
BioPhotometer®	Eppendorf (Hamburg, Germany)
Bio-Rad Mini Protean Tetra system	Biorad (Hercules, CA, USA)
Centrifuge 5415D, 5424R	Eppendorf (Hamburg, Germany)
Centri-Sep™ Spin Columns	Thermo Fisher Scientific (Waltham, MA, USA)
CO ₂ incubator C 170	BINDER (Tuttlingen, Germany)
E-BOX VX2	Vilber Lourmat (Eberhardzell, Germany)
FACSCanto™ II	BD Biosciences (Franklin Lakes, NJ, USA)
FACSVantage SE (sorting cells)	BD Biosciences (Franklin Lakes, NJ, USA)
Fluorescent microscope DMi8	Leica Microsystems (Wetzlar, Germany)
Freezer -20°C	Liebherr, (Biberach, Germany)
Freezer -80°C, TLE	Thermo Fisher Scientific (Waltham, MA, USA)
Freezing container Mr. Frosty™	Thermo Fisher Scientific (Waltham, MA, USA)
Fusion SL4 imaging system	Vilber Lourmat (Eberhardzell, Germany)
Heating block Thermomixer compact	Eppendorf (Hamburg, Germany)
Heraeus™ Multifuge™ X1R Centrifuge	Thermo Fisher Scientific (Waltham, MA, USA)
Ice machine FM-170AKE	Hoshizaki (Amsterdam, NL)
Illumina HiSeq 1500	Illumina (San Diego, CA, USA)
Incubator 9040-0013	Binder (Tuttlingen, Germany)
Light Cycler 480 II	Roche (Basel, CH)
Liquid Nitrogen Tank	Cryoson (Schöckrippen, Germany)
Magnetic stirrer MR3001	Heidolph (Schwabach, Germany)
Microplate reader GloMax® Discover	Promega (Madison, WI, USA)
Microscope ID03	Carl Zeiss (Oberkochen, Germany)
Mini Incubator	Labnet International (Edison, NJ, USA)
PCR cycler PeqSTAR 2xGradient	Peqlab (Wilmington, DE, USA)
pH meter inoLab® pH 7110	WTW (Weilheim, Germany)
Pipettes (0.25-2.00 µL, 2.0-20.0 µL, 20-200 µL, 200-1000 µL)	Gilson (Limburg, Germany)
Pipetus accu-jet pro®	Brand (Wertheim, Germany)
Precision scale PCB 2500-2	Kern & Sohn (Balingen-Frommern, Germany)
Q-POD® Remote Dispenser	Merck Millipore (Darmstadt, Germany)
RS-TR 5 Tube-roller	Phoenix instrument (Garbsen, Germany)
Spectrophotometer Nanodrop 1000	Thermo Fisher Scientific (Waltham, MA, USA)
Ultrapure water system Milli-Q™ Reference System	Merck Millipore (Darmstadt, Germany)
VARIOKLAV® Type 500	HP Medizintechnik (Oberschleißheim, Germany)
Vertical Autoclave VX-150	Systec (Linden, Germany)

Vi-CELL™ Cell Viability Analyzer XR	Beckman Coulter (Krefeld, Germany)
Vortexer	Cenco (Breda, NL)
Water Bath Type 1003	GFL (Burgwedel, Germany)
Xcell SureLock Mini Cell for SDS gel electrophoresis	Invitrogen (Darmstadt, Germany)

Table 11 List of used consumables.

Consumable	Product number	Supplier
5 mL Round Bottom Polystyrene Test Tube, Falcon®	352058	Thermo Fisher Scientific (Waltham, MA, USA)
5 mL Stripette® Serological Pipets	4487	Corning (Corning, NY, USA)
10 mL Stripette® Serological Pipets	4488	Corning (Corning, NY, USA)
25 mL Serological Pipets	760180	Greiner Bio One (Frickenhausen, Germany)
96-well Lightcycler plate	721982.202	Sarstedt (Nümbrecht, Germany)
96-well PCR plate	781400	Brand (Wertheim, Germany)
96-well Solid White PS Microplate	07-200-628	Corning (Corning, NY, USA)
96-well V-bottom, Greiner	M9686	Sigma-Aldrich (St. Louis, MO, USA)
Amersham Protran Nitrocellulose membrane, 0.45 µM	10600012	GE Healthcare (Little Chalfont, UK)
Combitips advanced® 0.5 mL	0030089634	Eppendorf (Hamburg, Germany)
Combitips advanced® 1.0 mL	0030089642	Eppendorf (Hamburg, Germany)
Combitips advanced® 5.0 mL	0030089669	Eppendorf (Hamburg, Germany)
Diamond Tower Pack D10	F167101	Gilson (Middleton, WI, USA)
Diamond Tower Pack D200	F167103	Gilson (Middleton, WI, USA)
Diamond Tower Pack D1000	F167104	Gilson (Middleton, WI, USA)
Disposable bags	759710	Brand (Wertheim, Germany)
DURAN® GL 45 Lab Bottles (10 mL, 250 mL, 500 mL, 1000 mL)	21801	DURAN Group (Mainz, Germany)
DURAN® Erlenmeyer flasks (25 mL, 50 mL, 250 mL, 500 mL, 1000 mL)	21216	DURAN Group (Mainz, Germany)
Sorenson low binding standard tips	Z719595	Sigma-Aldrich (St. Louis, MO, USA)
Gel-loading pipet tips	CSL4853	Sigma-Aldrich (St. Louis, MO, USA)
Micro tube 1.5 mL SafeSeal	72.706.400	Sarstedt (Nümbrecht, Germany)
Micro tube 2.0 mL SafeSeal	72.695.400	Sarstedt (Nümbrecht, Germany)
Mr. Frosty™ Freezing Container	5100-0001	Thermo Fisher Scientific (Waltham, MA, USA)
Novex Empty Gel Cassette, mini, 1.0 mm	NC2010	Thermo Fisher Scientific (Waltham, MA, USA)
Nunc™ Cryo Tube Vial	375418	Thermo Fisher Scientific (Waltham, MA, USA)
PARAFILM® M	P7793	Sigma-Aldrich (St. Louis, MO, USA)
PCR tubes 0.2 mL	710988	Biozym Scientific (Oldendorf, Germany)
Petri dish 10cm	82.1135.500	Sarstedt (Nümbrecht, Germany)
QIAshredder	79656	Qiagen (Hilden, Germany)
Sealing Tape, optically clear	95.1994	Sarstedt (Nümbrecht, Germany)
TC Dish 100 standard	83.3902	Sarstedt (Nümbrecht, Germany)
TC Flask T25, standard, Vent. Cap	83.3910.002	Sarstedt (Nümbrecht, Germany)

TC Flask T75, standard, Vent. Cap	83.3911.002	Sarstedt (Nümbrecht, Germany)
TC Flask T175, standard, Vent. Cap	83.3912.002	Sarstedt (Nümbrecht, Germany)
TC Flask T25, suspension, Vent. Cap	83.3910.502	Sarstedt (Nümbrecht, Germany)
TC Flask T75, suspension, Vent. Cap	83.3911.502	Sarstedt (Nümbrecht, Germany)
TC Flask T175, suspension, Vent. Cap	83.3912.502	Sarstedt (Nümbrecht, Germany)
TC Plate 6-well, standard	83.3920	Sarstedt (Nümbrecht, Germany)
TC Plate 12-well, standard	83.3921	Sarstedt (Nümbrecht, Germany)
TC Plate 24-well, standard	83.3922	Sarstedt (Nümbrecht, Germany)
TC Plate 48-well, standard	83.3923	Sarstedt (Nümbrecht, Germany)
TC Plate 96-well, standard	83.3924	Sarstedt (Nümbrecht, Germany)
TC Plate 6-well, suspension	83.3920.500	Sarstedt (Nümbrecht, Germany)
TC Plate 12-well, suspension	83.3921.500	Sarstedt (Nümbrecht, Germany)
TC Plate 24-well, suspension	83.3922.500	Sarstedt (Nümbrecht, Germany)
TC Plate 48-well, suspension	83.3923.500	Sarstedt (Nümbrecht, Germany)
TC Plate 96-well, suspension	83.3924.500	Sarstedt (Nümbrecht, Germany)
Tube 15ml, 120x17mm, PP	62.554.502	Sarstedt (Nümbrecht, Germany)
Tube 50ml, 114x28mm, PP	62.547.254	Sarstedt (Nümbrecht, Germany)
Vasco® Nitrile Blue	9209825	B. Braun (Melsungen, Germany)

2.1.12 Software and Programs

Table 12 List of used software and programs.

Application	Software	Developer/Link
Agarose gel documentation	E-Capt 15.06	Vilber Lourmat (Eberhardzell, Germany)
Data visualization and statistical analysis	GraphPad Prism 6.07	GraphPad Software (La Jolla, CA, USA)
DNA cloning and vector map visualization	SnapGene 3.3.4	GSL Biotech LLC (Chicago, IL, USA)
Flow cytometry data analysis	FlowJo 10.1r5	FlowJo, LLC (Ashland, OR, USA)
Flow cytometry setup and data acquisition	FACSDiva™ 8.0.1	BD Biosciences (Franklin Lakes, NJ, USA)
Gel visualization and Western Blot analysis	ImageJ version 1.50d	ImageJ developers, www.imagej.net
Manuscript preparation and analysis	Microsoft Office 2010	Microsoft (Redmond, WA, USA)
Mapping	STAR version 2.5.2b	STAR ¹⁹⁸
MLPA analysis	CoffalyserNet v140721.1958	MRC Holland (Amsterdam, NL)
Molecular biology and NGS analysis	Geneious 8.1.7	Biomatters Ltd (Auckland, NZ)
Multiple usage	NCBI database	www.ncbi.nlm.nih.gov
Preparation of protein domain graphs	IBS 1.0	CUCKOO Workgroup ¹⁵⁷
Reference manager	Mendeley Toolbar 1.19.2	Mendeley Ltd., Elsevier
RNA-Seq analysis	R program	www.R-project.org
Western Blot analysis	FusionCapt Advance 16.11	Vilber Lourmat (Eberhardzell, Germany)

2.2 Methods

2.2.1 Molecular biology methods

2.2.1.1 Chemical Transformation of recombinant bacteria

An aliquot of 50 μL of recombinant DH5 α *E.coli* bacteria was thawed on ice. 25 μL of recombinant bacteria were then gently added to a chilled tube containing 1 μL of plasmid DNA, 14 μL water and 10 μL 5xKCM. After 20 min on ice followed by 10 min at RT, 250 μL LB media was added and cells were incubated at 37°C for 1h at 220rpm. 100-150 μL of bacteria suspension was then plated on a pre-warmed LB_{Ampicillin/Kanamycin} plate and incubated at 37°C over night. On the next day, single colonies were picked for further expansion and subsequent plasmid DNA extraction.

2.2.1.2 Preparation of plasmid DNA

To isolate plasmid DNA from bacteria, the alkaline lysis extraction method was applied. For extraction of small amounts of plasmid DNA, a single colony was picked and incubated in 2 mL LB_{Ampicillin/Kanamycin} media for 8 to 10h at 37°C and 220 rpm. Plasmid DNA was extracted with *QIAprep Spin Miniprep Kit* according to the manufacturer's instructions, dissolved in EB buffer and stored at -20°C. For extraction of large amounts of plasmid DNA, a single colony was picked and incubated in 2 mL LB_{Ampicillin/Kanamycin} media for 8h at 37°C and 220 rpm. Bacteria suspension was then added to 100-200mL LB_{Ampicillin/Kanamycin} media and incubated over night at 37°C and 220rpm. On the following day, plasmid DNA was extracted with *Endofree Plasmid Maxi Kit* according to the manufacturer's instructions and dissolved in 200 μL TE buffer or water over night at 4°C. Concentration and purity of plasmid DNA was determined with spectrophotometer Nanodrop 1000. Aliquots of plasmid DNA were stored at -20°C.

2.2.1.4 Restriction digestion

Before sequencing, plasmid DNA constructs were screened for correct vector and insert size as well as successful mutagenesis by digestion with restriction enzymes and subsequent electrophoretic DNA separation. Reaction mixture containing the following components was incubated for at least 3h at 37°C.

1 µg Plasmid DNA	x µL
Restriction enzyme [20 000 u/µL]	1 µL
Restriction buffer [10x]	2 µL
H ₂ O	x µL
<hr/>	<hr/>
total volume	20 µL

2.2.1.5 Electrophoretic DNA separation

To separate DNA fragments by size for visualization or purification/extraction, gel electrophoresis was used. Depending on the fragment size, 0.8 to 1.5% agarose gels were used. Agarose was dissolved in 1xTAE or 1xTBE buffer with SYBRTM Safe DNA gel stain (1:10 000) by heating the flask in a microwave oven using 40-50 sec intervals and gentle swirling between intervals until the agarose was completely dissolved. Solution was cooled down to 50-60°C before pouring the gel into a gel tray. After 20-30 min when the gel was completely solidified, the agarose gel was placed into the gel box, the comb was removed and the gel box was filled with 1xTAE or 1xTBE buffer. DNA samples with 1:6 Gel Loading Dye were loaded into wells of the gel together with a molecular weight ladder into the first or last lane of the gel. Gel was run at 80-120 V for 30-50 min and DNA fragments were visualized with UV light. SYBRTM Safe DNA gel stain interacts with the DNA backbone and can be seen under UV light.

2.2.1.6 DNA purification

During cloning, DNA fragments were either directly purified with *QIAquick PCR Purification Kit* according to the manufacturer's instructions. If more than one DNA fragment was detectable, the desired DNA fragment was sliced from the agarose gel, placed in a labeled microfuge tube and isolated using the *QIAquick Gel Extraction Kit* according to the manufacturer's instructions.

2.2.1.7 DNA cloning

Human full-length KDM6A with N-terminal HA Tag was amplified from pCMV-HA-UTX and cloned into the pcDNA6/V5-His A vector with the *In-Fusion[®] HD Cloning Plus Kit* according to the manufacturer's instructions.

Lentiviruses expressing *KDM6A*-targeting shRNA's or non-target control shRNA targeting Renilla or eGFP (Table 6) were generated in the laboratory of Irmela Jeremias (Helmholtz Zentrum München, Germany) by cloning into a modified pCDH-EF1 α -MCS-T2A-copGFP vector. To enhance the shRNA expression, the EF1 α promoter was replaced by the viral promoter SFFV. The dsRED-miR30 fragment was amplified from the TRMPVIR vector and cloned into the pCDH-SFFV-MCS-T2A-copGFP vector. The 22mer shRNA target sequences were synthesized as part of 110 bp ss-DNA oligos (Eurofins Scientific, Luxembourg), annealed and cloned into the vector using XhoI and EcoRI.

For generation of *KDM6A* knockout clones, *KDM6A* specific gRNA targeting the splice site at the intron 3 and exon 4 border of *KDM6A* was designed using Benchling software and cloned into pSpCas9(BB)-2A-GFP vector. *KDM6A* gRNA forward and reverse strand (100 μ M) were annealed in NEB4 buffer at 95°C for 5 min followed by a slow cool down to RT. Ligation of annealed gRNA was performed as follows:

pSpCas9(BB)-2A-GFP	250 ng
Annealed Oligo [1:100]	0.3 μ L
FastDigest BpiI	1 μ L
T4 Ligase HC [20 u/ μ L]	1.5 μ L
T4 Buffer [10x]	2 μ L
H ₂ O	x μ L
<hr/>	
total volume	20 μ L

Reactions were run with the following cycling settings: [37°C/5 min - 20°C/5 min] x 55 - 37°C/60 min - 65°C/10 min - 4°C/ ∞ . 1 μ L of FastDigest BpiI was added and reaction was incubated at 37°C for 1h. Recombinant DH5 α *E.coli* bacteria were then transformed with 1 μ L of ligation reaction mixture. Correct sequence was confirmed by Sanger sequencing.

2.2.1.8 Mutagenesis

KDM6A mutations H1146A, L1103R, V1113Sfs*38 and E1325X were generated using the *QuikChange II XL Site-Directed Mutagenesis Kit* according to the manufacturer's instructions. Briefly, 50 ng of pcDNA6 HA *KDM6A* plasmid was amplified with

oligonucleotides containing the desired mutation. Correct sequence was confirmed by Sanger sequencing.

2.2.1.9 Sequencing

2.2.1.9.1 Sanger sequencing

Sequencing of plasmid DNA or PCR products was performed by the service-company Sequiserve (Vaterstetten, Germany). Somatic mutation E1325X was verified by Sanger sequencing both DNA strands of PCR-amplified gDNA using 3500/3500xL Genetic Analyzer. First, PCR was performed with AML393_FOR and AML393-REV primer located in the exon 27 flanking introns. The 790-bp PCR product was then purified with *QIAquick PCR Purification Kit* followed by a second PCR and sequence analysis with AML393-Sanger_FOR and AML393-Sanger_REV primer yielding a 373bp PCR product. For the second PCR, reaction mixture (6 μ L PCR grade water, 2 μ L Big Dye Terminator v1.1, and 1 μ L 10 μ M AML393-Sanger_FOR or REV primer) was mixed with 1 μ L of purified PCR product (80 ng/ μ L) from the first PCR reaction. Samples were run on a thermo cycler with the following cycling settings: 95°C/1 min - 96°C/30s - 50°C/30s - 60°C/4 min - 4°C/ ∞ . Samples were purified with a Centri-Sep™ spin column and then Sanger sequenced using 3500/3500xL Genetic Analyzer.

2.2.1.9.2 Targeted sequencing

Targeted, multiplexed amplicon resequencing covering the entire open-reading frame of *KDM6A* and mutational hotspots/entire open-reading frame of genes known to be recurrently mutated in myeloid malignancies was performed as described previously⁵¹.

2.2.1.10 Extraction of genomic DNA

Genomic DNA (gDNA) of 5×10^6 cells was isolated with the *QIAamp DNA Blood Mini Kit* manually or using a Qiacube instrument (Qiagen GmbH).

2.2.1.11 Multiplex Ligation-dependent Probe Amplification (MLPA) analysis

To screen AML cell lines or PDX samples for *KDM6A* exon deletions, MLPA analysis was carried out using the SALSA MLPA P445 *KDM6A* probe mix according to the

manufacturer's recommendations. 50 ng of purified gDNA was used as starting material. After hybridization, ligation and amplification steps, products were run on an ABI Prism 3500 XL Genetic Analyzer. The ratio of each relative probe signal from cell lines compared to human control samples (G1521, D1234999-G02, and D1234999-G01) was calculated.

2.2.1.12 Numerical aberrations

To identify and validate numerical *KDM6A* aberrations in AML cell lines, CytoScan HD Array (Affymetrix, Santa Clara, CA, USA) hybridization analysis was performed at the Leibniz Institute DSMZ-German Collection of Microorganisms and Cell Cultures (Braunschweig, Germany). The gDNA was prepared using the *Genra Puregene Kit*. Labeling, hybridization and scanning were performed at the Genome Analytics Facility, Helmholtz Centre for Infection Research (Braunschweig, Germany), all according to the manufacturer's protocol (Affymetrix). Data were analyzed by H. Quentmeier at the Leibniz Institute DSMZ-German Collection of Microorganisms and Cell Cultures (Braunschweig, Germany) using the Chromosome Analysis Suite software version 2.0.1.2 (Affymetrix).

2.2.1.13 RNA isolation

Total RNA was isolated from $3\text{-}5 \times 10^6$ cells using the *RNeasy Mini Kit* together with the *RNase-Free DNase Kit* according to the manufacturer's instructions. For homogenization of samples, QIAshredder columns were used.

2.2.1.14 cDNA synthesis

cDNA was synthesized by reverse transcription (RT) with the *SuperScriptTM IV First-Strand Synthesis System*.

1 µg total RNA	x µL
10 mM dNTP Mix	1 µL
Oligo (dT) ₁₈ primer	1 µL
H ₂ O	x µL
<hr/>	
total volume	15 µL

Reaction mixture was incubated at 65°C for 5 min and the following reagents were added.

RevertAid™ Premium Enzyme Mix	1 µL
RT buffer [5x]	4 µL

For cDNA synthesis, reaction mixture was incubated for 30 min at 50°C followed by 5min at 85°C. cDNA was stored at -20°C.

2.2.1.15 Quantitative real-time PCR

qRT-PCR assays were performed with *QuantiTect SYBR Green PCR Kit* using 500 ng of cDNA and the appropriate primers. 9 µL of reaction mixture containing SYBR Green Mix and primers was transferred into wells of a 96-well plate and 1 µL of cDNA [500 ng/µL] was added.

QuantiTect SYBR Green PCR Master [2x]	5 µL
Primer FOR [10 µM]	0.3 µL
Primer REV [10 µM]	0.3 µL
H ₂ O	x µL
<hr/>	
total volume	10 µL

Reactions were run on a Light Cycler 480 II with the following cycling settings: 95°C/15 min - [94°C/15s - 57°C/30s - 72°C/30s] x 45 - 40°C/30s - 4°C/∞. Fold changes were calculated using the $\Delta\Delta C_t$ method and normalized against *GAPDH* expression.

2.2.1.16 RNA Sequencing

2.2.1.16.1 Library preparation and sequencing

To construct bulk libraries from the prior isolated mRNA, a protocol adapted from the SCRBS-seq method was used¹⁹⁹. 50 ng of mRNA was reverse transcribed using Maxima H Minus Reverse Transcriptase and tagged with sample-specific barcodes and unique molecular identifiers (UMIs). Only 2 µM of the E3V6NEXT was used. Samples were pooled and purified by SPRI beads, followed by an Exonuclease I treatment to digest unattached primers. Full-length cDNA was pre-amplified by single primer PCR for

10 cycles with the modification of using *KAPA Hifi 2x ready mix kit*. For the *Nextera XT DNA Library Preparation kit* 4 ng of cDNA was used as input and library preparation performed according to the manufacturer's protocol, with the only exception of using a custom i5 primer (P5NEXTPT5). Sequencing was performed on an Illumina HiSeq 1500 on a flow cell with single end layout utilizing the standard Illumina sequencing primers and index primers. Sample reads were sequenced using 50 cycles and the UMI sequence using 16 cycles.

2.2.1.16.2 Data Processing

To obtain expression data the raw fastq files were processed by the zUMIs pipeline using default parameters²⁰⁰. Mapping to the human reference genome hg38 was performed by STAR¹⁹⁸ (version 2.5.2b) and the gene annotation GRCh38.84 was taken from Ensembl. Differential expression analysis was performed using limma²⁰¹. For this analysis genes with a read count below 10 in all of the samples were filtered out and library sizes scaled using the package edgeR²⁰². Count data was transformed to log2-counts per million and the mean variance calculated to compute the precision weights. In order to increase statistical power empirical Bayes moderation was applied and the false discovery rate calculated by the Benjamini-Hochberg procedure.

2.2.2 Cell biology methods

2.2.2.1 Cell culture cultivation and handling

All cells were grown and maintained under conventional cell culture conditions at 37°C and 5% CO₂. Cells were cultured according to the supplier's recommendation (DSMZ, Braunschweig, Germany). Before use, medium and trypsin were warmed to 37°C in a water bath.

Suspension cells were cultured in RPMI-1640 medium supplemented with 20% (v/v) FBS and 0.5% (v/v) Penicillin/Streptomycin. For culturing MM-1 and MM-6 cells, medium was additionally supplemented with 1 mM sodium pyruvate and 1 x Non-essential amino acids. To passage suspension cells, the amount of viable cells was counted on Vi-CELL™ Cell Viability Analyzer XR with Trypan Blue exclusion every 2-3 days. Fresh medium

together with cell suspension in an appropriate ratio (e.g. 3:1; 4:1; or 5:1) was placed in a new flask.

HEK293T cells were cultured in DMEM medium supplemented with 10% (v/v) FBS and 0.5% (v/v) Penicillin/Streptomycin. To passage HEK293T cells that are grown to 80-90% confluence, cells were gently washed with PBS and incubated in trypsin-EDTA solution for 5 min at 37°C in the incubator. After detachment of cells, medium in a 1:4 ratio was added to inactivate trypsin and the cell suspension was transferred to a conical tube. Cells were centrifuged (1100 rpm, 5 min, RT), resuspended in fresh medium and placed in a TC flask.

PDX AML samples were established and recovered from mice as previously described⁵¹. PDX cells were enriched with the *mouse cell depletion kit* according to the supplier's recommendation. For *in vitro* cultivation, PDX cells were kept in DD medium according to a previously described recommendation²⁰³ for up to 7 days. DD medium contained StemPro-34 SFM media supplemented with 2% (v/v) FBS, 1% (v/v) Penicillin/Streptomycin, 1% (v/v) L-glutamine, 10 ng/mL of rhIL3, rhTPO, rhFLT3-ligand, and rhSCF.

2.2.2.2 Cell thawing and freezing

For storage purposes, 5×10^6 viable cells were centrifuged (1100 rpm, 5 min, RT) and the cell pellet was resuspended in 5 mL FBS containing 10% (v/v) DMSO. 1 mL aliquots of the cell suspension were each dispensed into cryogenic storage vials (Nunc™ Cryo Tube). Vials were placed in an isopropanol freezing container (Mr. Frosty™ Freezing Container) and stored at -80°C overnight. For long-term storage, frozen cells were transferred to a tank of liquid nitrogen.

To thaw cells, frozen cells stored at -80°C or in liquid nitrogen were quickly thawed in a water bath at 37°C and transferred to a conical tube containing 5 mL of respective media. After centrifugation (1100 rpm, 5 min, RT), the cell pellet was resuspended in 2-4 mL fresh medium (amount depending on the appropriate cell density for each cell line) and the cell suspension was placed in 2-4 wells of a 48-well plate. After 1-3 days, suspension cells were gradually expanded by transferring cells to bigger wells (24-well or 12-well plate). Adherent cells were resuspended in 10 mL fresh medium and transferred to a TC flask T75.

PDX AML cell were thawed according to the protocol of Dominique Bonnet²⁰⁴ to obtain high viability. Briefly, cells were rapidly thawed in a 37°C water bath and 100 µL of DNase I (1 mg/mL) was added drop wise into the cryogenic vial. Cell suspension was gently mixed, incubated for 1 min and transferred into a 50 mL conical centrifuge tube. 1 mL FBS was added drop wise and cell suspension was gently mixed. After 1 min, 10 mL PBS with (v/v) 2% FBS was slowly added and incubated for 1 min. Volume was then slowly added up to 30 mL with PBS containing 2% (v/v) FBS. Cells were centrifuged (1100 rpm, 5 min, 4°C) and resuspended in DD medium.

2.2.2.3 Mycoplasma testing

To test for mycoplasma contamination in cell cultures, the *MycoAlert*® *Mycoplasma Detection kit*, which detects the enzymatic activity of mycoplasma, was used according to the supplier's recommendation. An aliquot (0.2 - 0.5 mL) was taken from each cell line grown in culture and transferred to a micro tube 4-6 days after thawing and subsequently every 7 days or before the start of an experiment. After centrifugation (1500 rpm, 10 min, RT), 25 µL of supernatant was transferred to a white bottom 96-well plate and mixed with 25 µL of MycoAlert™ Reagent. The plate was incubated for 5 min at RT to lyse mycoplasma cells and luminescence was measured with a Microplate reader GloMax® Discover (read A). After the addition of 25 µL of MycoAlert™ Substrate, reaction was incubated for 10 min at RT in the dark. During this time, mycoplasma enzymes react with the MycoAlert™ Substrate and generate ATP, which is then transferred into a light signal via the luciferase enzyme. Luminescence was measured a second time (read B). The ratio of B/A indicates the absence (<0.9) or presence (>1.1) of mycoplasma contamination.

2.2.2.4 Transient transfection

HEK293T cells were transiently transfected using the calcium-phosphate precipitation method. To have a confluency of 80-90%, 7×10^6 HEK293T cells were seeded in a 10 cm dish. On the next day, medium was removed and 10 mL of fresh medium was slowly added. After 4-5 h, 13 µg endotoxin-free plasmid DNA diluted in 450 µL sterile H₂O was mixed with 50 µL of 2M CaCl₂. The resulting mixture was slowly added to 500 µL HBS buffer to form Ca₃(PO₄)₂ - DNA complexes. After incubation for 3 to 4 min, the solution was added drop wise to the cells. Cells were incubated in the incubator and medium was changed after 13-15h. Cells were lysed 48h after transfection. For siRNA mediating

silencing of KDM6A expression, Lipofectamine 3000 reagent was used to transiently transfect HEK293T cells using 50 or 100 nM siRNA/well according to the supplier's recommendation.

Suspension cells were transfected with 100 nM siRNA or 1-2 μ g endotoxin-free plasmid DNA using the *Nucleofector Kit V* on the Amaxa Nucleofector II device according to the supplier's recommendation. The following preprogrammed settings were used, K562: T-016; MM-1: T-030/T-036. For siRNA mediated silencing of KDM6A expression, K562 cells were nucleofected two times with siRNA against *KDM6A* or negative control siRNA. After 72h, cells were nucleofected for a second time and incubated again for 72h, after which cells were used for subsequent analysis.

2.2.2.5 Stable transfection with lentivirus

Production of lentiviral particles expressing shRNA's against KDM6A or non-target control (Table 6) was performed as previously described^{205,206}. For transduction, 1×10^6 K562 cells in 1mL medium were placed in a 24-well plate and lentiviral particles together with 8 μ g/mL polybrene were added. After 24h, cells were washed three times with PBS and resuspended in fresh medium. After a few days, transgene positive cells were enriched in two consecutive rounds with one week in between by flow cytometry with the red fluorochrome gate using FACSVantage SE. Knockdown efficiency was determined by immunoblotting with the appropriate antibodies (Table 4).

2.2.2.6 CRISPR/Cas9-mediated gene editing

For generation of KDM6A knockout clones, K562 or MM-1 cells were transfected with 1 μ g (MM-1) or 2 μ g (K562) pSpCas9(BB)-2A-GFP-gRNA-KDM6A plasmid by nucleofection. After 48h, GFP positive cells were enriched by single-cell sorting into 96-well plates (V-bottom) with the FACSVantage SE. Cells were cultured until colonies were readily visible (10 to 30 days). To screen for KDM6A KO clones, cell lysis, PCR on lysates, and restriction digest were performed as previously described with minor modifications²⁰⁷. Briefly, for gDNA isolation cells in 96-well plate were washed two times with PBS, resuspended in 50 μ L/well lysis buffer SC, frozen at -80°C for 30 min, incubated at 56°C for 3 h, and finally Proteinase K heat inactivated at 85°C for 30 min. 2.5 μ L/well of the resulting crude cell lysate were directly subjected to PCR (25 μ L/rxn, 0.1 μ L MyTaqTM DNA Polymerase) using external screening primers (KDM6A_KO_FOR

and KDM6A_KO_REV) and following cycling settings: 95°C/5 min - [95°C/30s - 60°C/30s - 72°C/30s] x 45 - 72°C/40s - 4°C/∞. KDM6A KO clones were identified by restriction-fragment length polymorphism (RFLP) analysis of PCR products using HpyF10VI. Enzyme recognition site is lost after successful CRISPR/Cas9 targeting. Clones were confirmed by immunoblotting and Sanger sequencing. Sequences were analyzed and aligned with Geneious 8.1.7 and Benchling software.

2.2.2.7 MG132 treatment

HEK293T cells were transiently transfected as described under 2.2.2.4 with pcDNA6-HA-KDM6A WT or mutant plasmids. After 42h, medium was carefully removed and cells were incubated for 6h with 10 mL of fresh medium containing 50 μM of the proteasomal inhibitor MG132. Cells were then lysed and analyzed by immunoblotting.

2.2.2.8 Proliferation assay and cell counting

For proliferation assays with chemotherapeutic agents, 0.5 mL medium containing DMSO as control or increasing concentrations of the respective drugs were added to wells of a 48-well plate. Cells were resuspended in medium at 4×10^5 cells/mL and 0.5 mL of cell suspension corresponding to 2×10^5 cells was each added to the wells. After incubation for 72h or 96h, viable cells were counted on a Vi-CELL™ Cell Viability Analyzer XR. To count viable cells, cells were resuspended and 0.5 mL was transferred to a counting vial. The vial was then placed inside the Vi-CELL™ Cell Viability Analyzer XR and the amount of viable cells was measured by Trypan Blue exclusion.

For long-term proliferation, 3 mL of 4×10^5 cells/mL were placed in a TC flask T25 and 3 mL of medium containing DMSO as control or a certain drug concentration was added. The amount of viable cells was counted in duplicates every second day for 14 days. On day 4 and 8, 1 mL of cell suspension was transferred to a new TC flask T25 and 5 mL medium containing DMSO as control or a certain drug concentration was added.

2.2.2.9 Competitive growth assay

Competitive growth analysis in the presence of AraC was performed with the mixed population of lentiviral transduced K562 cells (10 days after transduction, not enriched for positive cells), containing both transduced shRNA-DsRed2(+) cells and untransduced

shRNA-DsRed2(-) cells. The mixed culture of native and transgene K562 cells (2×10^5 cells/mL) were placed in a TC flask T25 and treated with 111 nM of AraC every three days or left untreated for a time period of 24 days. The percentage of transduced DsRed2(+) cells was determined every 3 days by flow cytometry analysis with the red fluorochrome gate using FACSVantage SE. For flow cytometry analysis, cells were washed twice with PBS and resuspended in 0.5 mL buffer containing PBS, 3% [v/v] FBS and 1 $\mu\text{g/mL}$ DAPI. DAPI was used to exclude non-viable cells.

2.2.2.10 In vivo therapy trial

Patient-derived xenograft (PDX) cells expressing firefly luciferase were established as previously described⁵¹ in the laboratory of Irmela Jeremias (Helmholtz Zentrum München, Germany). 5×10^5 AML-491 or AML-393 cells were injected i.v. into groups of NSG mice (NOD scid gamma, The Jackson Laboratory, Bar Harbour, ME, USA), and tumor growth was regularly monitored by bioluminescence imaging (BLI) as previously described⁵¹. At defined imaging signals, mice were treated with a combination of AraC (100 mg/kg, i.p., days 1-4 and 14-17) and DaunoXome (1 mg/kg, i.v., days 1, 4, 14, 17). 28 days after start of therapy, BLI was performed and increase in BLI signals relative to day 0 were calculated. All animal trials were performed in accordance with the current ethical standards of the official committee on animal experimentation (Regierung von Oberbayern, number 55.2-1-54-2531-95-2010).

2.2.3 Protein biochemistry methods

2.2.3.1 Preparation of cell lysates

To extract whole cellular proteins, adherent cells were scraped off the culture dish using a cell scraper and the cell suspension was transferred into a pre-cooled conical tube on ice. For suspension cells, cells were transferred into a pre-cooled conical tube on ice. Cells were washed two times with 0.5-1.0 mL ice-cold PBS (1100 rpm, 5 min, 4°C) and the cell pellet was resuspended in ice-cold lysis buffer WCL (400 μL buffer for 1×10^7 cells). Cell lysates were incubated for 30-60 min on ice followed by centrifugation (13000 rpm, 30 min, 4°C) to pellet the cell debris. The supernatant was then transferred into a cooled micro tube and was stored at -20°C in aliquots to avoid repetitive freezing and thawing cycles.

Nuclear proteins were extracted with the *Qproteome Nuclear Protein kit* or *EpiQuik Total Histone Extraction kit* according to the supplier's recommendation. Aliquots of nuclear protein lysates were stored at -80°C.

2.2.3.2 Determination of protein concentration by Bradford Protein Assay

Total protein concentration in cell lysates was measured colorimetrically in a spectrophotometer using the Bradford method²⁰⁸. The Coomassie[®] Brilliant Blue G-250 dye binds to basic and aromatic amino acids of a protein which causes the dye to change its absorption maximum from 465 nm to 595 nm under acidic conditions. The measured absorbance at 595 nm correlates with the protein concentration. Bio-Rad Protein Assay Dye reagent was diluted 1:5 in H₂O and 2 µL of cell lysate were mixed with 18 µL H₂O. 20 µL of diluted cell lysates were then mixed with 980 µL of diluted Bio-Rad Protein Assay Dye and incubated for 5 min at RT. Absorption at 595 nm was measured against a blank control sample containing Bio-Rad Protein Assay Dye with 20 µL H₂O. To determine the protein concentration, a serial dilution of 20 µL BSA solution (200, 400, 600, 800 and 1000 µg/mL) was used as protein concentration reference standard.

2.2.3.3 SDS-Polyacrylamide gel electrophoresis

SDS-polyacrylamide gel electrophoresis (SDA-PAGE) was used to separate denatured proteins based on their molecular weight. Depending on the molecular weight of the protein of interest, separating gels in the range of 8 to 15% were used. For separating low molecular weight proteins (e.g. histone H3), a higher acrylamide concentration of 15% was used. First, the separating gel was poured into a gel cassette, overlaid with H₂O, and allowed to polymerize for 30 min. The overlaid water was then removed and the acrylamide solution for a stacking gel was poured on top of the separating gel. A comb with 10, 12 or 15 combs was inserted. After polymerization, the gel was used or stored with wet tissue in the fridge up to several days.

Separating gel (e.g. 10%)

H ₂ O dest.	6.9 mL
30% acrylamide/bisacrylamide	4.0 mL
1.5 M Tris-HCl buffer (pH 8.8)	3.8 mL
10% SDS in H ₂ O dest.	0.15 mL
10% APS in H ₂ O dest.	0.15 mL
TEMED	0.009 mL

Stacking gel

H ₂ O dest.	3.4 mL
30% acrylamide/bisacrylamide	0.83 mL
1.5 M Tris-HCl buffer (pH 6.8)	0.63 mL
10% SDS in H ₂ O dest.	0.05 mL
10% APS in H ₂ O dest.	0.05 mL
TEMED	0.005 mL

Samples containing equal amount of proteins (e.g. 30 µg) from lysates were mixed with 4:1 Lämmli buffer (total volume: 12 or 16 µL) and samples were boiled for 5 min at 95°C. Samples were allowed to cool down and shortly centrifuged. Samples and a molecular weight protein ladder were loaded in wells. Gels were run in a Xcell SureLock Mini Cell with 1x Electrophoresis buffer at 40 mA (stacking gel) and 60-80 mA (separating gel).

2.2.3.4 Western Blot

Separated proteins were transferred to a nitrocellulose membrane using a wet electroblotting system (Biorad Mini Protean Tetra system) with transfer blotting solution at 100 mA and 4°C overnight. Immunoblot was blocked with 5% (w/v) nonfat dried milk or 5% BSA (w/v) in TBST for 60-90 min at RT and incubated with respective primary antibody solution (Table 4; diluted antibody in 5% (w/v) milk- or BSA-TBST) for 1 h at RT or overnight at 4°C. After washing 3 times for 10 min in TBST, immunoblot was incubated for 1 h at RT with respective secondary antibody (Table 4) diluted 1:10000 in 5% milk- or BSA-TBST. After washing 3 times for 10 min in TBST, proteins of interest were detected using enhanced chemoluminescence (ECL). Immunoblot was incubated with Pierce ECL solution for 5 min and proteins were visualized on Fusion SL imaging

system. Western blot signals were quantified using ImageJ and relative protein levels were normalized to loading control.

2.2.3.6 Statistical analysis

All results are expressed as the mean \pm SD of at least three independent experiments unless stated otherwise. The significance of differences was calculated by unpaired, two-tailed Student's *t*-test. *P* values at <0.05 were considered significant by Student's *t* test. Calculation of IC₅₀ values and Pearson's correlation were performed using GraphPad Prism software.

3 Results

3.1 Investigation of *KDM6A* during AML progression

The histone demethylase *KDM6A* is frequently targeted by somatic loss-of-function mutations in newly diagnosed cancer types^{145,183–188} including leukemia^{153,192–194}. In this work, the clonal evolution dynamics of *KDM6A* during progression of AML was addressed by investigating the VAF of *KDM6A* mutations and expression levels of *KDM6A* in diagnosed and relapsed AML.

3.1.1 Analysis of *KDM6A* mutations in AML patients at diagnosis

To get insight into the biological relevance of *KDM6A* mutations at diagnosis, we first analyzed their locations, type of mutations and VAFs in AML patients. Given the low frequency of *KDM6A* mutations in AML, *KDM6A* mutations were analyzed in patients from two AMLCG trials, AMLCG-99 (NCT00266136; $n=6$) and AMLCG-2008 (NCT01382147; $n=9/664$)²¹, and our CN-AML diagnosis-relapse cohort ($n=2/50$)⁴⁸. In addition, three *KDM6A* mutated patients (UPN-393, UPN-202, and UPN-432) were identified and analyzed in the Laboratory of Leukemia Diagnostics, University Hospital LMU Munich. Analysis of their locations showed that the majority of mutations are either located at or within the proximity of the tetratricopeptide repeat (TPR) or the JmjC domain (Figure 9a). 65% ($n=13/20$) of patients harbor either frameshift insertions/deletions or nonsense mutations suggesting a loss-of-function phenotype. As *KDM6A* escapes X chromosome inactivation in females and therefore has two active copies of *KDM6A*, VAF of *KDM6A* mutations is shown separately for both genders (Figure 9b). In the majority of patients ($n=12/20$), the mutation occurred only in a subpopulation of AML cells, with a VAF below 15% (Figure 9b).

3.1.2 Gain of *KDM6A* mutations in AML patients at relapse

In our recent study⁴⁸, we analyzed paired diagnosis and relapse samples of 50 CN-AML patients and found two patients with *KDM6A* mutations, L1103R and V1113Sfs*38. Cancer cells harboring these mutations were discovered to be subclonal at diagnosis (VAFs < 6%) but became the major clone at relapse (VAFs > 73%; Figure 10a).

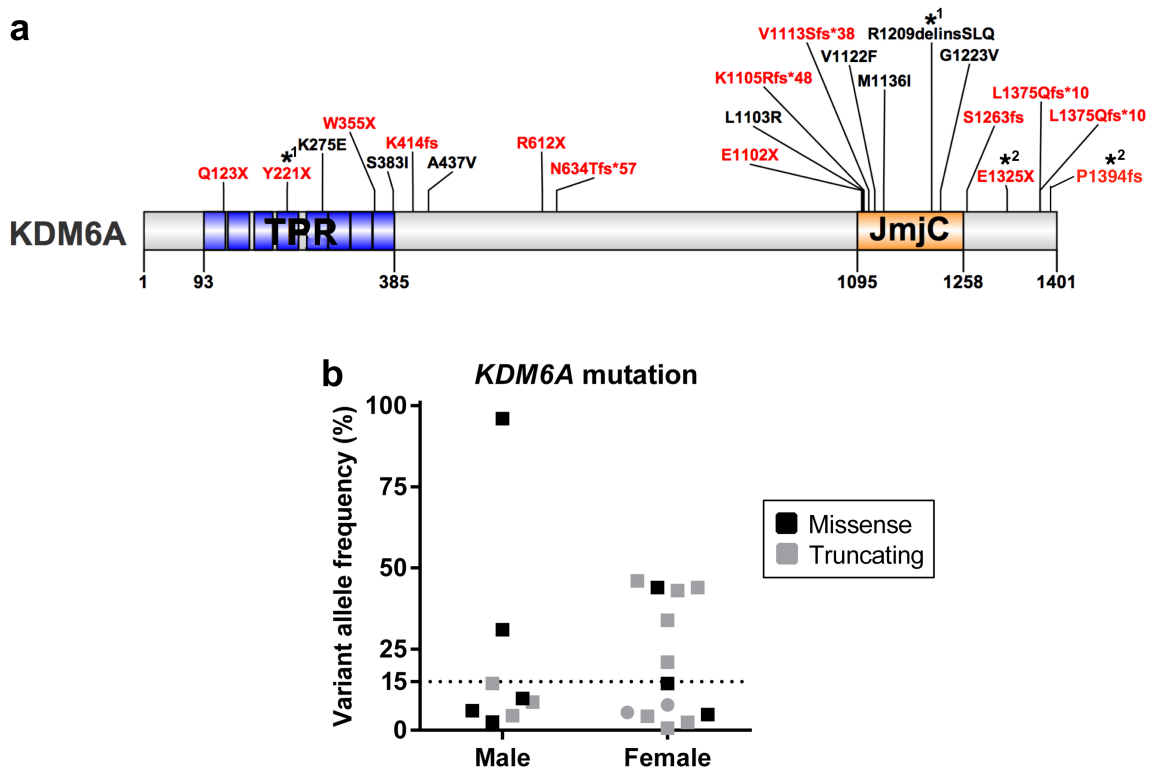


Figure 9 *KDM6A* mutations at diagnosis. **a**, Schematic overview of *KDM6A* protein structure (NP_066963.2) and mutations (red=truncating; black=missense) identified in patients with newly diagnosed AML, illustrated using IBS software¹⁵⁷. Location of mutations is displayed and amino-acid positions are indicated below the graph. Asterisk (*) signifies two patient harboring two mutations each. Presented *KDM6A* mutations are from AMLCG-99 trial, AMLCG-2008 trial, a CN-AML diagnosis-relapse cohort⁴⁸ and this work. TPR, tetratricopeptide repeat; JmjC, Jumonji C. **b**, Overview of variant allele frequency (VAF) of *KDM6A* mutations at diagnosis. The types of mutation including missense and truncating mutations are highlighted with their respective color. VAFs are shown separately for male and female patients and a VAF of 15% is pointed out by a dotted line.

The analyses of three additional AML patients harboring *KDM6A* mutations, for which a matched diagnosis and relapse samples was available, also revealed an increase in VAF of *KDM6A* mutations at relapse compared to diagnosis (Figure 10a, Supplementary Figure 1). Mutations N634Tfs*57 and L1375Qfs*10, which were already present as a major clone at diagnosis, were found to be further enriched at relapse. The mutant clone E1325X showed the most striking increase at relapse (68.2% VAF relative to blast count), as it was barely detectable at diagnosis (0.58% VAF). A second *KDM6A* mutation, P1394fs, was detectable in the same patient at diagnosis with a 12.8-fold greater VAF (8.1%) than E1325X (Supplementary Figure 1a). Intriguingly, the frameshift mutation, which is located at the very C-terminal end (1394/1401 AS), was lost at relapse.

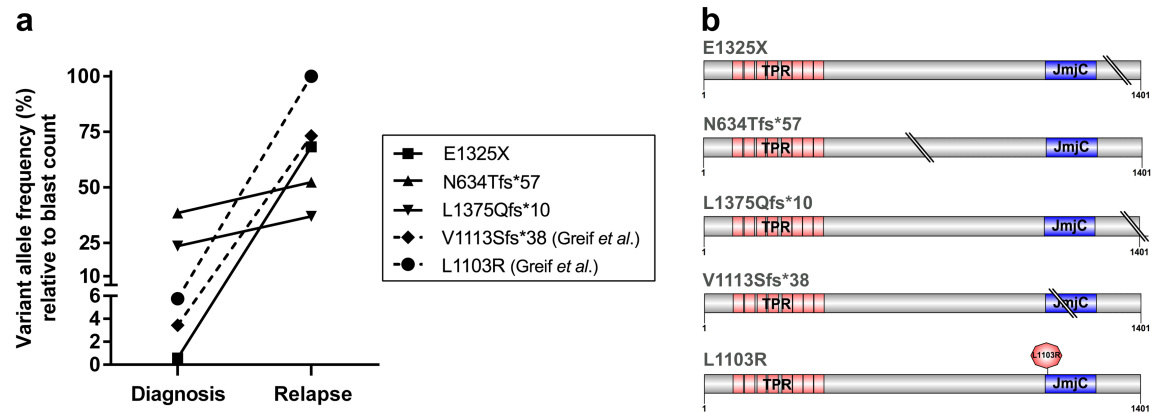


Figure 10 Gain of recurrent *KDM6A* mutations at relapse. **a**, Comparison of variant allele frequency (VAF) between diagnosis and relapse of 5 AML patients with *KDM6A* mutations. Due to variations in blast count, VAF was calculated relative to the respective blast count. Raw data for mutation L1130R and V1113Sfs*38 originate from our previous study⁴⁸. **b**, Schematic overview of *KDM6A* mutant structures illustrated with IBS software¹⁵⁷. The locations of premature stop codons originating from point or frameshift mutations are shown with two straight oblique lines. The position of point mutation L1103R is highlighted with a red dot. Amino acid positions are indicated below the graphs. TPR, tetratricopeptide repeat; JmjC, Jumonji C.

The majority of *KDM6A* mutations (4/5) are frameshift or stop mutation resulting in a premature stop codon and inactivation of *KDM6A* (Figure 10b).

Forms of induction therapy were according to standard German AML protocols, but varied between patients (Table 13). Whereas patient CN-017 and CN-025 received the TAD regimen (6-TG, AraC, and DNR), other three patients received induction therapy including sequential high dose AraC with mitoxantrone (S-HAM) alone, or in combination with AraC plus DNR followed by S-HAM. One chemotherapeutic agent, AraC, was part of the treatment schedule in all five patients. Comparison of time to relapse between patients showed early relapse in two patients (UPN-432 and CN-025) and a relatively late relapse in one patient, UPN-202 (Table 13). Of interest, early relapse patient CN-025 acquired chromosomal alterations during disease progression. The X chromosome not carrying the *KDM6A* mutation was lost at relapse⁴⁸.

Table 13 Patients characteristics.

UPN	Age at Diagnosis	Gender	<i>KDM6A</i> mutation	Karyotype at Diagnosis	Karyotype at Relapse	Time to Relapse	Induction Therapy
202	56	Female	L1375Qfs*10	Normal	Normal	2294	S-HAM
393	43	Female	E1325X	N/A	46,XX,ins(10;11)(p12;q23q23)[13]/46,XX[6]	1373	AD HAM
432	32	Female	N634Tfs*57	Normal	Normal	250	S-HAM
CN-017 ⁴⁸	80	Female	V1113Sfs*38	Normal	Normal	1203	TAD TAD
CN-025 ⁴⁸	66	Female	L1103R	Normal	N/A; -X, +8, +20	122	TAD

Time to relapse in days. A, AraC; D, DNR; H, high dose; M, Mitoxantrone; N/A, not available; S, sequential; T, 6-Thioguanine. Data for patients CN-017 and CN-025 originate from our previous study⁴⁸.

3.1.3 Proteasomal degradation of *KDM6A* mutants in HEK293T cells

Given the high frequency of truncating mutations (Figure 9a; $n=13/20$), mutant *KDM6A* is presumably inactivated by degradation mechanisms such as non-sense mediated mRNA decay or degradation by the proteasome. To investigate the stability of some of the recurrent *KDM6A* mutants at the protein level, HEK293T cells were transiently transfected with *KDM6A* WT and mutant expression constructs. Cells were then treated with the proteasomal inhibitor MG132 for 6h and protein expression was analyzed by immunoblotting with a HA antibody (*KDM6A* constructs have a N-terminal HA tag). Protein expression of the patient-related *KDM6A* mutants V1113Sfs*38, E1325X, and L1103R was significantly reduced compared to WT (Figure 11). MG132 mediated proteasomal inhibition resulted in a significantly elevated expression of these mutants and restored their expression in the range of WT levels. In contrast, WT and the demethylase-dead mutant H1146A did not change after treatment with MG132 (Figure 11). These results suggest that the three patient-related *KDM6A* mutants are rapidly degraded by the proteasome leading to reduced *KDM6A* protein levels and a loss-of-function phenotype.

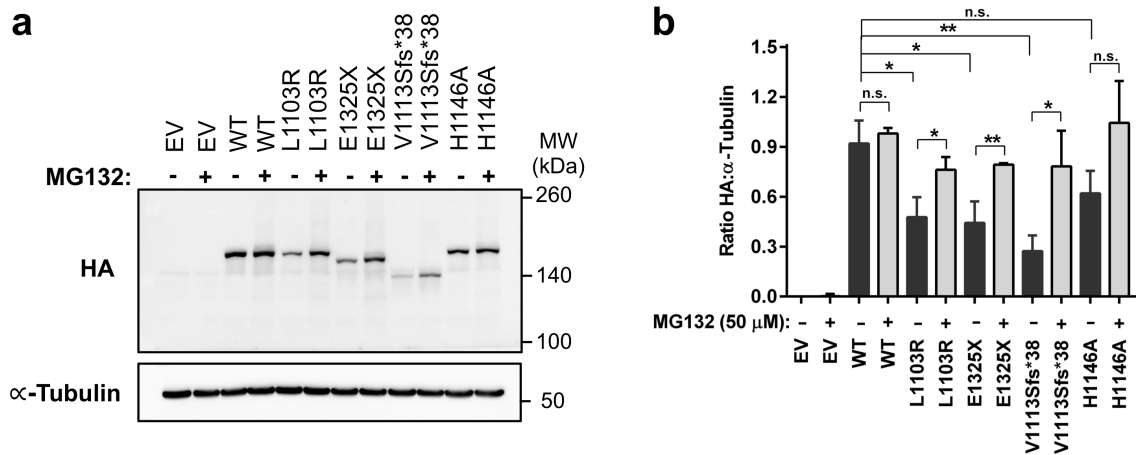


Figure 11 Recurrent KDM6A mutants are degraded by the proteasome. **a**, Immunoblot showing the effect of MG132 treatment (50 μ M, 6h) on HA tagged KDM6A protein expression in HEK293T cells transiently transfected with KDM6A WT or mutants (N-terminal HA tag). Immunoblots are representative of three independent experiments. EV, empty vector; WT, wild type; MW, molecular weight; α -Tubulin, loading control. **b**, The mean ratio of HA relative to α -tubulin expression \pm s.d. is given for three independent experiments. Unpaired, two-tailed Student's *t*-test; * P <0.05; ** P <0.01; n.s., not significant. EV, empty vector; WT, wild type.

3.1.4 *KDM6A* mutation independent protein expression at diagnosis and relapse

To investigate if *KDM6A* protein levels change during disease progression in AML samples without *KDM6A* mutations, matched diagnosis and relapse samples of 5 AML patients were analyzed. Compared to time point of diagnosis, three patients (#1, #2, #3) showed a strong decrease in *KDM6A* protein expression at relapse (Figure 12). On the contrary, *KDM6A* expression was increased at relapsed in two patients (#4, #5). Of note, the karyotype of these patients changed from normal to aberrant at relapse (Table 14). In addition, trisomy 21 was lost at relapse in patient #5 (Table 14). Heterogeneous expression levels are observed when comparing *KDM6A* protein levels at diagnosis or relapse between patients (Figure 12). All three male patients have similar low *KDM6A* protein levels than the two female patients. Overall, *KDM6A* expression, especially at relapse, appears to be heterogeneous between patients and strong changes during disease progression can be observed.

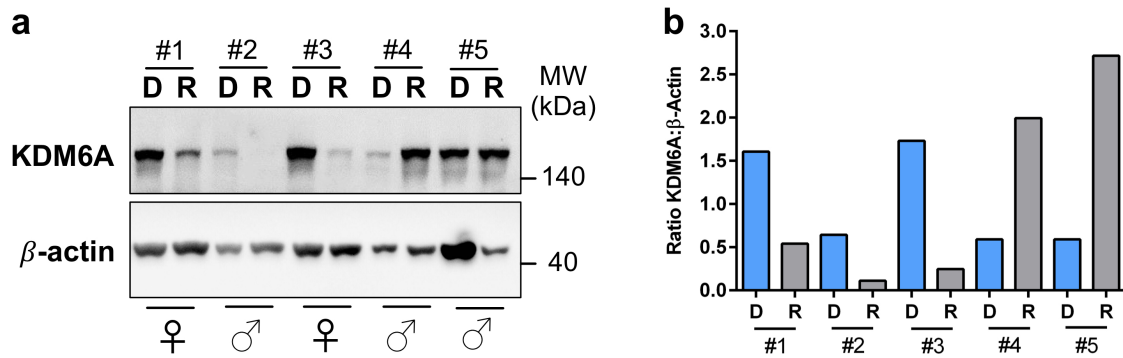


Figure 12 KDM6A protein expression patterns in diagnosed and relapsed AML. a, Immunoblotting for KDM6A expression in 5 AML patients at diagnosis (D) and relapse (R). Their respective gender is shown below. MW, molecular weight; β -actin, loading control. **b,** The ratio of KDM6A to β -actin expression is displayed.

Table 14 Patients characteristics of samples analyzed by immunoblotting.

UPN	Age at Diagnosis	Sex	Karyotype at Diagnosis	Karyotype at Relapse	Time to Relapse	Induction Therapy
#1	38	Female	47,XX,+8[15]/46,XX[2]	47,XX,+8[6]/47,sl,t(2;13)(p21;p11)[2]/47,sl,t(1;13)(p36;q?3),t(1;20)(q21;q13),t(1;8)(q21;q22),t(3;4)(q2?8;q3?4),t(3;5)(q1?;q3?5), t(5;9)(q31;p22),t(6;13)(q2?;q?3),t(9;15)(q3?4;q1?5)[cp8]/46,XX[2]	137	S-HAM
#2	76	Male	Normal	N/A	176	S-HAM
#3	57	Female	Normal	Normal	468	TAD9 HAM
#4	71	Male	Normal	46,XY,t(1;22)(p13;q11),der(5)t(5;19)(q12;q?),der(15)t(5;15)(q?q?),der(19)t(15;19)(q?q?)[5]/46,XY,t(11;13)(p1?;q1?)[3]/46,XY[1]	209	S-HAM
#5	44	Male	47,XY,+21[16]/46,XY[6]	46,XY,i(7)(q10),der(9)(p?),del(9)(p1?)[9]	860	TAD HAM

Time to relapse in days. A, AraC; D, DNR; H, high dose; M, Mitoxantrone; N/A, not available; S, sequential; T, 6-Thioguanine. TAD9, TAD for 9 days.

3.1.5 Status of KDM6A in PDX relapsed AML cells

A patient-derived xenograft (PDX) mouse model of AML was used to further investigate the mutational status and expression of KDM6A at relapse. PDX relapsed AML samples were established from primary patients' cells by the group of Irmela Jeremias at the Helmholtz Zentrum München (Table 9). PDX cells were shown to share close relationship to the patient sample and can be serially retransplanted to provide PDX cells for *in vitro* or *in vivo* experiments⁵¹.

First, KDM6A mRNA and protein levels were analyzed in 8 PDX relapsed AML samples. Heterogeneous expression patterns of KDM6A were observed for mRNA (Figure 13a) as well as protein expression (Figure 13b). PDX AML-393, -573, and -579 cells showed low mRNA levels, which correlated with protein expression. A correlation between mRNA and protein levels was observed for all samples except for AML-372.

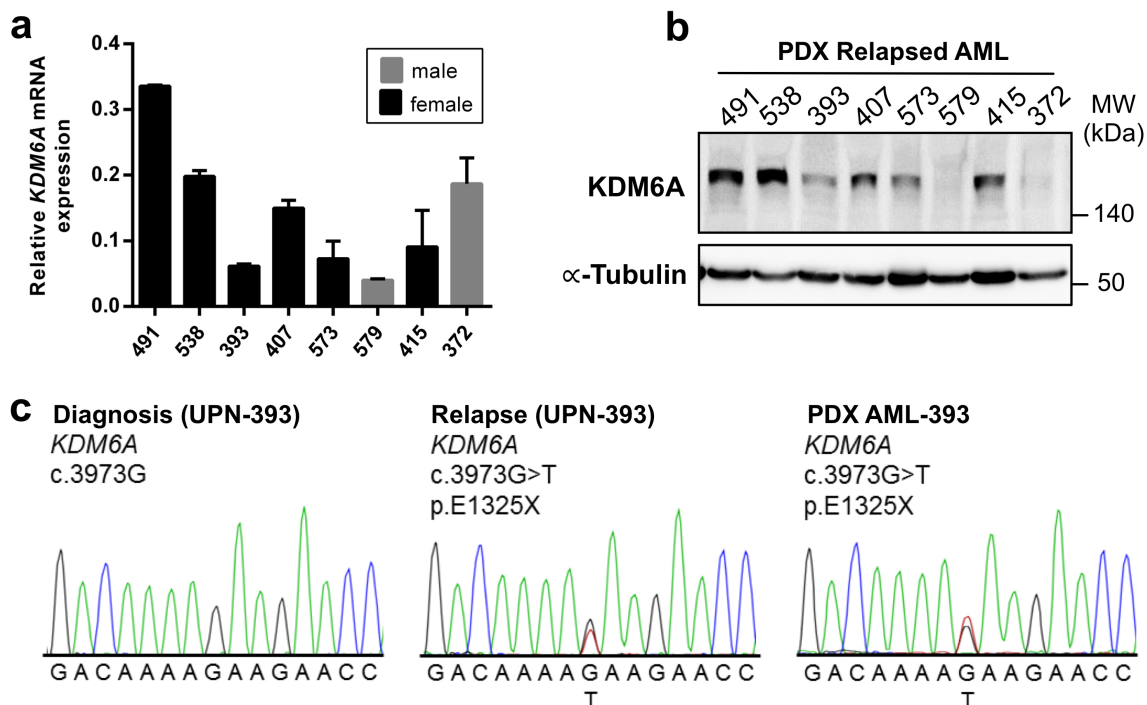


Figure 13 Heterogeneous KDM6A expression patterns in PDX cells of relapsed AML patients. **a,b,** KDM6A mRNA (**a**) and protein (**b**) expression was analyzed in eight PDX relapsed AML cells. KDM6A mRNA expression is shown relative to GAPDH expression. Male samples are highlighted as grey bar blots. For Western Blot, α -Tubulin was used as a loading control. **c,** DNA sequencing chromatogram showing a KDM6A mutation in the gDNA of female primary AML patient UPN-393 at relapse and in PDX AML-393 cells, established from the primary relapse sample. The mutation is not detectable in diagnosis material of the same patient by Sanger sequencing.

To investigate if *KDM6A* exon deletions or missense/truncating mutations are present, which might explain the reduced *KDM6A* expression observed in some of the PDX cells, multiplex ligation-dependent probe amplification (MLPA) and targeted sequencing was performed. MLPA analysis showed that none of the analyzed PDX AML cells harbor *KDM6A* exon deletions (Supplementary Figure 2). Targeted sequencing revealed a *KDM6A* stop mutation E1325X in PDX AML-393 cells. PDX AML-393 was established from primary cells of patient UPN-393 at relapse (mutation was already mentioned in chapter 3.1.2). The cancer cells harboring *KDM6A* mutation E1325X at relapse (UPN-393) regenerated to a stable population after transplantation into immunodeficient mice (PDX AML-393; Supplementary Figure 1a), which was verified by Sanger sequencing (Figure 13c). No additional *KDM6A* mutations were detected.

No molecular weight band corresponding to the premature stop mutation E1325X (estimated protein weight: 145 kDa) in the female PDX AML-393 cells was observed. To investigate if this mutant is undetectable due to rapid proteasomal degradation, PDX AML-393 cells were treated *in vitro* with the proteasomal inhibitor MG132 for 6h. No increase in overall *KDM6A* expression, but also no appearance of an additional band corresponding to E1325X was observed (Supplementary Figure 3). These results might point towards a nonsense-mediated mRNA decay.

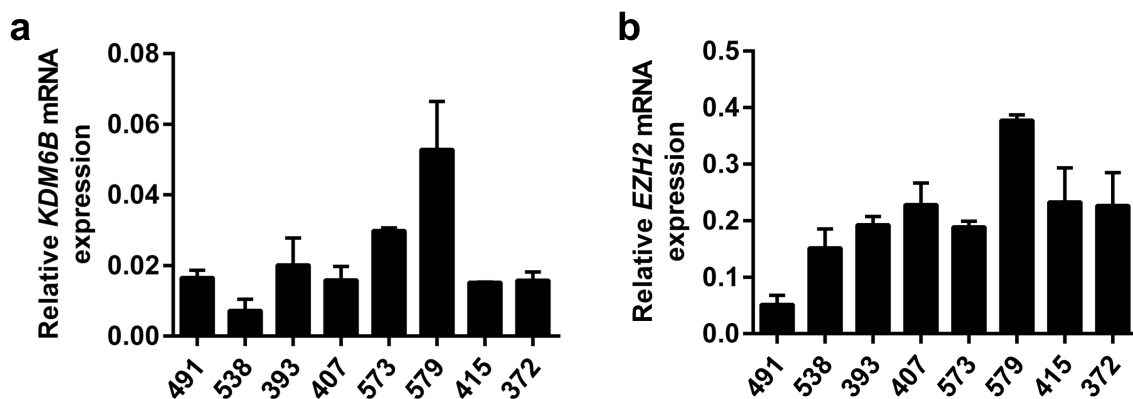


Figure 14 *KDM6B* and *EZH2* mRNA levels in PDX relapsed AML cells. **a,b**, qRT-PCR for *KDM6B* (**a**) and *EZH2* (**b**) in eight PDX relapsed AML samples. The mean \pm s.d. relative to the endogenous control *GAPDH* for three experiments is shown.

The histone demethylase KDM6B and the histone methyltransferase EZH2 remove or add, respectively, methyl groups at the same lysine residue as KDM6A and therefore might be able to compensate for KDM6A loss. *KDM6B* and *EZH2* mRNA levels were slightly increased in AML-579 cells, whereas AML-538 showed low *KDM6B* and AML-491 low *EZH2* mRNA levels (Figure 14). Concomitant loss of UTY, a catalytically inactive homolog of KDM6A that is encoded on the Y chromosome, was recently shown to be lost or reduced in conjunction with *KDM6A* mutations in pancreatic cancers with squamous differentiation in male patients¹⁹⁶. Analysis of the mRNA level of *UTY* in male PDX AML samples of which PDX AML-579 showed reduced KDM6A expression, revealed normal *UTY* levels (Figure 21).

Most patients with recurrent *KDM6A* mutations received the “3+7” or TAD regimen as induction therapy. Both schedules include the cytotoxic agents AraC and DNR suggesting that *KDM6A* mutant cells might be less sensitive to AraC and/or DNR treatment. To test this hypothesis, drug sensitivity of two PDX AML models of the same adverse ELN classification⁵¹ with i) *KDM6A* WT and strong expression (AML-491) and ii) *KDM6A* mutant and weak expression (AML-393) was investigated *in vivo*. Mice bearing AML-491 or AML-393 were treated with two cycles of AraC and DaunoXome (DNX; liposomal DNR) and tumor burden was analyzed before and after treatment. Treatment dramatically decreased the tumor burden in *KDM6A* WT AML-491 bearing mice compared to control ($P=0.0157$), whereas only a modest drop in tumor burden was observed in treated AML-393 bearing mice (Figure 15).

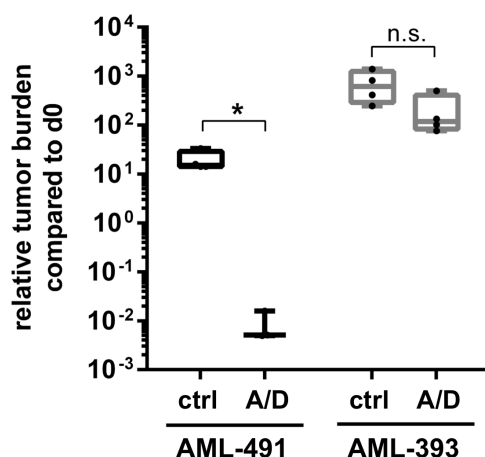


Figure 15 Decreased *in vivo* drug sensitivity in *KDM6A* mutant PDX AML-393 cells. Comparison of tumor load reduction under *in vivo* chemotherapy in AML-491 and AML-393 bearing animals. Tumor burden was quantified by bioluminescence before (d0) and after (d28) two cycles of treatment with AraC (days 1-4, 14-17) and DNX (days 1, 4, 14, and 17) (A/D) or control treated animals (ctrl). Relative tumor burden at day 28 compared to d0 was calculated. Unpaired, two-tailed Student's *t*-test; * $P=0.0157$; n.s., not significant.

3.2 KDM6A in AML cell lines

3.2.1 Mutation and expression analysis of KDM6A in AML cell lines

KDM6A exon deletion mutations have been observed in AML cell lines, MONO-MAC-6 (MM-6) and THP-1¹⁴⁵. To identify the frequency of *KDM6A* deletions in leukemia, MLPA analysis for the *KDM6A* gene in 40 myeloid leukemia cell lines (Table 8) was performed. Obtained peak ratios were then compared to two healthy donor control samples (male and female). MLPA analysis confirmed the reported exon deletions in MM-6 (exon 3-10) and THP-1 (exon 1-16) and revealed two additional AML cell lines, OCI-AML3 and HL-60, with in-frame deletions in exon 3-4 and 5-6, respectively (Figure 16).

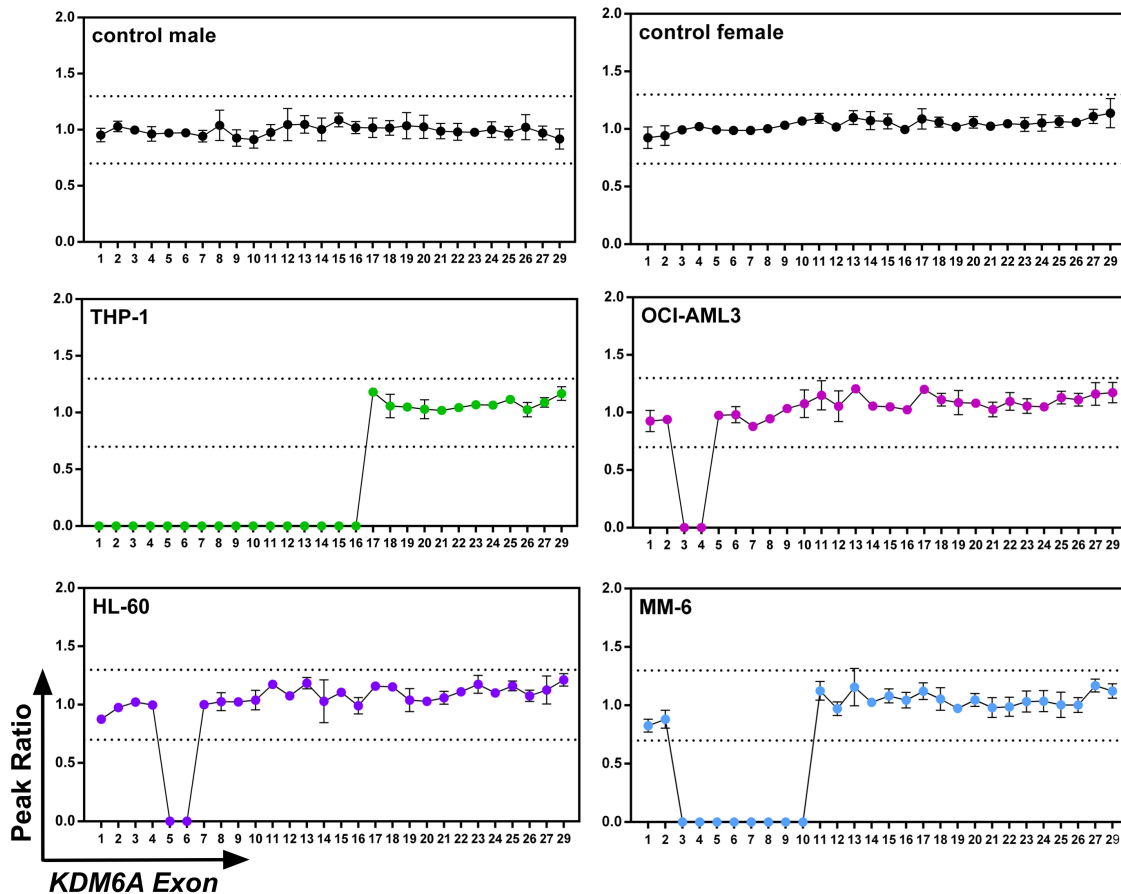


Figure 16 Identification of *KDM6A* exon deletions in AML cell lines. The peak ratio for each *KDM6A* exon specific probe, detected by quantitative MLPA analysis, is shown. Results for 4/40 of the investigated myeloid cell lines (summarized in Table 8) and two healthy donor control samples (male and female) are shown. The area of a normal peak ratio lies within the two dotted lines and ranges from 0.7 to 1.3. Mean \pm s.d. are given for at least two independent experiments.

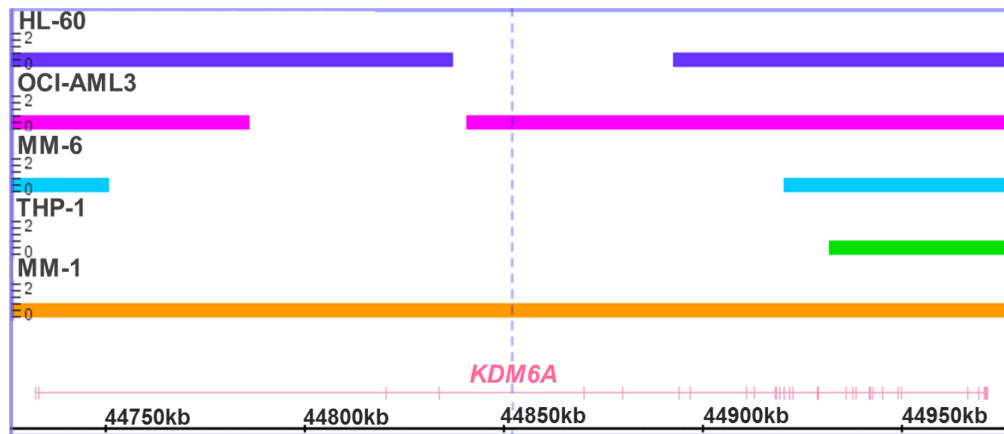


Figure 17 Identification of *KDM6A* aberrations in AML cell lines. AML cell lines HL60, OCI-AML3, MM-6, and THP-1 were analyzed by CytoScan HD Array hybridization analysis for *KDM6A* aberrations. MM-1 serves as a WT control. Bar thickness ranging from 0 to 2 indicates the copy number (CN) status. Haploidy (CN = 1) in cell lines from male patients is due to the X chromosomal localization of *KDM6A*. HL-60, the only cell line derived from a female patient, has lost one X chromosome.

These deletions were confirmed by independent CytoScan HD Array hybridization analysis at the Leibniz Institute DSMZ-German Collection of Microorganisms and Cell Cultures in Braunschweig (Figure 17). In addition, X chromosomal haploidy was detected in the female AML cell line HL-60 suggesting that HL-60 cells have lost the other X chromosome (Figure 17).

Exon deletions in MM-6 lead to a frameshift with two premature stop codons in exon 11, whereas in-frame deletions in THP-1 might result in a truncated protein of approximately 71 kDa (WT: 154 kDa). In-frame deletions in OCI-AML3 and HL-60 lead to a truncated protein of approximately 147 kDa. Although low to intermediate mRNA levels were detectable in the mutant cell lines, *KDM6A* protein expression was completely absent (Figure 18). The anti-*KDM6A* antibody used for *KDM6A* protein expression analysis, detects amino acids surrounding Ala490 of human *KDM6A* protein. Therefore, the antibody should be able to detect the truncating forms of *KDM6A* in OCI-AML3 and HL-60 if these are expressed.

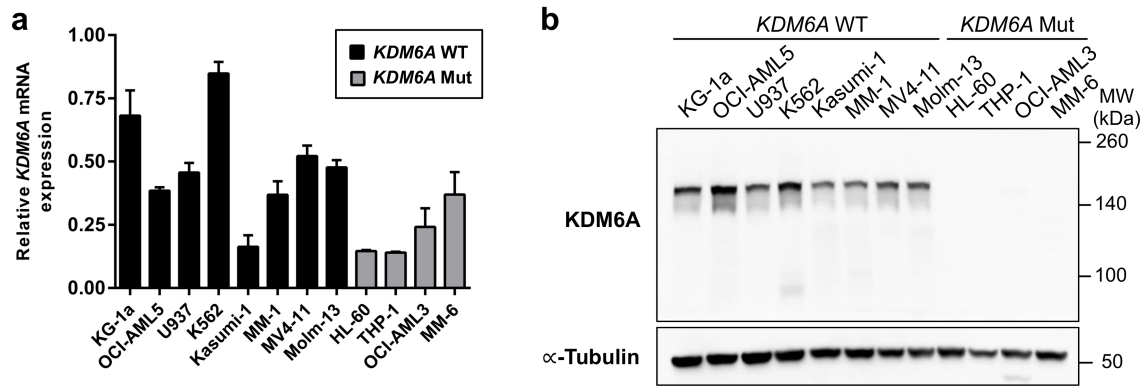


Figure 18 Loss of KDM6A protein expression in *KDM6A* mutant AML cell lines. **a,b**, qRT-PCR (**a**) and immunoblot analysis (**b**) for KDM6A in *KDM6A* WT and mutant human leukemia cell lines. **a**, The mean \pm s.d. relative to the endogenous control *GAPDH* for three experiments is shown. **b**, α -Tubulin was used as a loading control and blots are representative of three independent experiments. MW, molecular weight.

3.2.2 Global H3K27 methylation in *KDM6A* WT and mutant AML cell lines

To investigate the impact of KDM6A loss on global H3K27 mono-, di-, and tri-methylation, immunoblotting in *KDM6A* WT and mutant cell lines was performed. Mutant cells showed increased H3K27 tri-methylation, whereas H3K27 di- and mono-methylation levels were similar between WT and mutant cells (Figure 19a). Global H3K27me3 was inversely correlated with KDM6A levels ($r=-0.76$; $P=0.0042$; Figure 19b) indicating a KDM6A dependent epigenetically altered phenotype.

The sister cell lines MM-1 and MM-6 were established from the peripheral blood of a 64-year-old man with AML at relapse²⁰⁹. We found that MM-1 and MM-6 have an identical mutation profile (e.g. *FLT3* V592A, *KMT2A/MLLT3* fusion), but only MM-6 harbor *KDM6A* exon deletions, which result in a loss of KDM6A expression exclusively in MM-6 cells⁴⁸. In comparison to MM-1, *KDM6A* mutant MM-6 cells showed a trend for decreased H3K27 mono- or di-methylation and increased H3K27 tri-methylation⁴⁸.

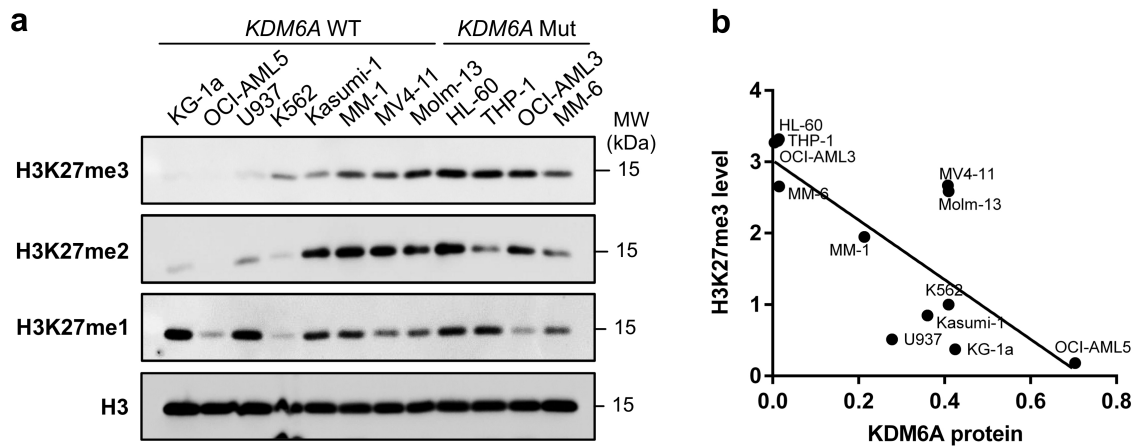


Figure 19 High H3K27 tri-methylation in *KDM6A* mutant cells. **a**, Immunoblotting for global H3K27 mono-, di- and tri-methylation levels in *KDM6A* WT and mutant human leukemia cell lines. Total H3 was used as a loading control. Blots are representative of three independent experiments. MW, molecular weight. **b**, Negative correlation between *KDM6A* protein expression and global H3K27me3 level in *KDM6A* WT and mutant human leukemia cell lines (Pearson's correlation; $r=-0.76$, $*P=0.0042$). Mean values of three independent analyzes are shown.

3.2.3 Analysis of H3K27 modifiers in AML cell lines

In addition, the H3K27 demethylase *KDM6B* or methyltransferase *EZH2* can influence the global H3K27 methylation status and compensate for *KDM6A* loss. Therefore, the mRNA levels of *KDM6B* and *EZH2* were analyzed via qPCR. For both genes, mRNA levels were similar between mutant and WT cells (Figure 20). *EZH2* mRNA levels were especially low in KG-1a and U937 cells (Figure 20b). Both cell lines were found to have strong mono-methylation and low tri-methylation of H3K27 (Figure 19a).

Mutations in the *KDM6A* homolog *UTY* were recently reported to occur frequently in *KDM6A* mutated male hematopoietic cell lines and solid organ cancers¹⁹⁷. Analysis of *UTY* mRNA levels showed loss of *UTY* mRNA expression in two *KDM6A* mutant (OCI-AML3 and MM-6) and three *KDM6A* WT cell lines (Figure 21).

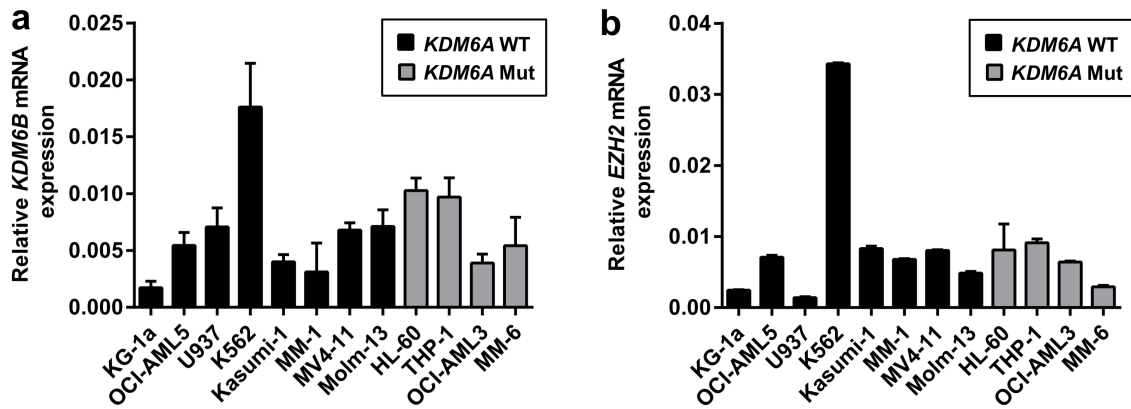


Figure 20 *KDM6B* and *EZH2* mRNA expression in *KDM6A* WT and mutant cell lines. a,b, qRT-PCR analysis for *KDM6B* (a) or *EZH2* (b) in *KDM6A* WT and mutant human leukemia cell lines. The mean \pm s.d. relative to *GAPDH* for three experiments is shown.

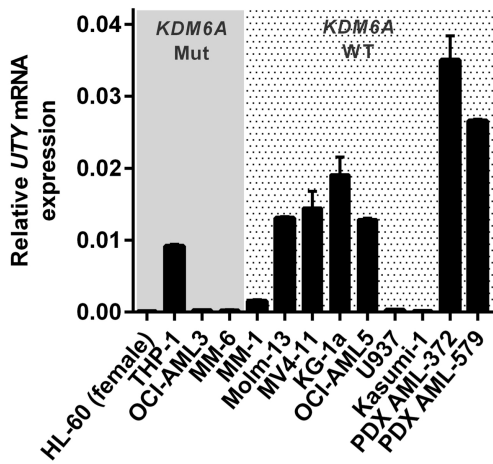


Figure 21 *UTY* mRNA expression in *KDM6A* mutant and WT cells. qRT-PCR for *UTY* in male *KDM6A* WT and mutant AML cell lines. The female cell line HL-60 was used as a negative control. In addition, two male PDX relapsed AML samples are shown. The mean \pm s.d. relative to *GAPDH* for three experiments is displayed.

3.3 Investigation of the role of KDM6A in chemotherapy resistance

Due to the observed inactivating mutations or mutation-independent, heterogeneous expression patterns of KDM6A in AML patients, the effect of reduced or depleted KDM6A expression regarding H3K27 tri-methylation, proliferation, and drug resistance was investigated. Therefore, stable *KDM6A* knockdown (KD) and knockout (KO) models were generated.

3.3.1 shRNA mediated knockdown of *KDM6A* in K562 cells

3.3.1.1 Generation of stable *KDM6A* knockdown cells

To generate stable KDM6A KD cells, the myeloid cell line K562 was transduced with lentivirus expressing different short hairpin RNA's (shRNA's) against *KDM6A*. As control, shRNA against Renilla (*shRenilla*) or GFP (*shGFP*), which are not expressed in the cell, were used. Of several tested shRNA's, *shKDM6A* #3, #4, and #7 decreased KDM6A protein expression by 70% (#3, #4) or 90% (#7; Figure 22a). Compared to K562

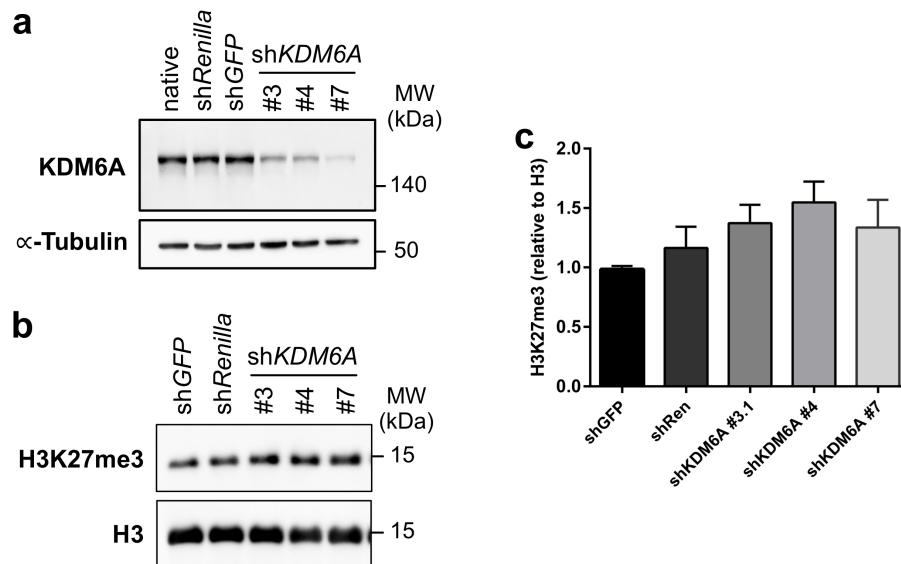


Figure 22 KDM6A expression and H3K27 tri-methylation in *KDM6A* KD K562 cells. **a**, Immunoblot showing knockdown (KD) of KDM6A protein expression in K562 cells lentiviral transduced with three different shRNA's against *KDM6A*. *shRenilla* and *shGFP* serve as controls. Blot is representative of three independent experiments. α -Tubulin, loading control. **b**, Immunoblotting for global H3K27 tri-methylation in *KDM6A* KD and ctrl K562 cells. Blot is representative of three independent experiments. H3, loading control; MW, molecular weight. **c**, The mean \pm s.d. of H3K27me3 levels relative to H3 for *KDM6A* ctrl and KD K562 cells are displayed ($n=3$).

native cells, KDM6A protein expression was not affected by *shRenilla* or *shGFP* (Figure 22a). Comparison of H3K27 tri-methylation levels between *KDM6A* KD and ctrl cells showed only a trend for higher tri-methylation in cells where KDM6A expression was downregulated (Figure 22b,c).

3.3.1.2 Effect of *KDM6A* knockdown on chemotherapy sensitivity

To investigate if reduced expression of KDM6A correlates with increased resistance towards chemotherapeutic agents commonly used in the induction therapy of AML, the half-inhibitory concentration (IC_{50}) of the respective drugs was determined in *KDM6A* KD or ctrl cells after 72h.

KDM6A KD cells displayed decreased sensitivity towards AraC treatment (Figure 23c) applying doses within the range of reported AraC plasma concentrations in patients²¹⁰ (Figure 23d). Only KD with the most potent *shKDM6A* #7 resulted in a significantly increased resistance to AraC (Figure 23c). However, the effect of *KDM6A* KD on response towards DNR or 6-TG was not as prominent or even absent: only KD cells *shKDM6A* #7 were slightly more resistant to DNR treatment (Figure 23b), and no change in IC_{50} values was observed after 6-TG treatment for all constructs (Figure 23a).

Since induction therapy typically involves continuous treatment of AML patients for seven (“7+3”) or 10 days (TAD regimen), *KDM6A* KD and ctrl cells were treated multiple times (day 0, 4, and 8) for a prolonged time course. For each drug, a concentration corresponding to their respective IC_{40} to IC_{50} values was chosen.

Prolonged treatment with 6-TG (1000 nM) showed no difference in the amount of viable cells between control and KD cells after 14 days (Figure 24a). Differences in growth under AraC (150 nM) treatment started at day 4, and resulted in a significant proliferative advantage for *KDM6A* KD cells compared to control (Figure 24b). Growth of both control groups was completely arrested under DNR (20 nM) treatment after day 8, whereas *KDM6A* KD cells were strongly proliferating (Figure 24c). *KDM6A* KD efficiency and proliferative advantage under DNR were positively correlated. In contrast, no differences in growth were observed without drug treatment (Figure 24d).

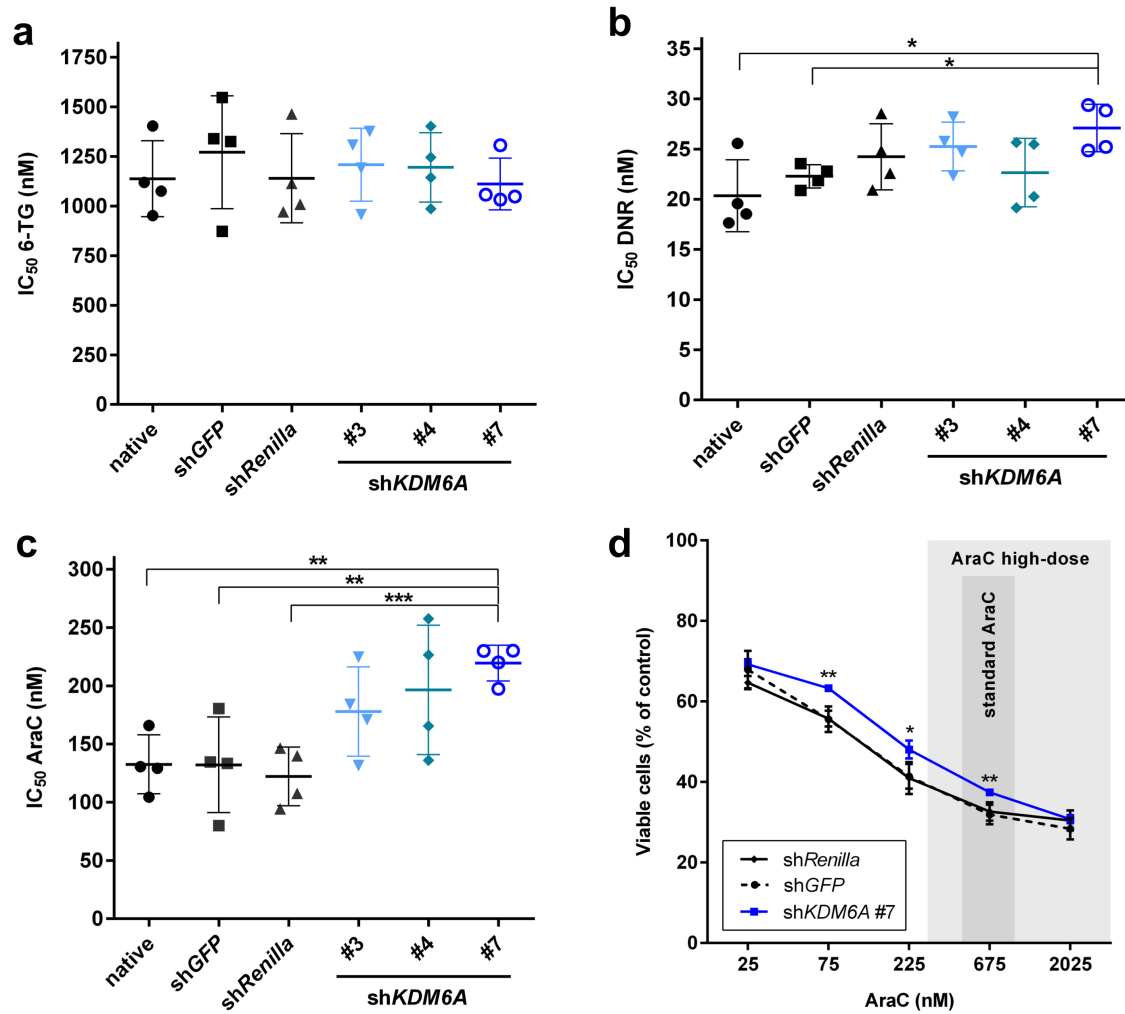


Figure 23 Knockdown of *KDM6A* confers decreased AraC resistance in K562 cells. **a,b,c**, Comparison of IC₅₀ values for 6-TG (**a**), DNR (**b**), and AraC (**c**) between control and *KDM6A* KD in K562 cells. Cells were treated for 72h with the respective drug. Mean of IC₅₀ values \pm s.d. are shown ($n=4$). Unpaired, two-tailed Student's *t*-test; * $P<0.05$; ** $P<0.01$; *** $P<0.001$. **d**, AraC dose-response analysis in K562 cells with modified *KDM6A* expression, shControl and sh*KDM6A* #7, after 72h. The mean \pm s.d. is given ($n=3$). The area shaded in dark grey and light grey indicates the range of steady-state plasma concentrations measured in patients during standard AraC (100-200mg/m²) and after high-dose AraC (3000mg/m²) treatment, respectively²¹⁰. Unpaired, two-tailed Student's *t*-test; * $P<0.05$; ** $P<0.01$.

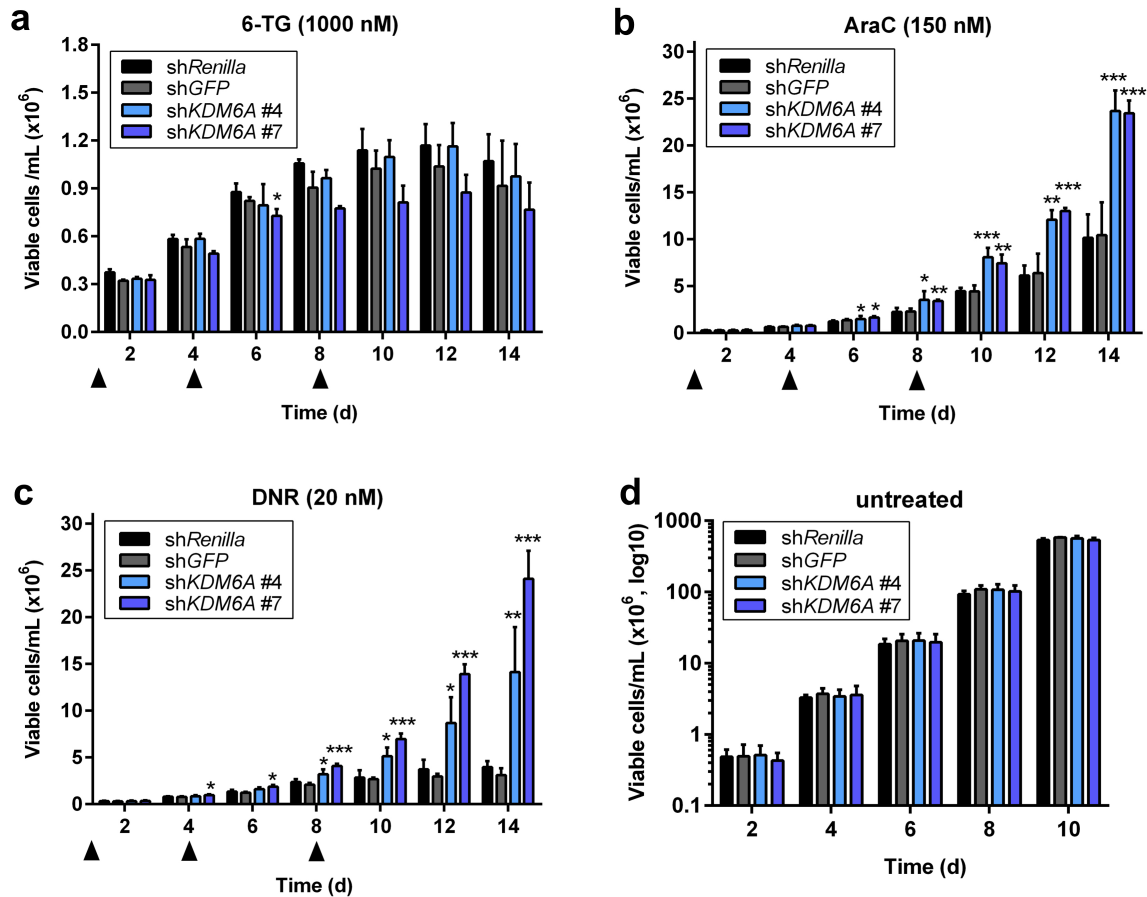


Figure 24 *KDM6A* KD confers a proliferative advantage during multiple treatments with AraC and DNR but not 6-TG. **a,b,c,d**, Long-term proliferation assay measuring the amount of viable K562 cells, shControl and sh*KDM6A*, every 2 days for 10 or 14 days. Cells were treated with 1000 nM 6-TG (**a**), 150 nM AraC (**b**), and 20 nM DNR (**c**) on day 0, 4 and 8 as indicated with the triangle or left untreated (**d**). Mean \pm s.d. are given for three independent experiments. Unpaired, two-tailed Student's *t*-test; * P <0.05; ** P <0.01; *** P <0.001.

3.3.1.3 Selective growth advantage of *KDM6A* KD cells

To further investigate if downregulation of *KDM6A* might lead to a growth advantage either under normal conditions or when treated with AraC, a competitive growth assay was performed. K562 cells were transduced with lentivirus expressing shRNA against Renilla (sh*Renilla*) or *KDM6A* (sh*KDM6A*) #3. The mixed population of lentiviral transduced K562 cells, which was not enriched for positive cells by FACS, contained both transduced shRNA-DsRed2(+) and native, shRNA-DsRed2(-) cells. The transduction efficiency ranged from 18% (sh*KDM6A* #3) to 32% (sh*Renilla*).

In the presence of AraC (111 nM) for 24 days, sh*KDM6A* #3 cells showed a significant growth advantage compared to native untransduced cells (Figure 25). In contrast, the amount of K562 cells transduced with sh*Renilla* did not change over the treatment period. In the absence of AraC, the percentage of sh*Renilla* or sh*KDM6A* #3 cells remained stable (Figure 25).

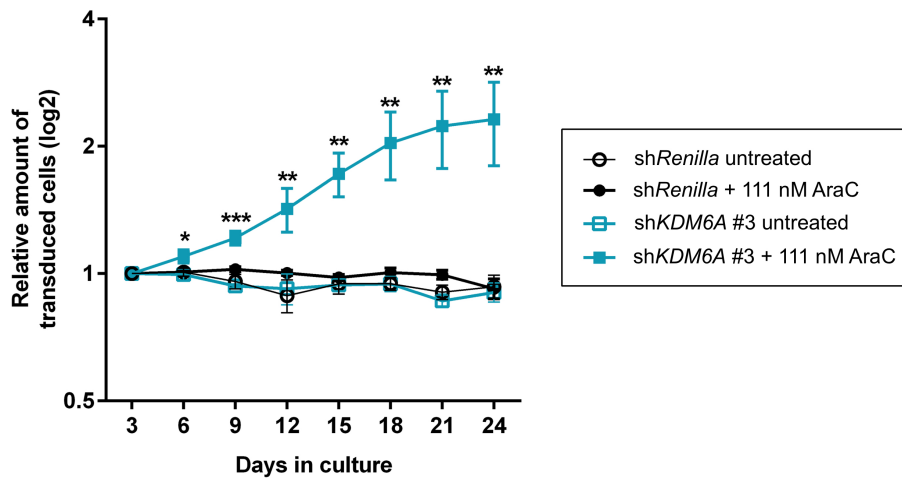


Figure 25 Knockdown of *KDM6A* in K562 cells leads to a competitive growth advantage in the presence of AraC. Mixed population of K562 native and lentiviral transduced cells, sh*Renilla* or sh*KDM6A* #3, were treated with 111 nM AraC (approximately IC₇₅ value) or left untreated. Cells were treated every three days for a time period of 24 days. The amount of transduced, DsRed2(+) cells relative to day 0 with a log₂ scale is shown. The mean values \pm s.d. of three independent experiments are displayed. Unpaired, two-tailed Student's *t*-test; * $P < 0.05$; ** $P < 0.01$; *** $P < 0.001$.

3.3.2 CRISPR/Cas9-mediated knockout of *KDM6A* in K562 cells

To confirm the results obtained by lentiviral mediated KD of *KDM6A* and compare the effect of KD vs. KO, CRISPR/Cas9-mediated genome editing was applied to knockout *KDM6A* in K562 cells.

3.3.2.1 Generation of *KDM6A* knockout single cell clones

K562 single cell *KDM6A* KO clones were generated by nucleofection with Cas9 and a *KDM6A* specific guide RNA (gRNA) targeting the intron 3 - exon 4 border of the *KDM6A* locus (Figure 26b). Single cell clones were screened and potential *KDM6A* KO clones were identified by restriction-fragment length polymorphism (RFLP) analysis of PCR

products using HpyF10VI (Figure 26a). Recognition site of HpyF10VI was completely lost in two single cell clones (Figure 26a) and Sanger sequencing confirmed successful CRISPR/Cas9 targeting in these clones (Figure 26b). Homozygous deletions of GCA (KO #1) or AGCA (KO #2) both generate a *KDM6A* frameshift mutation A112Vfs*12 and result in a complete loss of KDM6A protein expression (Figure 26c). Comparison of H3K27 tri-methylation levels between *KDM6A* WT and KO single cell clones showed only a trend for higher tri-methylation in cells with lost KDM6A protein expression (Figure 27).

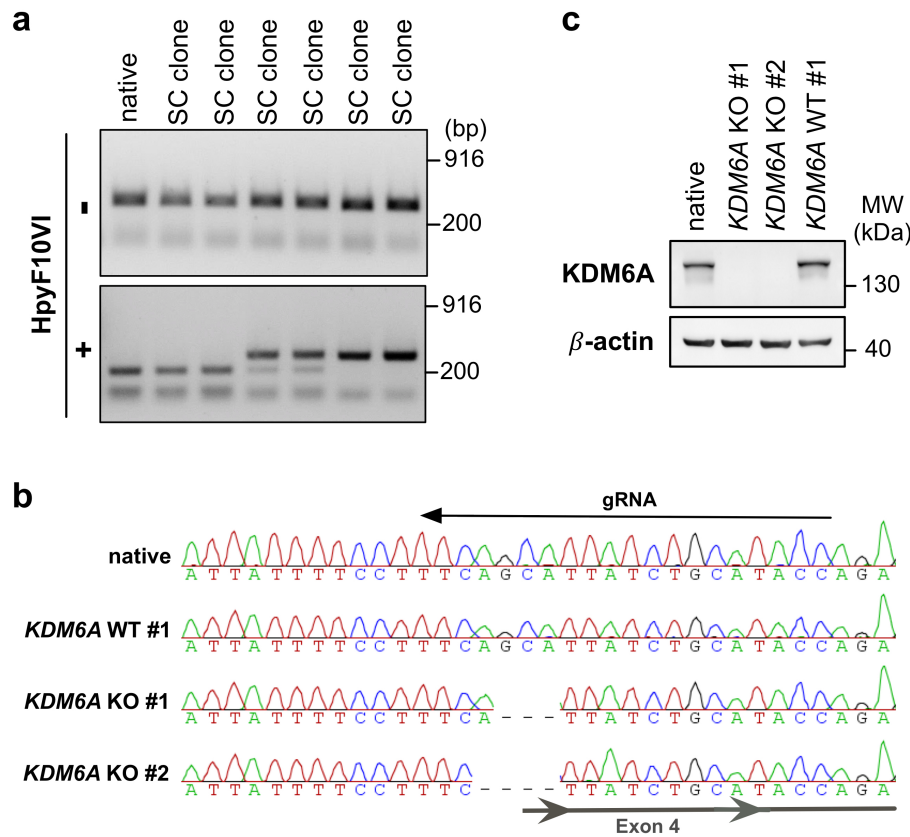


Figure 26 Generation of *KDM6A* KO K562 single cell clones. **a**, Screening PCR followed by restriction digest with HpyF10VI of generated single cell clones. Enzyme recognition site is lost after successful CRISPR/Cas9 targeting. SC, single cell. **b**, DNA sequencing chromatogram showing *KDM6A* frameshift mutations A112Vfs*12 in *KDM6A* KO K562 clone #1 and #2 compared with parental cells and a WT #1 clone. WT #1 clone was tested negative for *KDM6A* KO after CRISPR/Cas9 targeting. **c**, Immunoblot showing loss of KDM6A protein in *KDM6A* KO K562 single cell clones. Results of one representative experiment are shown ($n=3$). MW, molecular weight; β -actin, loading control.

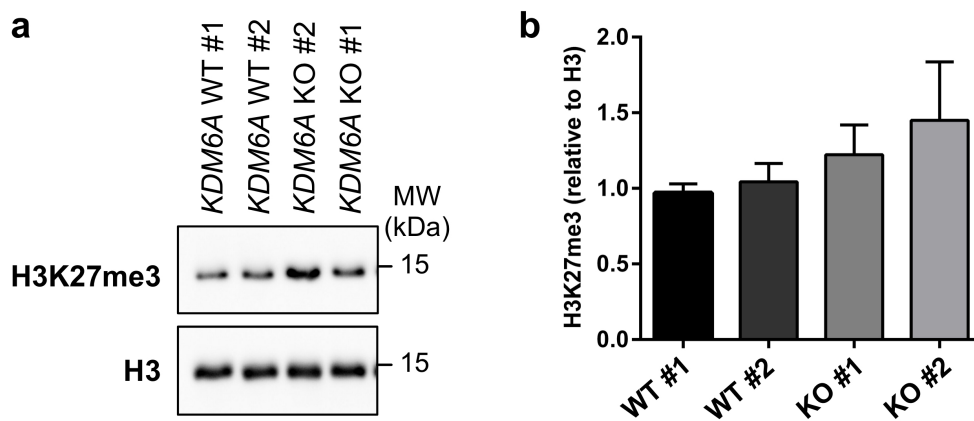


Figure 27 Analysis of H3K27 tri-methylation in *KDM6A* WT and KO cells. a, Immunoblotting for global H3K27 tri-methylation in *KDM6A* WT and KO K562 single cell clones. Blot is representative of three independent experiments. H3, loading control; MW, molecular weight. **b**, The mean \pm s.d. of H3K27me3 levels relative to H3 levels for *KDM6A* WT and KO K562 single cell clones are shown ($n=3$).

3.3.2.2 Effect of *KDM6A* loss in K562 cells on chemotherapy sensitivity

In order to investigate the effect of *KDM6A* loss on drug sensitivity, the established *KDM6A* KO single cell clones #1 and #2 were treated with AraC, DNR, and 6-TG for 72h. Their respective IC_{50} values were then compared to the IC_{50} values of a *KDM6A* WT single cell clone and K562 native cells.

After AraC treatment for 72h, IC_{50} values were significantly increased for both *KDM6A* KO clones compared to controls (Figure 28a). Some of the applied AraC doses were within the range of reported AraC plasma concentrations in patients²¹⁰ (Figure 28d).

A trend towards higher IC_{50} values or no difference between KO and control cells after DNR or 6-TG treatment, respectively, was seen (Figure 28b,c).

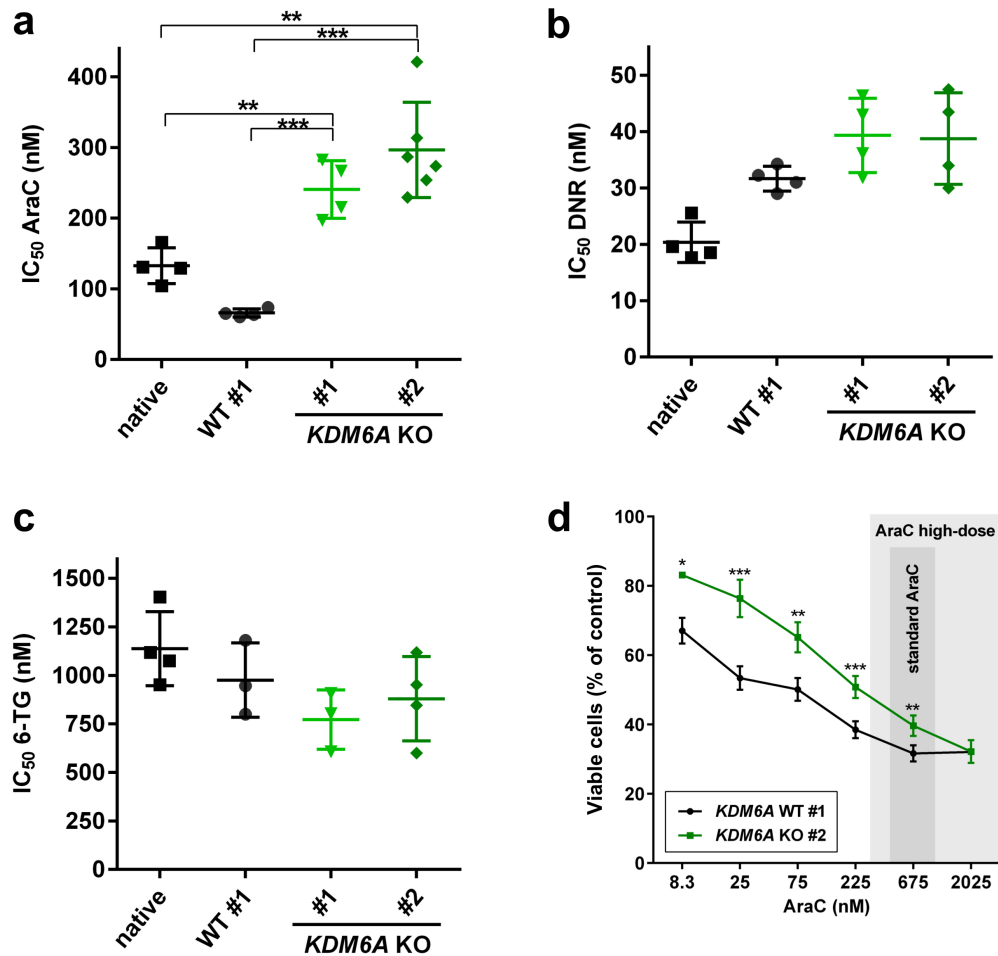


Figure 28 Loss of *KDM6A* results in decreased sensitivity towards AraC but not DNR and 6-TG treatment. **a,b,c** Comparison of IC₅₀ values for AraC (**a**), DNR (**b**) and 6-TG (**c**) between K562 control cells (native, WT #1) and *KDM6A* KO clones #1 and #2 (72h treatment). Mean of IC₅₀ values \pm s.d. ($n=3-4$) are shown. Unpaired, two-tailed Student's *t*-test; ** $P<0.01$; *** $P<0.001$. **d**, AraC dose-response analysis in K562 cells with modified *KDM6A* expression, *KDM6A* WT #1 and KO #2, after 72h. The mean \pm s.d. is given ($n=4$). The area shaded in dark grey and light grey indicates the range of steady-state plasma concentrations measured in patients during standard AraC (100-200mg/m²) and after high-dose AraC (3000mg/m²) treatment, respectively²¹⁰. Unpaired, two-tailed Student's *t*-test; * $P<0.05$; ** $P<0.01$; *** $P<0.001$.

3.3.3 CRISPR/Cas9-mediated knockout of *KDM6A* in MM-1 cells

The sister cell lines MM-1 and MM-6 have originally been established in culture from the same male AML patient at relapse²¹¹. Whereas MM-1 cells express *KDM6A*, MM-6 cells have lost *KDM6A* expression due to a *KDM6A* exon deletion mutation (Figure 30a), rendering them a good model to examine the implications of *KDM6A* loss within a similar genetic background. In our previous study⁴⁸, we observed that MM-6 cells are less

sensitive to AraC treatment than MM-1 cells. To study if KDM6A loss is responsible for this drug resistance phenotype, KDM6A expression was deleted in *KDM6A* WT MM-1 cells by CRISPR/Cas9 genome editing.

3.3.3.1 Generation of *KDM6A* KO MM-1 single cell clones

MM-1 single cell *KDM6A* KO clones were generated by nucleofection with Cas9 and a *KDM6A* specific guide RNA (gRNA) targeting the intron 3 - exon 4 border of the *KDM6A* locus (Figure 29). Due to poor transfection efficiency and low tolerance for single cell culture, only few single cell colonies were visible after a few weeks. Single cell clones were screened by immunoblotting for KDM6A expression. Compared to MM-1 parental and WT single cell clones, KDM6A protein expression was lost in a single clone (Figure 29b). Sanger sequencing revealed that the last 74 bp of Intron 3 and 29 bp of exon 4 were deleted in this clone resulting in a *KDM6A* frameshift mutation A112Vfs*3 (Figure 29a).

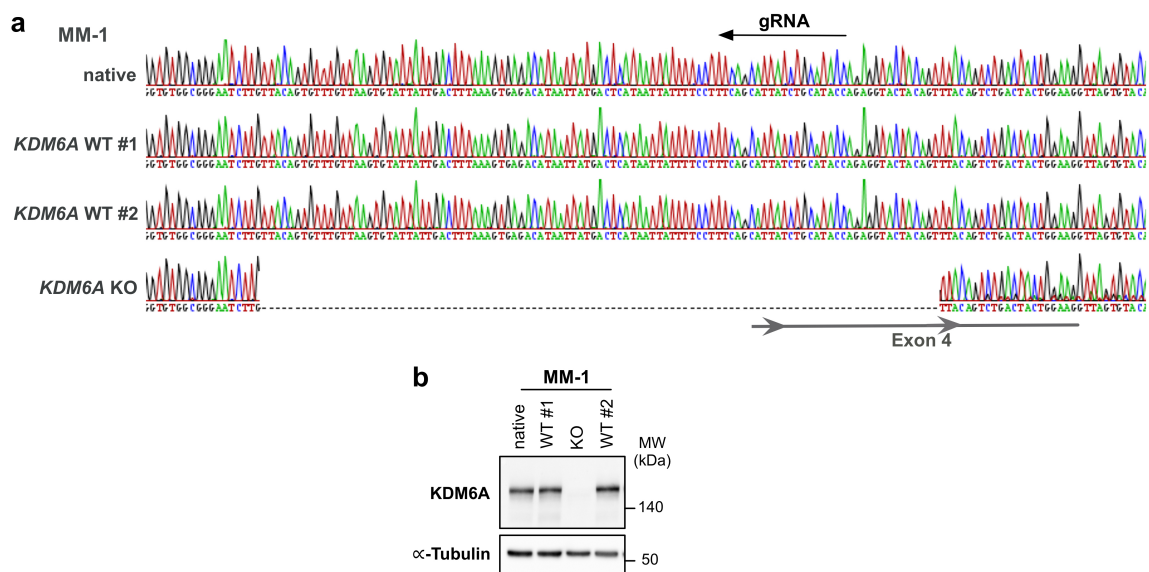


Figure 29 Generation of *KDM6A* KO and WT MM-1 single cell clones. **a**, DNA sequencing chromatogram showing *KDM6A* frameshift mutation A112Vfs*3 of a *KDM6A* KO MM-1 clone which is absent in native MM-1 cells and two *KDM6A* WT clones. WT #1 and #2 clones were tested negative for *KDM6A* KO after CRISPR/Cas9 targeting. **b**, Immunoblotting for KDM6A expression in *KDM6A* WT and KO cells. Results of one representative experiment are shown ($n=2$). MW, molecular weight; α -Tubulin, loading control.

3.3.3.2 Effect of *KDM6A* loss in MM-1 cells on chemotherapy sensitivity

In our previous study⁴⁸, we treated *KDM6A* WT MM-1 and *KDM6A* mutant MM-6 cells with AraC for 72h and found that MM-6 were 4.3-fold more resistant than MM-1. Comparison of the IC₅₀ values of AraC after treatment for 96h showed that loss of *KDM6A* expression in MM-1 significantly increased the IC₅₀ of AraC compared to both WT clones (3.4- to 8.8-fold increase; Figure 30b). *KDM6A* KO MM-1 cells were also significantly less sensitive to 6-TG and DNR treatment than *KDM6A* WT MM-1 cells (Figure 30c,d). Compared to native MM-1 cells, MM-6 showed a 2.5-fold increase in IC₅₀ of DNR (Figure 30c). A very similar resistance to DNR was observed in *KDM6A* KO

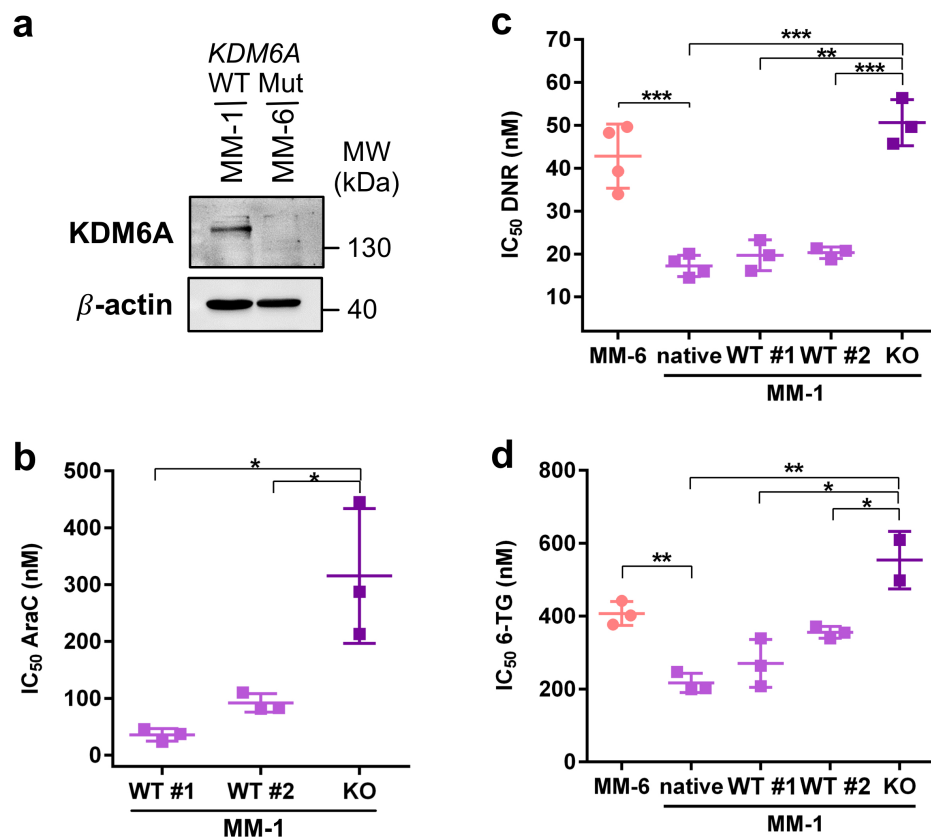


Figure 30 *KDM6A* loss in MM-1 recapitulates the drug phenotype of the *KDM6A* mutant sister cell line MM-6. **a**, Immunoblot showing loss of *KDM6A* protein expression in *KDM6A* mutant MM-6 cells. MW, molecular weight; β -actin, loading control. **b,c,d**, Comparison of IC₅₀ values for AraC (**b**), DNR (**c**), and 6-TG (**d**) between MM-6 and MM-1 cells including MM-1 native, two *KDM6A* WT and one *KDM6A* KO clone. Cells were treated for 96h with the respective drug. Mean \pm s.d are given for three independent experiments. Unpaired, two-tailed Student's *t*-test; **P*<0.05; ***P*<0.01; ****P*<0.001.

MM-1 cells: KO cells showed a 2.5- or 2.6-fold increase of IC₅₀ values for DNR compared to WT #1 or #2 cells. Treatment with 6-TG showed that *KDM6A* KO MM-1

cells were 1.6- to 2.1-fold more resistant than *KDM6A* WT MM-1 cells (Figure 30d). A 1.9-fold decrease in 6-TG sensitivity was observed in native MM-1 compared to MM-6 cells (Figure 30d).

3.4 Identification of *KDM6A* target genes with different KD/KO approaches

To identify genes involved in *KDM6A*-mediated drug resistance, genomewide RNA expression (RNA-Seq) analysis was performed in K562 cells treated with siRNA or shRNA against *KDM6A* under native conditions and after AraC treatment. Furthermore, differentially expressed genes in *KDM6A* KO K562 single cell clones were compared to *KDM6A* WT cells.

3.4.1 siRNA-mediated silencing of *KDM6A*

First, different si*KDM6As*' with various concentrations were tested in HEK293T cells to identify potent siRNAs against *KDM6A*. Of several tested, one was successful in strongly reducing *KDM6A* expression compared to control (si*SCR*) or native cells (Figure 31). Transient transfection of HEK293T cells with si*SCR* or si*KDM6A* showed stable reduction of *KDM6A* protein levels in si*KDM6A* treated cells for all investigated time points (Figure 31). To investigate which genes are differentially expressed in *KDM6A* KD cells, K562 cells were nucleofected with the respective siRNAs, si*SCR* or si*KDM6A*. To maximize the time of *KDM6A* silencing and thereby potentially the amount of differentially expressed genes, K562 cells were nucleofected two times (2 x 72h) and RNA was isolated on day 6. Transient *KDM6A* KD in K562 cells reduced *KDM6A* protein levels by $73.6 \pm 9.7\%$ compared to control ($n=6$; Figure 32a) and resulted in transcriptional downregulation of 39 genes and upregulation of 7 genes (Figure 32b).

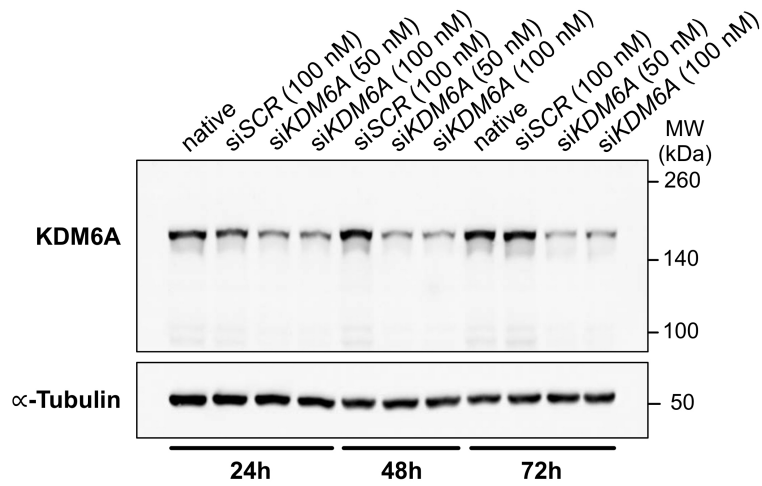


Figure 31 Time course of siRNA-mediated silencing of *KDM6A* in HEK293T cells. Immuno-blot showing reduction of KDM6A protein levels in HEK293T cells transfected with two different concentrations of siRNA targeting KDM6A (*siKDM6A*) for 24h, 48h and 72h. *siSCR* was used as a control showing the same KDM6A expression levels as native cells. MW, molecular weight; α -Tubulin, loading control.

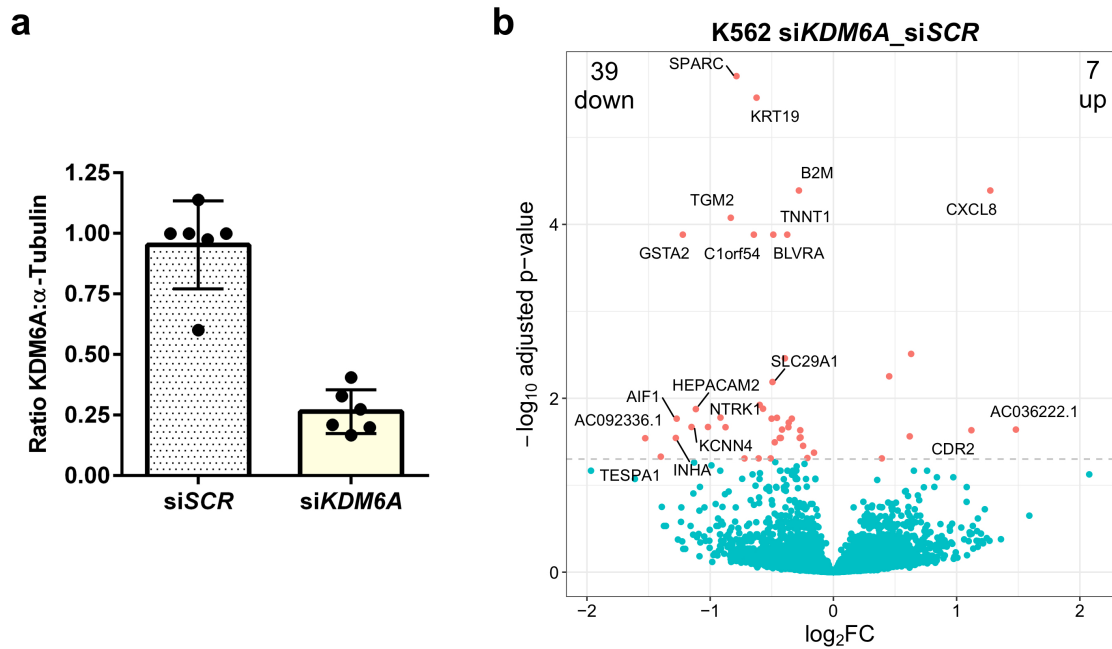


Figure 32 Identification of differentially expressed genes in K562 cells treated with siRNA targeting *KDM6A*. **a**, Knockdown efficiency of *siKDM6A* compared with control (*siSCR*) after two rounds of nucleofection (2x72h; 300 nM) in K562 is shown for six independent experiments (mean \pm s.d.). The ratio of KDM6A to α -Tubulin protein expression was calculated for each experiment. **b**, Volcano plot of \log_2 FC and $-\log_{10}$ adjusted *P* value (transcripts with $P < 0.05$ are highlighted in red) for genes differentially expressed after siRNA-mediated knockdown of *KDM6A* in K562 cells. Differential genes for *siKDM6A* compared with *siSCR* after two rounds of nucleofection (2x72h) are shown ($n=6$).

3.4.2 shRNA-mediated knockdown of *KDM6A*

To identify *KDM6A* target genes in stable *KDM6A* KD K562 cells, RNA-Seq analysis was performed under native conditions and after AraC treatment. For the most potent *shKDM6A* #7, transcriptional deregulation was detected in 295 genes compared to 7 or 54 deregulated genes during *shKDM6A* #3 or #4 mediated KD, respectively (Figure 33a). Only 3 genes showed transcriptionally deregulation in all three *shKDM6As*, but 44 genes overlapped when *shKDM6A* #4 was compared with #7 (Figure 33a). Whereas the majority of differentially expressed genes (39/46) was downregulated in the siRNA-mediated KD (Figure 32b), *shKDM6A* #7 KD resulted in similar transcriptional down- (150, 50.8%) and upregulation (145, 49.2%; Figure 33c).

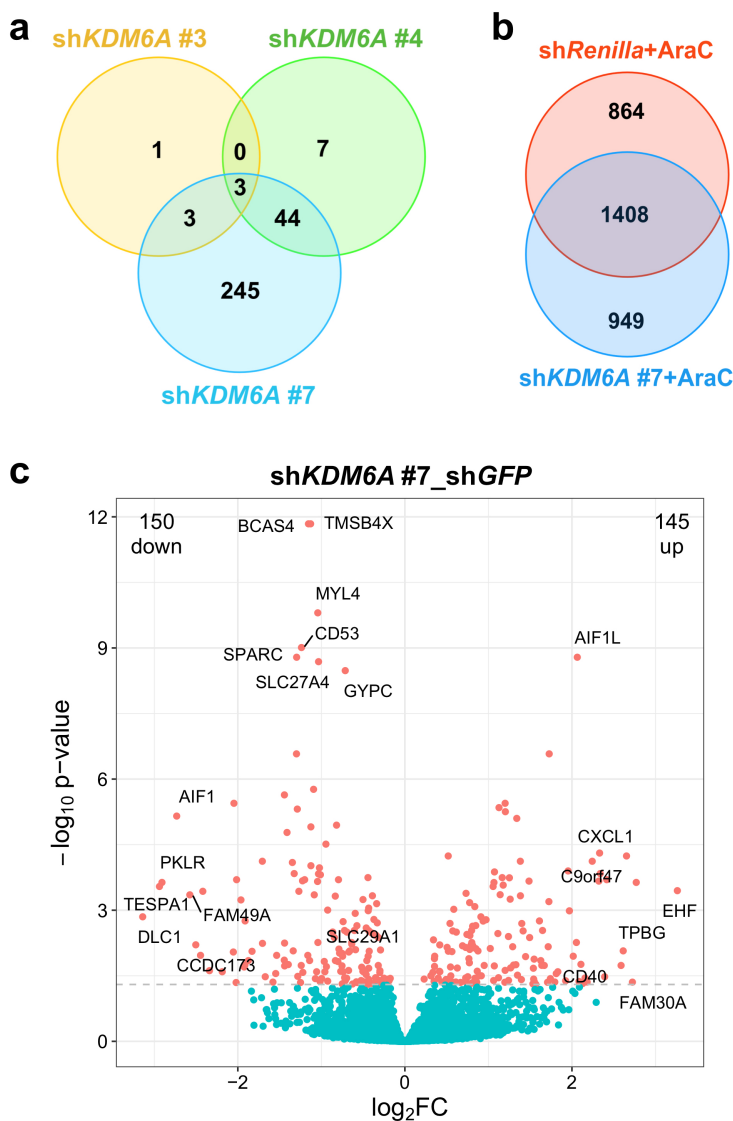


Figure 33 Identification of differentially expressed genes in *KDM6A* KD K562 cells. **a**, Overlap between differentially expressed genes ($P < 0.05$) in three different *shKDM6A* KD K562 cells. Differentially expressed genes of each *shKDM6A* (#3, #4, and #7) compared to *shGFP* control cells are shown ($n=6$). **b**, AraC specific gene expression changes ($P < 0.05$) in *shKDM6A* #7 K562 cells compared with *shRenilla* control cells ($n=6$). Differentially expressed genes in AraC (150 nM, 72h) treated samples were acquired by comparison with the respective untreated samples. **c**, Volcano blot of $\log_2 FC$ and $-\log_{10} P$ value (transcripts with $P < 0.05$ are highlighted in red) showing differentially expressed genes of *shKDM6A* #7 K562 compared with *shGFP* K562 cells.

Treatment with AraC (150 nM, 72h) during shRNA-mediated KD led to increased transcriptional deregulation (sh*KDM6A* #7: 2,357; sh*Renilla*: 2,272) in comparison to the native state with 40.3% (949/2,357) of genes exclusively being deregulated in sh*KDM6A* #7 (Figure 33b).

3.4.3 CRISPR/Cas9-mediated knockout of *KDM6A*

To detect *KDM6A* target genes and compare these with the differentially expressed genes in *KDM6A* KD cells, RNA-Seq was performed in *KDM6A* KO K562 cells.

Comparison of *KDM6A* KO #1 or #2 with *KDM6A* WT #1 cells revealed transcriptional deregulation of 1679 and 1187 genes, respectively (Figure 34a,b).

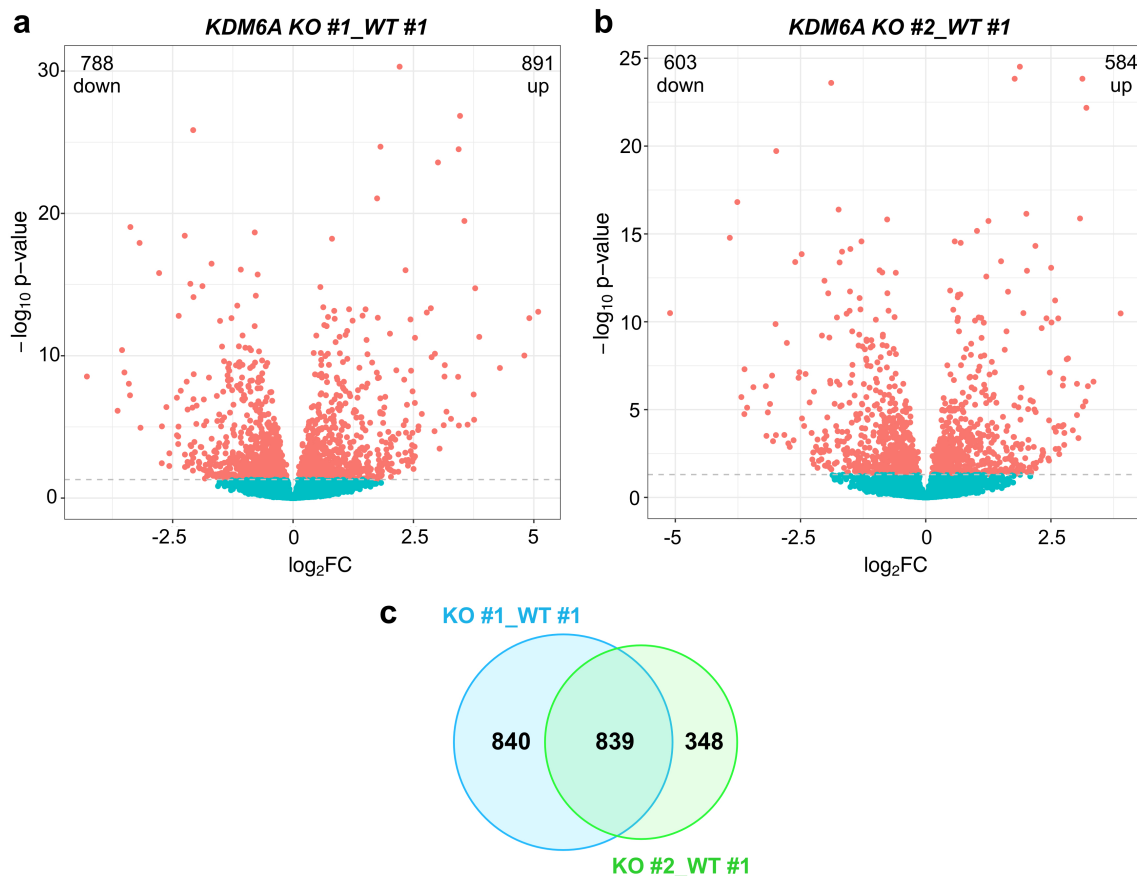


Figure 34 Identification of differentially expressed genes in *KDM6A* KO K562 cells. a,b, Volcano plot of \log_2 FC and $-\log_{10} P$ value (transcripts with $P < 0.05$ are highlighted in red) showing differentially expressed genes of *KDM6A* KO #1 (a) and *KDM6A* KO #2 (b) compared with *KDM6A* WT #1 K562 cells. **c,** Overlap between differentially expressed genes ($P < 0.05$) in *KDM6A* KO #1 and #2 K562 cells. Differentially expressed genes of each *KDM6A* KO compared to *KDM6A* WT #1 are shown ($n=6$).

Of these genes, 839 differentially expressed genes were found in both *KDM6A* KO single cell clones (Figure 34c). The top 20 of these differential expressed genes of both *KDM6A* KO #1 and #2 cells compared with *KDM6A* WT #1 cells with the highest \log_2 fold change (FC) are summarized in Table 15.

Table 15 Summary of top 20 differentially expressed genes found in both *KDM6A* KO K562 single cell clones. The top 20 differentially expressed genes in both *KDM6A* KO #1 and #2 K562 cells compared to *KDM6A* WT #1 K562 cells are listed. Genes with the strongest \log_2 fold change and the respective \log_{10} *P*-values are shown.

Gene Name	\log_2 FC	\log_{10} <i>P</i> -value	Gene Name	\log_2 FC	\log_{10} <i>P</i> -value
<i>ZFP42</i>	5.09	-15.68	<i>FAM49A</i>	-4.28	-10.59
<i>CD36</i>	4.91	-15.14	<i>BCRP2</i>	-3.64	-7.89
<i>AC109492.1</i>	4.80	-12.25	<i>TIMP4</i>	-3.55	-12.69
<i>MS4A6A</i>	3.56	-22.64	<i>LPCAT2</i>	-3.50	-10.91
<i>CALB1</i>	3.47	-30.62	<i>FAM9B</i>	-3.41	-9.98
<i>IGFBP5</i>	3.44	-6.73	<i>TESPA1</i>	-3.39	-9.08
<i>MS4A4A</i>	3.44	-27.88	<i>SNCA</i>	-3.38	-22.16
<i>OOSP1</i>	3.43	-10.56	<i>SRGN</i>	-3.19	-20.89
<i>MAP3K7CL</i>	3.15	-10.58	<i>PLA2G4A</i>	-3.17	-6.56
<i>PII6</i>	3.13	-6.77	<i>PAWR</i>	-2.72	-6.67

FC, fold change.

3.4.4 Overlap of KDM6A target genes between different silencing approaches

Due to the observed drug resistance in both KDM6A silencing approaches (KD and KO), differentially expressed genes of both RNA-Seq analyses were compared. Of the 295 deregulated genes in *shKDM6A* #7 cells, 112 genes overlapped with those differentially expressed in *KDM6A* KO #1 and #2 single cell clones (Figure 35). The top 20 of these genes with the highest \log_2 FC in *KDM6A* KO #1 cells compared to control are shown in Table 16 (all 112 genes are listed in Supplementary Table 1).

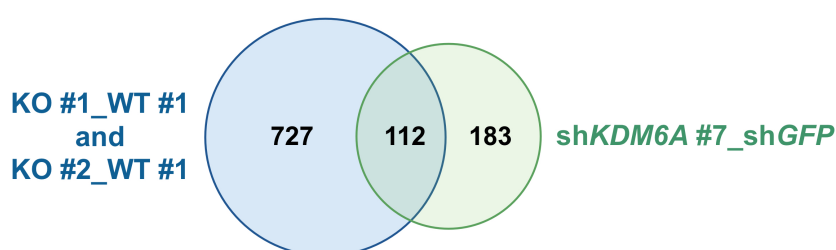


Figure 35 Identification of transcriptional deregulated genes in both KDM6A silencing systems. Overlap between differentially expressed genes ($P < 0.05$) in *shKDM6A* #7_shGFP and *KDM6A* KO #1_WT #1 with *KDM6A* KO #2_WT #1 K562 cells are shown ($n=6$).

Table 16 Summary of top 20 differentially expressed genes in both KDM6A silencing approaches. The \log_2 fold changes and the respective \log_{10} P -values are listed for the top 20 of the 112 differentially expressed genes found in all three *KDM6A* silenced K562 cells compared to controls: *shKDM6A* #7_shGFP, *KDM6A* KO #1_WT #1 and *KDM6A* KO #2_WT #1.

Gene Name	<i>shKDM6A</i> #7_shGFP		<i>KDM6A</i> KO #1_WT #1		<i>KDM6A</i> KO #2_WT #1	
	\log_2 FC	\log_{10} P -value	\log_2 FC	\log_{10} P -value	\log_2 FC	\log_{10} P -value
<i>CD36</i>	2.05	-4.33	4.91	-15.14	3.35	-8.55
<i>CALB1</i>	2.32	-6.11	3.47	-30.62	3.13	-27.47
<i>CAVI</i>	1.63	-3.76	2.78	-15.61	2.31	-11.91
<i>HPGD</i>	1.67	-3.62	2.48	-9.39	2.14	-7.30
<i>ERRFI1</i>	1.81	-3.35	2.30	-6.77	1.59	-3.43
<i>C9orf47</i>	2.77	-6.06	2.26	-3.83	3.02	-6.40
<i>HBBP1</i>	1.14	-5.70	2.14	-11.08	1.54	-6.29
<i>CXCL1</i>	2.65	-6.96	2.04	-5.01	2.74	-8.30
<i>FNI</i>	1.61	-4.96	1.89	-8.14	1.91	-8.15
<i>TSPAN5</i>	1.55	-3.81	1.87	-6.95	1.61	-5.36
<i>FAM49A</i>	-2.57	-5.69	-4.28	-10.59	-3.62	-9.34
<i>LPCAT2</i>	-1.29	-8.24	-3.50	-10.91	-1.91	-8.61
<i>TESPA1</i>	-2.94	-5.94	-3.39	-9.08	-3.19	-8.26

Results

<i>SNCA</i>	-1.06	-3.41	-3.38	-22.16	-0.64	-5.43
<i>DLC1</i>	-3.14	-5.07	-2.57	-4.49	-2.72	-4.28
<i>PEAR1</i>	-1.44	-3.78	-2.41	-8.89	-2.52	-9.16
<i>SERPINF1</i>	-0.57	-3.02	-2.37	-15.35	-2.61	-16.12
<i>ADTRP</i>	-0.75	-3.97	-2.33	-9.44	-1.39	-6.38
<i>CD53</i>	-1.24	-12.54	-2.21	-10.15	-2.77	-10.99
<i>AIFI</i>	-2.73	-8.03	-2.09	-8.13	-2.23	-7.92

FC, fold change.

Gene set enrichment analysis, an analytical method that evaluates RNA-Seq data at the level of gene sets²¹², revealed no gene sets that share common biological functions. Therefore, KDM6A regulated genes were compared with known key candidate genes in AraC, DNR, and 6-TG metabolic pathways. To eliminate cell type specific changes, RNA-Seq data of the sister cell lines MM-1 and MM-6 was included in the analysis. For the metabolic pathway of AraC, the AraC influx transporter *SLC29A1* was found to be consistently downregulated in si*KDM6A*, sh*KDM6A* #7 and both *KDM6A* KO cells compared to their controls (Figure 36). In addition, *SLC29A1* mRNA was downregulated in *KDM6A* mutant MM-6 cells compared to *KDM6A* WT MM-1 cells. *SLC29A1*, also known as ENT1, is a membrane transporter important for the cellular uptake of nucleosides and its analogues²¹³.

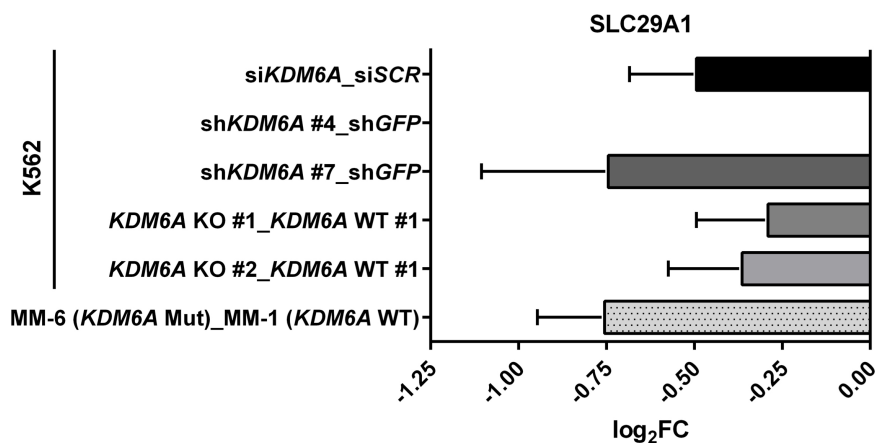


Figure 36 Differential expression of *SLC29A1* in *KDM6A* silenced cells. Horizontal bar plot showing log₂ FC with confidence interval of differentially expressed gene *SLC29A1*. RNA-Seq data from *KDM6A* silencing approaches (siRNA, shRNA, CRISPR/Cas9) in K562 cells and MM-6 vs. MM-1 are shown ($n=6$).

For the metabolic pathway of DNR, the aldo-keto reductases *AKR1C1* and *AKR1C2*, which are members of the drug-metabolizing enzyme family called AKR1C, were found to be differentially expressed in *KDM6A* silenced cells. An upregulation of *AKR1C1* and *AKR1C2* mRNA was observed in both shRNA and KO approaches but not in si*KDM6A* KD cells (Figure 37). In *KDM6A* mutant MM-6 cells, only *AKR1C2* mRNA was also upregulated compared to MM-1 cells (Figure 37b).

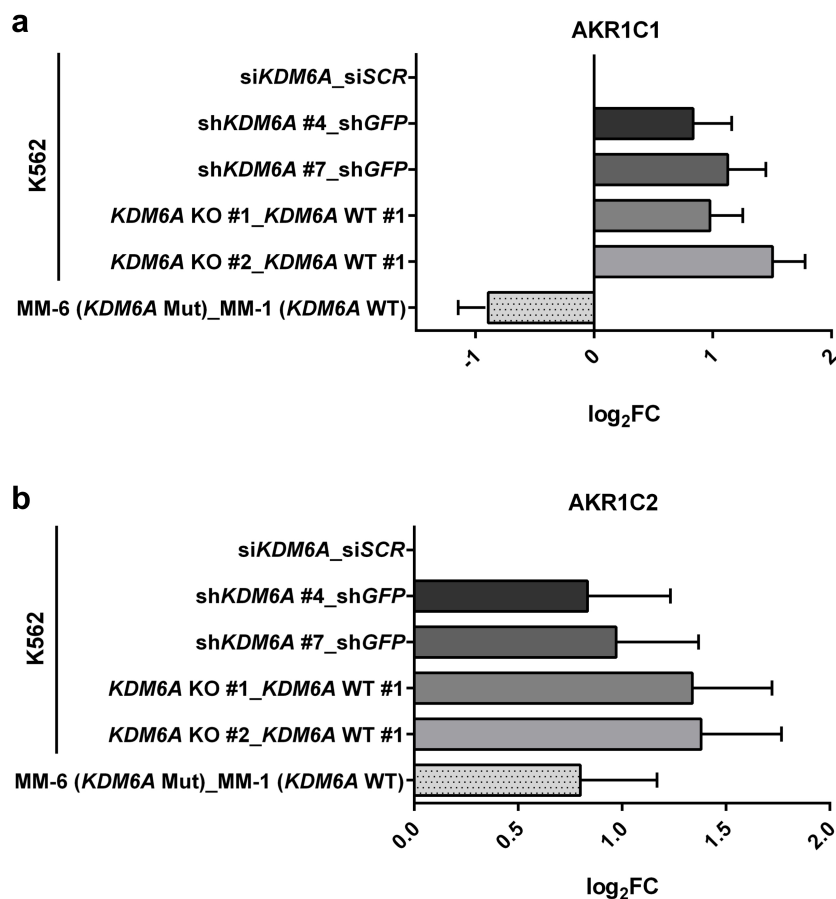


Figure 37 Differential expression of *AKR1C1* and *AKR1C2* in *KDM6A* silenced cells. Horizontal bar plot showing log₂ FC with confidence interval of differentially expressed genes *AKR1C1* (a) and *AKR1C2* (b). RNA-Seq data from *KDM6A* silencing approaches (siRNA, shRNA, CRISPR/Cas9) in K562 cells and MM-6 vs. MM-1 are shown ($n=6$).

4 Discussion

4.1 Inactivation of KDM6A during the clonal evolution of AML

In AML, frequency of patients with *KDM6A* mutations ranges from 0.7 to 4.0% and the majority of mutations are missense mutations^{19,21,31,48}. In this work, the investigated *KDM6A* mutations AML patients at diagnosis were somatic missense and truncating mutations. In contrast to T-ALL¹⁵³ and pediatric ALL¹⁹⁴, where inactivating *KDM6A* mutations were almost exclusively detected in the catalytic JmjC domain, the investigated mutations were also located at or within the proximity of the TPR domain. *KDM6A* mutations most likely lead to a loss of KDM6A expression by facilitating nonsense-mediated mRNA decay or proteasomal degradation of premature stop codons. Therefore, these mutations lead to an inactivation of KDM6A. Although the catalytic inactive mutant H1146A is normally expressed in HEK293T cells, point mutations in specific, highly conserved residues (e.g. L1103R)²¹⁴, might facilitate a destabilization of the protein and subsequent proteasomal degradation. Mutations or deletions targeting the catalytic SET domain of KMT2D were reported to destabilize KMT2D¹⁶⁴. It may be that the JmjC domain is responsible not only for the H3K27 demethylase activity but also for maintaining protein stability of KDM6A.

KDM6A mutation E1325X was previously described in an AML patient at diagnosis and was present in a subclone only³¹. Given that many *KDM6A* mutations are present as subclones in this work and other studies^{21,31}, one could speculate that these mutations occur at a later time point during AML evolution. Investigation of clonal relationships in a cohort of 1540 AML patients by Papaemmanuil and Gerstung *et al.*³¹ revealed that mutations in the *KDM6A* gene mostly occur after the acquisition of mutations in genes like *ASXL1*, *DNMT3A*, *IDH1/2*, *NPM1*, *NRAS*, *TP53*, *TET2*, *RAD21*, *RUNX1*, *NFI*, *PHF6*, *EP300*, *STAG2*, or *SF3B1*. Only the *KIT* gene is probably targeted by mutations after *KDM6A*³¹. The heterogeneous mixture of subclones and small number of patients with *KDM6A* mutations hinders the definition of common mutational patterns. In the present study, *KDM6A* mutations co-occurred with mutations in genes such as *KRAS*, *BCOR*, *Rad21*, *WT1*, *NPM1*, *ASXL1*, *RUNX1*, *TP53*, *FLT3*, and *ABCG2*, but no solid conclusion can be drawn whether *KDM6A* mutations occurred in the same clone or in separate clones. It is possible that the type of co-occurring mutation influences the ELN

risk group assessment, because *KDM6A* mutated patients are diversely grouped³¹. For example, *TP53* mutations were reported to be enriched in myeloid malignancies with *KDM6A* mutations and dual loss of p53 and Kdm6a strongly shortened the latency of Kdm6a loss induced CMML compared to mice with single gene loss¹⁷⁰.

Given the low frequency of diagnosed AML patients with *KDM6A* mutations and limited availability of relapse material, we were able to analyze matched diagnosis and relapse samples in a total of five AML patients. Of these, two patients were part of our CN-AML diagnosis-relapse cohort⁴⁸. The consistent outgrowth of the *KDM6A* mutated population at relapse in all investigated patients, which varied only in their outgrowth intensities, suggests that mutations in the *KDM6A* gene contribute to clonal survival during chemotherapy by at least two possible mechanism. One, KDM6A inactivation could increase the mutational diversity and thus adaptability of the leukemia, leading to clonal survival. Two, KDM6A loss may lead to chemotherapy resistance and clonal survival during therapy.

So far, many studies have focused on identifying driver genes at diagnosis, but only few have compared gene alterations between diagnosis and relapse to identify possible recurrent relapse signatures. Several studies in ALL report compelling evidence that *KDM6A* alternations in ALL are more prevalent at relapse than at diagnosis. For instance, whole-exome sequencing analysis in three adult patients with Philadelphia chromosome negative ALL at diagnosis and relapse after allo-HSCT showed a recurrent somatic *KDM6A* frameshift mutation, N855Rfs*20, in one patient²¹⁵. Although the changes in the variant frequencies were not drastic (34% vs. 44%), the *KDM6A* mutated clone outcompeted the other clones and evolved into the dominant clone at relapse²¹⁵. In pediatric B-ALL patients, *KDM6A* mutations were reported to be enriched at relapse in two patients²¹⁶. Additionally, investigation of copy number alterations (CNA) during progression of adult B-ALL revealed that copy number deletions of *KDM6A* occur specifically at relapse²¹⁷. Recurrent mutations of *KDM6A* are not limited to leukemia and were recently associated with a risk of bladder recurrence²¹⁸. Although not specific for *KDM6A*, high levels of relapse-associated clones at diagnosis predict a shorter remission than low levels in certain cases of childhood ALL⁶⁵. In this study, maybe due to the small number of cases ($n=5$), no correlation between VAF of individual *KDM6A* mutations at diagnosis and time to relapse could be observed.

As *KDM6A* is not X-inactivated¹⁵², females have two active gene copies and thus higher *KDM6A* expression than males⁴⁸. Consistent with these reports, *KDM6A* protein levels in

KDM6A non-mutated patients were lower in males than in females. Of note, all five patients with recurrent *KDM6A* mutations in this study were females. Of these patients, patient CN-025 lost the X chromosome carrying *KDM6A* WT at relapse⁴⁸. The AML cell line HL-60 harboring a *KDM6A* exon deletion also lost the other X chromosome. In line with these observations, a loss of heterozygosity was observed among 16 female cancer cell lines with *KDM6A* inactivating mutations on one allele¹⁴⁵. Patient CN-025, who lost the other X chromosome, had an extremely short remission with a time to relapse of only 122 days. Although the possibility remains that gain of additional alterations contribute to a short remission, complete loss of *KDM6A* WT expression might play a role in accelerating the progression of AML. Consistent with this notion, *KDM6A* deficiency was found to accelerate and promote cancer progression dependent on its expression dosage in a mouse lymphoma model²¹⁹.

In our recent study, we found a positive correlation between *KDM6A* expression and overall survival in CN-AML patients⁴⁸. This correlation appears to be gender-specific, because shortened overall and relapse-free survival was only observed in male CN-AML patients⁴⁸. Female cells likely have more functional reserves to compensate for *KDM6A* inactivation compared with male cells carrying only a single copy. In T-ALL, pathogenesis seems to be facilitated through a loss in demethylase activity and thus females benefit from two functional copies¹⁵³. On the contrary, male mice with loss of *KDM6A* do not develop AML, because the Y-linked homolog *UTY* facilitates *KDM6A*-similar noncatalytic functions¹⁹⁷. Expression levels of *UTY* were not analyzed in the AMLCG-99 cohort and thus no conclusion about the prognostic impact of *UTY* and the functional redundancy between *KDM6A* and *UTY* in male CN-AML patients can be drawn from our recent study.

Results from this work suggest that at least two mechanisms exist to regulate *KDM6A* activity. On the one hand, *KDM6A* can be inactivated by loss-of-function mutations. On the other hand, *KDM6A* mutation-independent mechanisms seem to contribute to low protein expression at relapse. A possible mechanism to downregulate *KDM6A* in females during AML progression could be loss of chromosome X, because the X chromosome is among the most frequently aneuploid chromosomes in female cancers²²⁰.

Other possible regulatory mechanisms are altered epigenetic pathways including DNA hypermethylation, histone modifications, and misregulation of miRNAs or deregulated protein degradation. A recent study by Göllner *et al.*²²¹ found that a subset of AML

patients lost protein expression of the histone H3K27 methyltransferase EZH2 during disease progression. EZH2 protein levels were reduced by proteasomal degradation through EZH2 phosphorylation at Threonine 487 and binding of E3 ubiquitin protein ligases²²¹. Whereas treatment with the proteasomal inhibitor bortezomib restored EZH2 levels in some AML patients²²¹, *in vivo* treatment of PDX AML-393 bearing mice with bortezomib showed no upregulation of KDM6A expression in this study (data not shown). These findings suggest that KDM6A levels might be reduced during AML progression by other regulatory mechanisms than protein degradation.

Karyotype changes from normal to complex aberrant may have an impact on KDM6A protein expression during disease progression. Of note, the karyotype of patient #5 at relapse was completely distinct from the primary tumor, which differentiates it as a second malignancy. This might explain why KDM6A protein expression is higher in this specific relapse sample compared to diagnosis.

The type of induction therapy included S-HAM, TAD or AraC plus DNR and thus the applied drug combinations varied between AML patients. The component all induction regimens have in common is AraC. Although the number of cases is small, the results from the *in vivo* therapy of PDX bearing mice with AraC and liposomal DNR indicate that *KDM6A* mutated cells are resistant to therapy whereas *KDM6A* WT cells are not. Unfortunately, no viable cells from these two patients were available at diagnosis to establish a PDX model and to compare drug sensitivity between diagnosis and relapse in PDX samples from the same patient. Overall, the *in vivo* findings are in agreement with results obtained from patients and suggest that chemotherapy might select for clones which possess a *KDM6A* mutation or have reduced KDM6A expression.

4.2 Deletions of *KDM6A* facilitate an altered epigenetic phenotype in AML cell lines

Van Haaften and colleagues¹⁴⁵ were the first to identify *KDM6A* exon deletion mutations in a broad spectrum of cancer cell lines. In this work, extended analysis of 40 myeloid leukemia cell lines revealed *KDM6A* exon deletions in 10% of AML cell lines. Exon deletions in MM-6 and THP-1 cells were detected as reported previously¹⁴⁵. In addition, exon deletion mutations were found in OCI-AML3 and HL60 cells and these findings were independently validated. Although both deletions are short and in-frame, *KDM6A* protein expression is completely lost. Recently, *KDM6A* expression was reported to be lost in the cell line MV4-11¹⁹⁷. In contrast, MV4-11 cells used in this study harbor no *KDM6A* exon deletion and showed normal *KDM6A* protein expression. Cell line identity of MV4-11 was confirmed by fingerprint analysis. The discrepancy could be explained by clonal evolution of sublines during cultivation or other yet unexplained mechanisms.

Genomic loss of *UTY* in hematopoietic and solid organ cancer cell lines was demonstrated to occur more frequently in cells with inactivating *KDM6A* mutations than in *KDM6A* WT cells^{145,197}. Additionally, *UTY* was reported to be lost or reduced in conjunction with *KDM6A* mutations in pancreatic cancers with squamous differentiation in male patients¹⁹⁶. Consistent with these findings, reduced expression of *UTY* mRNA was found to occur quite frequently in *KDM6A* mutant AML cell lines (2/3), but also in some *KDM6A* WT cell lines (3/7). In contrast, PDX AML-579 and AML-372 cells with low *KDM6A* protein expression showed *UTY* mRNA levels comparable to *UTY* WT cell lines. Of note, the sister cell lines MM-1 and MM-6, which have been originally established in culture from the same male AML patient at relapse²¹¹, both lost *UTY* expression. We demonstrated previously that *KDM6A* mutant MM-6 cells are more resistant to AraC treatment than *KDM6A* WT MM-1 cells⁴⁸. In *KDM6A*-deficient male mice, *UTY* can compensate for *KDM6A* loss and suppress myeloid leukemogenesis cells¹⁹⁷. Because *UTY* mRNA expression is lost in both cell lines, the impact of *KDM6A* loss in these sister cell lines can be studied without possible interference from *UTY*.

The steady state of H3K27 methylation is kept tightly regulated by the histone H3K27 methyltransferase *EZH2* and demethylases *KDM6A* and *KDM6B*. Despite their opposing roles on H3K27 methylation, loss-of-function mutations in both *KDM6A* and *EZH2* genes were detected in a mutually exclusive manner in CMML patients¹⁹⁵.

Mutations in *EZH2* and *KDM6A* or *KDM6B* appear to be mutually exclusive in AML as well. In addition, *EZH2* and *KDM6B* mRNA levels were similar in AML cell lines with different *KDM6A* gene status, suggesting that the increase of global H3K27me3 in *KDM6A* mutated AML cell lines is a direct consequence of KDM6A loss.

Consistent with this notion, both KDM6A silencing approaches in K562 cells led to a modest increase of global H3K27me3. Recently, inactivation or loss of KDM6A was linked to a modest increase of global H3K27me3 in urothelial bladder carcinomas¹⁸⁹. During malignant T-cell transformation in a NOTCH1-induced T-ALL mouse model, KDM6A deficiency caused a genomewide redistribution of H3K27me3, but did not change the global levels of H3K27me3¹⁵³. Hence, increased H3K27me3 are direct consequence of KDM6A loss, but results from several studies suggest that the magnitude of increase as well as its impact on regulatory mechanisms might vary depending on the investigated tumor type.

4.3 Inactivation of KDM6A confers drug resistance in AML

Despite high initial remission rates, a substantial fraction of patients with AML relapse. In addition to established cytogenetic risk factors, certain molecular genetic lesions such as *RUNX1*, *TP53*, and *FLT3/ITD* mutations have been associated with an increased risk of relapse in AML^{52,222–225}. Still, reliable biomarkers for predicting the therapeutic response to induction therapy are mostly lacking^{52,226}. The search for relapse promoting biomarkers is further complicated by the heterogeneity of AML. Recently, SAMHD1 was reported to be a promising biomarker for AraC resistance in patients with AML⁹¹. By decreasing the levels of active AraC (Ara-CTP), SAMHD1 was found to mediate resistance to AraC. SAMHD1 levels at diagnosis were inversely correlated with the clinical response to AraC based therapy in two cohorts of adult patients with AML⁹¹. Another potential candidate gene for AraC resistance in AML is the H3K27 methyltransferase EZH2. Low EZH2 expression correlate with poor overall survival and event-free survival in AML patients²²¹. Loss of EZH2 and subsequent reduction of H3K27me3 levels were identified as a novel pathway of acquired resistance to cytotoxic drugs such as AraC and DNR but also to tyrosine kinase inhibitors (e.g. PKC412)²²¹.

In this work, we identified KDM6A as a novel biomarker for drug resistance in AML. Suppression of KDM6A protein expression induced chemoresistance of AML cell lines *in vitro* and of PDX cells *in vivo*. In contrast to AraC for which a dependency on KDM6A expression dosage was only observed after short-term treatment, resistance to DNR appears to be dependent on KDM6A expression dosage during prolonged treatment. Stronger suppression of KDM6A results in increased growth advantage under DNR therapy indicating that regulation of chemoresistance mediating KDM6A target genes depends on KDM6A expression dosage. Although not in the context of chemoresistance, level of KDM6A expression were found to have an impact on leukemogenesis in mouse models^{197,219}.

Induction therapy typically involves continuous treatment of AML patients for seven (7+3 schedule) or 10 days (TAD regime). During prolonged *in vitro* treatment, we observed a strong increase in resistance of AML cell lines with KDM6A loss to AraC and DNR, whereas only a modest increase was seen after short-term treatment *in vitro*. This shows that even smaller differences in drug sensitivity observed after short-term therapy can significantly impact long-term therapy.

In our previous study⁴⁸ we demonstrated that the *KDM6A* mutant MM-6 cells were significantly more resistant to AraC short-term treatment than its sister cell line MM-1

(*KDM6A* WT). In contrast, only a trend for increased DNR resistance was seen after short-term treatment for 72h. In this work, we extended treatment time, which resulted in a significant increase of DNR resistance in MM-6 compared to MM-1 cells. Additionally, we demonstrated that deletion of *KDM6A* in MM-1 recapitulates the same drug resistant phenotype observed in MM-6. These findings are in agreement with our previous results and clearly support our hypothesis that *KDM6A* deficiency induces drug resistance in AML. Besides increased resistance towards AraC and DNR, *KDM6A* deficient MM-1 and *KDM6A* mutant MM-6 cells are less sensitive to 6-TG treatment. As this was not the case for *KDM6A* deficient K562 cells, 6-TG resistance might be cell type dependent. To date, a link between *KDM6A* loss and altered cytotoxic drug sensitivity has only been reported in a mouse B cell lymphoma model²¹⁹, but not for AML. AraC, which is only occasionally used in the treatment of lymphomas, was reported to show the most significant sensitivity changes upon *KDM6A* knockdown in mouse B lymphoma cells²¹⁹. In contrast to our findings in AML, lymphoma cells with *KDM6A* knockdown were more sensitive to AraC but showed increased resistance towards 6-TG, 3-MA-34, and CDDP²¹⁹. One possible explanation for the discrepancy between the AraC sensitivity of *KDM6A* deficient murine B lymphoma cells and *KDM6A* deficient human AML cells could be tissue specific activation or repression of regulatory genes involved in drug sensitivity. Overall, these results suggest for the first time that AML clones with a *KDM6A* loss are selected for during therapy with cytotoxic agents including AraC and DNR.

Given the tumor suppressor function of *KDM6A*, the design and application of therapeutic approaches targeting *KDM6A* deficient cancer cells is rather difficult. A potential vulnerability that can be exploited is its dependency on increased EZH2 activity because cells with a *KDM6A* deficiency were reported to be more sensitive for H3K27me3 inhibition in certain tumor types^{182,189}. Van der Meulen *et al.*¹⁸² demonstrated in both murine and human *in vitro* T-ALL model systems that *KDM6A* loss renders cells more sensitive to treatment with DZNep, an epigenetic compound that targets EZH2. Notably, no increased sensitivity to DZNep treatment was observed in *KDM6A* mutant AML cell lines in this work (data not shown). Given that DZNep is not specific for EZH2 and also acts as a *S*-adenosylhomocysteine hydrolase inhibitor, *KDM6A* deficient cells were also treated with a specific EZH2 inhibitor (GSK126). Consistent with our findings from DZNep treatment, treatment with GSK126 showed no differences in growth between *KDM6A* WT and deficient AML cell lines (data not shown). Probably due to its largely demethylase independent tumor suppressor functions, *KDM6A* deficient squamous-like

pancreatic cancers do not respond differently to EZH2 inhibition, but are selectively sensitive to BET inhibitors¹⁹⁶. To exploit potential vulnerabilities upon KDM6A loss in AML, screening for diverse types of inhibitors should be performed in the future.

4.4 Identification of key KDM6A target genes involved in mediating drug resistance

Various mechanisms of drug resistance in AML have been proposed in the last decades. Possible mechanisms of resistance include drug inactivation, decreased drug influx or increased drug efflux, altered DNA repair mechanisms, protective microenvironment, altered apoptotic pathway and cell cycle⁶⁷.

AraC for instance can only exert its cytotoxic effect via DNA polymerase inhibition and incorporation into DNA after cellular uptake and conversion into its active triphosphate form. Hence, deregulation of genes involved in AraC metabolism can profoundly impact AraC sensitivity. One of the factors affecting AraC sensitivity in AML patients is DCK, which is believed to be the key rate-limiting activating enzyme by phosphorylating AraC to AraC monophosphate (Ara-CMP). Low levels of DCK were reported to correlate with low AraC sensitivity^{87,88} and to predict shorter DFS^{83,89}. Besides AraC activating enzymes, increased activity of inactivating enzymes can also impact the responsiveness to AraC⁹¹. Upon loss of EZH2, the effectiveness of AraC in AML cell lines and primary cells was reported to be diminished due to an activation of *HOX* gene family members (e.g. *HOXB7* and *HOXA9*)²²¹. Given that no gene sets with shared common biological functions were found by gene set enrichment analysis in KDM6A deficient cells, differential expressed genes were compared with known candidate genes in drug resistance pathways.

Among the key candidate genes in AraC metabolism, we consistently found differential expression of the drug influx transporter gene *SLC29A1*, also known as *ENT1*, in KDM6A deficient cells. SLC29A1 is the most abundant nucleotide transporter in blasts from AML patients and leukemia cell lines²²⁷. It is responsible for the cellular uptake of AraC and the DNA methyltransferase inhibitors decitabine and 5-azacytidine²²⁷. Previous studies showed that KD or inhibition of SLC29A1 in AML cell lines confers AraC resistance^{95,228}. A trend for inverse correlation of SLC29A1 protein expression and AraC sensitivity was also observed in AML cell lines⁹¹. In AraC based therapy, AML patients with low SLC29A1 levels were reported to have shorter disease-free or overall survival and a

reduction of ENT1 expression was observed at relapse compared to remission⁹⁶. Consistent with these findings, we demonstrate that both K562 and MM-6 cells with KD/KO of *KDM6A*, which are less sensitive to AraC based treatment, have decreased mRNA expression of *SLC29A1*. Furthermore, combinational treatment with AraC and a selective SLC29A1 small molecule antagonist called NBMPR resulted in increased cell survival compared to AraC alone (data not shown). Collectively these results show that loss of *KDM6A* induces decreased AraC sensitivity in AML cells by reducing the expression of the AraC influx transporter SLC29A1 and thereby decreasing the intracellular amount of AraC (Figure 38). Hence, we propose a novel mechanism of AraC resistance upon loss of *KDM6A* in AML although the possibility cannot be ruled out that other target genes of *KDM6A* might contribute to AraC resistance as well.

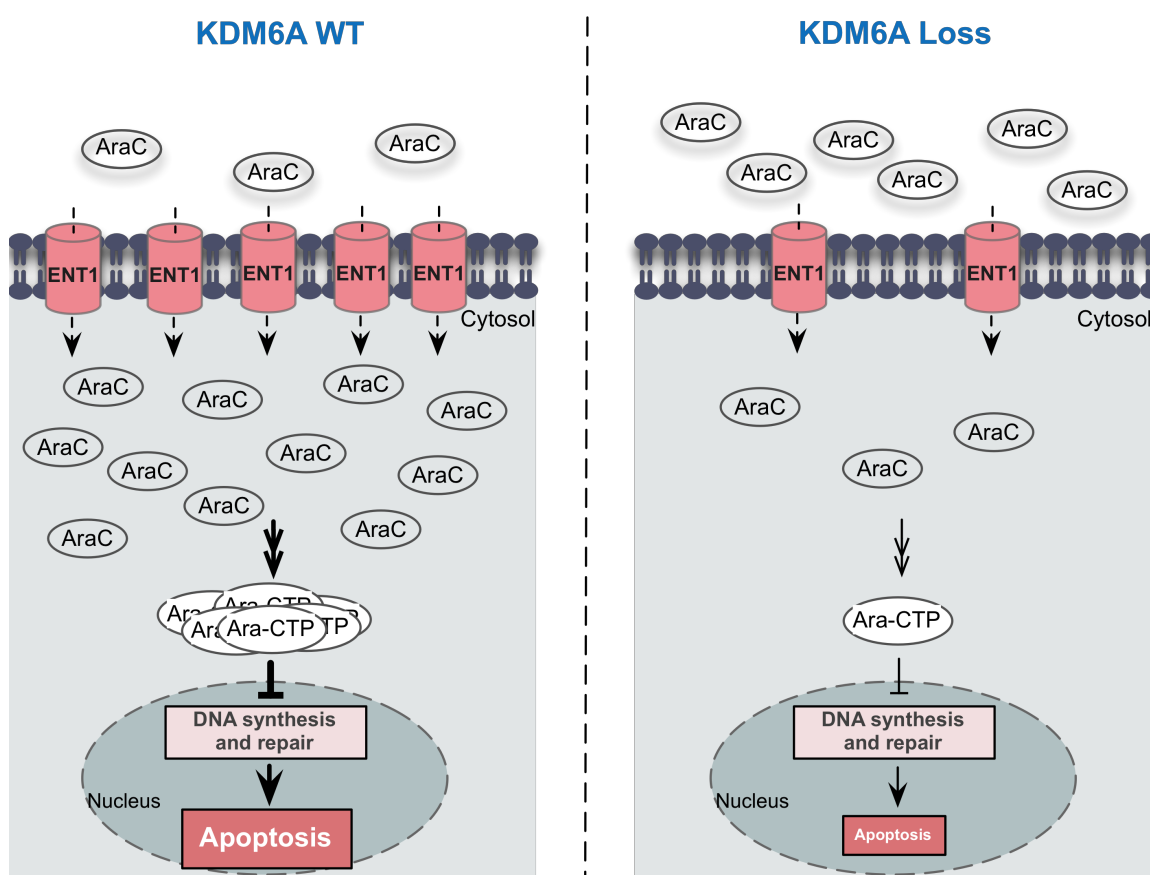


Figure 38 Proposed model for *KDM6A*-controlled AraC resistance in AML cells. In *KDM6A* WT cells, ENT1 (SLC29A1) facilitates the transport of AraC across the cell membrane of AML cells leading to high amounts of intracellular AraC and subsequent high levels of active AraC (Ara-CTP). Ara-CTP blocks DNA synthesis and repair resulting in enhanced induction of apoptosis (left panel). In *KDM6A* deficient AML cells, loss of *KDM6A* leads to the reduction of ENT1 expression thereby decreasing intracellular AraC levels and preventing/reducing the induction of apoptosis (right panel).

To further elucidate the mechanism of *SLC29A1* regulation by KDM6A, ChIP-seq analysis for H3K27me3 in KDM6A deficient and WT cells should be performed in the future. Additionally, ChIP-seq analysis for H3K27 acetylation seems promising since KDM6A was reported to regulate gene expression during myeloid leukemogenesis mainly by modifying levels of H3K27 acetylation, H3K4 monomethylation and chromatin accessibility¹⁹⁷. Consistent with previous findings that KDM6A is not solely a transcriptional activator¹⁹⁷, we observed gene expression changes with similar up- and downregulation after KD and KO of *KDM6A* in myeloid cells suggesting that KDM6A regulates gene expression not only by modifying levels of H3K27 methylation. It will be important to understand the extent to which the drug resistant promoting effects of KDM6A depend upon its catalytic activity as compared to its noncatalytic structural contributions to COMPASS complex integrity and chromatin remodeling factor activity. Given that the cellular uptake of DNR is not facilitated by SLC29A1 (Stief *et al.*, manuscript submitted), other mechanisms appear to induce DNR resistance in KDM6A deficient cells. One possible mechanism leading to DNR resistance might be upregulation of the metabolizing enzymes AKR1C1 and AKR1C2 in KDM6A deficient cells. AKR1C1 and AKR1C2 belong to a family of aldo-keto reductases (AKR1C1-AKR1C4), which share over 86% homology and catalyze NADPH dependent aldehyde or ketone reductions^{229,230}. Although their natural substrates are steroids and prostaglandins, these aldo-keto reductases can metabolize and inactivate anticancer drugs and thus were implicated in chemotherapeutic drug resistance in cancer^{230,231}. For instance, resistance to cisplatin was found to be induced by upregulation of AKR1C1 in human ovarian cancer cells²³² or of both AKR1C1 and AKR1C3 in human colon cancer cells²³³. In leukemic U937 cells, induction of AKR1C1 and AKR1C3 expression was demonstrated to facilitate reduction of DNR efficacy²³⁴. Whereas AKR1C3 expression was not differentially regulated, we observed upregulation of AKR1C1 and AKR1C2 in DNR resistant leukemic cells upon reduction or loss of *KDM6A*. However, we exclusively found a consistent upregulation of AKR1C2, but not AKR1C1, across different cell lines in both K562 cells with *KDM6A* KD/KO and *KDM6A* mutant MM-6 cells. Interestingly, AKR1C2, but not AKR1C1, was reported to display enzymatic activity with DNR metabolism²³⁰ supporting our hypothesis that AKR1C2 plays a role in conferring resistance to DNR in KDM6A deficient cells. The role of AKR1C2 in DNR resistance seems promising and should be further investigated by deleting or overexpressing AKR1C2 in AML cells. Additionally, upregulation of AKR1C2 is the major factor responsible for DNR resistance in KDM6A

deficient cells, specific inhibition of AKR1C2^{230,235} should re-sensitize cells to DNR treatment.

In summary, these findings suggest that two different proteins mediate resistance to AraC and DNR, respectively, in KDM6A deficient cells. AraC resistance is achieved by downregulation of the drug influx transporter SLC29A1, whereas upregulation of AKR1C2 most likely promotes resistance to DNR. Future studies are planned to unravel the mechanisms behind KDM6A target gene regulation.

5 Summary

Acute myeloid leukemia (AML) is an aggressive hematologic cancer resulting from the malignant transformation of myeloid progenitors. Despite an initiate response to intensive chemotherapy, relapse caused by intrinsic or acquired drug resistance remains a major hurdle in the treatment of AML. KDM6A (or UTX) is a histone 3 lysine 27 (H3K27)-specific demethylase and a member of the COMPASS-like complex, which is important for H3K4 methylation and chromatin enhancer activation. *KDM6A* is targeted by inactivating mutations in a variety of cancer types with frequency of occurrence ranging from 0.7 to 4% in AML. Although recent studies reported a crucial role for the tumor suppressor KDM6A in the development of cancer including leukemia, its functions during clonal evolution of AML from diagnosis to relapse are still unresolved.

It was the aim of this project to characterize the clonal evolution dynamics of KDM6A during AML progression and to investigate if KDM6A loss facilitates tolerance to drugs that are commonly used in the induction therapy for AML. In a diagnosis-relapse cohorte of 50 cytogenetically normal AML patients, we initially discovered *KDM6A* as a novel relapse-associated gene in two patients. Subclones harboring a *KDM6A* mutation were selected for during AML progression and evolved into the major clone at relapse. By comparing the variant allele frequency of *KDM6A* mutations in AML patients with matched diagnosis and relapse samples, we found three additional AML patients with enrichment of *KDM6A* loss-of-function mutations at relapse. During disease progression, loss of KDM6A can also occur in a mutation-independent fashion suggesting that loss of KDM6A is also facilitated by other regulatory mechanisms. Increase of global H3K27me3 in *KDM6A* mutant or deleted cells is a direct consequence of KDM6A inactivation, but to which extend the relapse-promoting effects of KDM6A depend upon its enzymatic activity need further investigation.

To investigate whether loss of KDM6A leads to increased resistance towards drugs commonly used in the treatment of AML, KDM6A expression was silenced by different approaches including siRNA, shRNA and CRISPR/Cas9-mediated genome editing in the myeloid leukemia cell lines K562 and MM-1. Compared to control, *KDM6A* knockdown and knockout K562 cells showed a strong proliferative advantage after cytarabine (AraC) and daunorubicin (DNR) but not 6-thioguanine (6-TG) treatment. Loss of KDM6A in MM-1 phenocopied the drug resistance phenotype observed in the sister cell line MM-6

(*KDM6A* mutant). RNA-Seq analysis in K562 cells treated with siRNA or shRNA against *KDM6A* revealed differentially expressed genes, of which two are key candidate genes in AraC and DNR metabolic pathways. AraC resistance, at least partly, might be achieved by reduction of the AraC influx transporter SLC29A1 (or ENT1). In contrast, resistance to DNR in *KDM6A* deficient cells might be mediated by upregulation of the drug metabolizing enzymes AKR1C1 and AKR1C2.

In conclusion, these results show that mutations in *KDM6A* are associated with the outgrowth of drug-resistant clones and highlight *KDM6A* as a novel mediator of drug resistance in AML.

6 Zusammenfassung

Die akute myeloische Leukämie (AML) ist eine aggressive hämatologische Neoplasie, die aus der malignen Umwandlung myeloischer Vorläufer entsteht. Obwohl die Mehrheit der Patienten auf eine intensive Chemotherapie anspricht, ist ein Krankheitsrückfall aufgrund intrinsischer oder erworbener Arzneimittelresistenz häufig. Das Rezidiv ist daher eine der größten Herausforderungen bei der Behandlung von AML. KDM6A (oder UTX) ist eine Histon 3 Lysin 27 (H3K27)-spezifische Demethylase und Mitglied des COMPASS-artigen Komplexes, welcher für die H3K4 Methylierung und die Aktivierung von Chromatin Enhancern wichtig ist. Inaktivierende *KDM6A* Mutationen wurden in einer Vielzahl von Krebsarten gefunden und haben eine Häufigkeit von 0,7 bis 4% in der AML. Obwohl kürzlich durchgeführte Studien eine entscheidende Rolle für KDM6A als Tumorsuppressor bei der Krebsentstehung, einschließlich Leukämien, beschrieben haben, sind dessen Funktionen während des Fortschreitens der AML von Diagnose zu Rezidiv noch ungeklärt.

Ziel dieses Projektes war es, die klonale Evolutionsdynamik von KDM6A während der AML-Progression zu bestimmen. Des Weiteren sollte untersucht werden, ob der Verlust von KDM6A zu einem veränderten Ansprechen auf Medikamente, die üblicherweise in der Induktionstherapie für AML eingesetzt werden, führt. In einer Diagnose-Rezidiv-Kohorte von 50 zytogenetisch normalen AML Patienten entdeckten wir KDM6A als neues, rezidiv-assoziiertes Gen bei zwei Patienten. Subklone mit einer *KDM6A* Mutation hatten einen selektiven Vorteil während der AML-Progression und entwickelten sich in den Hauptklon im Rezidiv. Durch Vergleich der Allelhäufigkeit von *KDM6A* Mutationen bei AML Patienten, bei denen übereinstimmende Diagnose- und Rezidivproben verfügbar waren, fanden wir drei weitere AML Patienten mit einer Anreicherung von *KDM6A* Mutationen im Rezidiv. Während des Fortschreitens der Krankheit kann der Verlust von KDM6A auch mutationsunabhängig auftreten, was darauf hindeutet, dass die Expression von KDM6A auch durch andere Mechanismen reguliert wird. Die Zunahme von globalem H3K27me3 in *KDM6A* mutierten oder reprimierten Zellen ist eine direkte Folge der KDM6A Inaktivierung. Weitere Untersuchungen müssen aber erst zeigen, in wie fern die enzymatische Aktivität die rezidiv-spezifische Selektion beeinflusst.

Um zu untersuchen, ob der Verlust von KDM6A zu einer erhöhten Resistenz gegenüber Medikamenten führt, die üblicherweise bei der Behandlung von AML eingesetzt werden,

wurde die *KDM6A* Expression durch verschiedene Ansätze wie siRNA, shRNA und CRISPR/Cas9 in den myeloischen Leukämie Zelllinien K562 und MM-1 reprimiert. Im Vergleich zur Kontrolle zeigten *KDM6A* Knockdown (KD) und Knockout (KO) K562 Zellen einen starken proliferativen Vorteil nach Behandlung mit Cytarabin (AraC) und Daunorubicin (DNR), aber nicht 6-Thioguanin (6-TG). KO von *KDM6A* in MM-1 Zellen resultierte im gleichen Resistenzphänotyp wie der der Schwesterzelllinie MM-6 (*KDM6A* mutiert).

Die RNA-Seq-Analyse in K562 Zellen, die mit siRNA oder shRNA gegen *KDM6A* behandelt wurden, zeigte differentiell exprimierte Gene, von denen zwei eine wichtige Rolle im AraC- und DNR-Stoffwechselweg spielen. Die Resistenz gegen AraC, zumindest teilweise, könnte durch die reduzierte Expression des AraC Transporters SLC29A1 (oder ENT1) erreicht werden. Im Gegensatz dazu könnte die Resistenz gegen DNR in *KDM6A*-reprimierten Zellen durch eine Hochregulierung der Arzneimittel metabolisierenden Enzyme AKR1C1 und AKR1C2 vermittelt werden.

Zusammenfassend zeigen die Ergebnisse dieser Arbeit, dass *KDM6A* Mutationen die Selektion von Chemotherapie-resistenten Klonen im Rezidiv begünstigen. Somit spielt *KDM6A* eine wichtige Rolle bei der Vermittlung der Chemotherapie-Resistenz in der AML.

7 References

1. Greaves, M. Leukaemia ‘firsts’ in cancer research and treatment. *Nat. Rev. Cancer* **16**, 163–172 (2016).
2. Smith, A. *et al.* The Haematological Malignancy Research Network (HMRN): a new information strategy for population based epidemiology and health service research. *Br. J. Haematol.* **148**, 739–53 (2010).
3. Visser, O. *et al.* Incidence, survival and prevalence of myeloid malignancies in Europe. *Eur J Cancer* **48**, 3257–3266 (2012).
4. German Centre for Cancer Registry Data, Robert Koch Institute, 28.08.2018
5. Weltermann, A. *et al.* Impact of cytogenetics on the prognosis of adults with de novo AML in first relapse. *Leukemia* **18**, 293–302 (2004).
6. Shen, Y. *et al.* Gene mutation patterns and their prognostic impact in a cohort of 1185 patients with acute myeloid leukemia. *Blood* **118**, 5593–5603 (2011).
7. Schlenk, R. F. *et al.* Mutations and Treatment Outcome in Cytogenetically Normal Acute Myeloid Leukemia. *N. Engl. J. Med.* **358**, 1909–1918 (2008).
8. Bennett, J. M. *et al.* Proposals for the classification of the acute leukaemias. French-American-British (FAB) co-operative group. *Br. J. Haematol.* **33**, 451–8 (1976).
9. Vardiman, J. W., Harris, N. L. & Brunning, R. D. The World Health Organization (WHO) classification of the myeloid neoplasms. *Blood* **100**, 2292–2302 (2002).
10. Vardiman, J. W. *et al.* The 2008 revision of the WHO classification of myeloid neoplasms and acute leukemia: rationale and important changes. *Blood* **114**, 937–952 (2008).
11. Arber, D. A. *et al.* The 2016 revision to the World Health Organization classification of myeloid neoplasms and acute leukemia. *Blood* **127**, 2391–2405 (2016).
12. Keating, M. J. *et al.* Cytogenetic pattern in acute myelogenous leukemia: a major reproducible determinant of outcome. *Leukemia* **2**, 403–12 (1988).
13. Fenaux, P. *et al.* Cytogenetics and their prognostic value in de novo acute myeloid leukaemia: a report on 283 cases. *Br. J. Haematol.* **73**, 61–7 (1989).
14. Dastugue, N. *et al.* Prognostic significance of karyotype in de novo adult acute myeloid leukemia. The BGMT group. *Leukemia* **9**, 1491–8 (1995).
15. Grimwade, D. *et al.* The importance of diagnostic cytogenetics on outcome in AML: analysis of 1,612 patients entered into the MRC AML 10 trial. The Medical Research Council Adult and Children’s Leukaemia Working Parties. *Blood* **92**, 2322–33 (1998).
16. Byrd, J. C. *et al.* Pretreatment cytogenetic abnormalities are predictive of induction success, cumulative incidence of relapse, and overall survival in adult patients with de novo acute myeloid leukemia: results from Cancer and Leukemia Group B (CALGB 8461). *Blood* **100**, 4325–4336 (2002).
17. Döhner, H., Weisdorf, D. J. & Bloomfield, C. D. Acute Myeloid Leukemia. *N. Engl. J. Med.* **373**, 1136–1152 (2015).
18. Rockova, V. *et al.* Risk stratification of intermediate-risk acute myeloid leukemia : integrative analysis of a multitude of gene mutation and gene expression markers. *Blood* **118**, 1069–1076 (2011).
19. The Cancer Genome Atlas Research Network. Genomic and Epigenomic Landscapes of Adult De Novo Acute Myeloid Leukemia. *N. Engl. J. Med.* **368**, 2059–2074 (2013).
20. Welch, J. S. *et al.* The origin and evolution of mutations in acute myeloid leukemia. *Cell* **150**, 264–78 (2012).

21. Metzeler, K. H. *et al.* Spectrum and prognostic relevance of driver gene mutations in acute myeloid leukemia. *Blood* **128**, 686–699 (2016).
22. Gaidzik, V. I. *et al.* *TET2* Mutations in Acute Myeloid Leukemia (AML): Results From a Comprehensive Genetic and Clinical Analysis of the AML Study Group. *J. Clin. Oncol.* **30**, 1350–1357 (2012).
23. Prassek, V. V. *et al.* Genetics of acute myeloid leukemia in the elderly: mutation spectrum and clinical impact in intensively treated patients aged ≥ 75 years. *Haematologica* haematol.2018.191536 (2018). doi:10.3324/haematol.2018.191536
24. Chou, W.-C. *et al.* *TET2* mutation is an unfavorable prognostic factor in acute myeloid leukemia patients with intermediate-risk cytogenetics. *Blood* **118**, 3803–3810 (2011).
25. Delhommeau, F. *et al.* Mutation in *TET2* in Myeloid Cancers. *N. Engl. J. Med.* **360**, 2289–2301 (2009).
26. Ernst, T. *et al.* Inactivating mutations of the histone methyltransferase gene *EZH2* in myeloid disorders. *Nat. Genet.* **42**, 722–726 (2010).
27. Ley, T. J. *et al.* *DNMT3A* Mutations in Acute Myeloid Leukemia. *N. Engl. J. Med.* **363**, 2424–2433 (2010).
28. Figueroa, M. E. *et al.* Leukemic *IDH1* and *IDH2* Mutations Result in a Hypermethylation Phenotype, Disrupt *TET2* Function, and Impair Hematopoietic Differentiation. *Cancer Cell* **18**, 553–567 (2010).
29. Rose, D. *et al.* Subtype-specific patterns of molecular mutations in acute myeloid leukemia. *Leukemia* **31**, 11–17 (2017).
30. Shih, A. H., Abdel-Wahab, O., Patel, J. P. & Levine, R. L. The role of mutations in epigenetic regulators in myeloid malignancies. *Nat. Rev. Cancer* **12**, 599–612 (2012).
31. Papaemmanuil, E. *et al.* Genomic Classification and Prognosis in Acute Myeloid Leukemia. *N. Engl. J. Med.* **374**, 2209–2221 (2016).
32. Cancer Genome Atlas Research Network *et al.* Genomic and Epigenomic Landscapes of Adult De Novo Acute Myeloid Leukemia. *N. Engl. J. Med.* **368**, 2059–2074 (2013).
33. Vassiliou, G. S. *et al.* Mutant nucleophosmin and cooperating pathways drive leukemia initiation and progression in mice. *Nat. Genet.* **43**, 470–475 (2011).
34. Wartman, L. D. *et al.* Sequencing a mouse acute promyelocytic leukemia genome reveals genetic events relevant for disease progression. *J. Clin. Invest.* **121**, 1445–1455 (2011).
35. Mupo, A. *et al.* A powerful molecular synergy between mutant Nucleophosmin and *Flt3-ITD* drives acute myeloid leukemia in mice. *Leukemia* **27**, 1917–20 (2013).
36. Grimwade, D., Ivey, A. & Huntly, B. J. P. Molecular landscape of acute myeloid leukemia in younger adults and its clinical relevance. *Blood* **127**, 29–42 (2016).
37. Döhner, H. *et al.* Diagnosis and management of acute myeloid leukemia in adults: recommendations from an international expert panel, on behalf of the European LeukemiaNet. *Blood* **115**, 453–474 (2010).
38. Döhner, K. *et al.* Mutant nucleophosmin (*NPM1*) predicts favorable prognosis in younger adults with acute myeloid leukemia and normal cytogenetics: interaction with other gene mutations. *Blood* **106**, 3740–6 (2005).
39. Thiede, C. *et al.* Prevalence and prognostic impact of *NPM1* mutations in 1485 adult patients with acute myeloid leukemia (AML). *Blood* **107**, 4011–20 (2006).
40. Nowell, P. C. The clonal evolution of tumor cell populations. *Science (80-.)*. **194**, 23–8 (1976).
41. Jaiswal, S. *et al.* Age-related clonal hematopoiesis associated with adverse outcomes. *N. Engl. J. Med.* **371**, 2488–98 (2014).
42. Young, A. L., Challen, G. A., Birmann, B. M. & Druley, T. E. Clonal haematopoiesis

- harbouring AML-associated mutations is ubiquitous in healthy adults. *Nat. Commun.* **7**, 12484 (2016).
43. Jan, M. *et al.* Clonal evolution of preleukemic hematopoietic stem cells precedes human acute myeloid leukemia. *Sci. Transl. Med.* **4**, 149ra118 (2012).
 44. Desai, P. *et al.* Somatic mutations precede acute myeloid leukemia years before diagnosis. *Nat. Med.* **24**, 1015–1023 (2018).
 45. Krönke, J. *et al.* Clonal evolution in relapsed NPM1-mutated acute myeloid leukemia. *Blood* **122**, 100–8 (2013).
 46. Shlush, L. I. *et al.* Identification of pre-leukaemic haematopoietic stem cells in acute leukaemia. *Nature* **506**, 328–33 (2014).
 47. Grove, C. S. & Vassiliou, G. S. Acute myeloid leukaemia: a paradigm for the clonal evolution of cancer? *Dis. Model. Mech.* **7**, 941–951 (2014).
 48. Greif, P. A. *et al.* Evolution of Cytogenetically Normal Acute Myeloid Leukemia During Therapy and Relapse: An Exome Sequencing Study of 50 Patients. *Clin. cancer Res.* **24**, 1716–1726 (2018).
 49. Rothenberg-Thurley, M. *et al.* Persistence of pre-leukemic clones during first remission and risk of relapse in acute myeloid leukemia. *Leukemia* **32**, 1598–1608 (2018).
 50. Anderson, K. *et al.* Genetic variegation of clonal architecture and propagating cells in leukaemia. *Nature* **469**, 356–361 (2011).
 51. Vick, B. *et al.* An Advanced Preclinical Mouse Model for Acute Myeloid Leukemia Using Patients' Cells of Various Genetic Subgroups and In Vivo Bioluminescence Imaging. *PLoS One* **10**, e0120925 (2015).
 52. Burnett, A., Wetzler, M. & Löwenberg, B. Therapeutic advances in acute myeloid leukemia. *J. Clin. Oncol.* **29**, 487–94 (2011).
 53. Fernandez, H. F. *et al.* Anthracycline Dose Intensification in Acute Myeloid Leukemia. *N. Engl. J. Med.* **361**, 1249–1259 (2009).
 54. Löwenberg, B. *et al.* High-Dose Daunorubicin in Older Patients with Acute Myeloid Leukemia. *N. Engl. J. Med.* **361**, 1235–1248 (2009).
 55. Lee, J.-H. *et al.* Prospective Randomized Comparison of Idarubicin and High-Dose Daunorubicin in Induction Chemotherapy for Newly Diagnosed Acute Myeloid Leukemia. *J. Clin. Oncol.* **35**, 2754–2763 (2017).
 56. Wang, J. *et al.* Meta-Analysis of Randomised Clinical Trials Comparing Idarubicin + Cytarabine with Daunorubicin + Cytarabine as the Induction Chemotherapy in Patients with Newly Diagnosed Acute Myeloid Leukaemia. *PLoS One* **8**, e60699 (2013).
 57. Patel, J. P. *et al.* Prognostic relevance of integrated genetic profiling in acute myeloid leukemia. *N. Engl. J. Med.* **366**, 1079–89 (2012).
 58. Cheson, B. D. *et al.* Revised Recommendations of the International Working Group for Diagnosis, Standardization of Response Criteria, Treatment Outcomes, and Reporting Standards for Therapeutic Trials in Acute Myeloid Leukemia. *J. Clin. Oncol.* **21**, 4642–4649 (2003).
 59. FDA granted regular approval to enasidenib for the treatment of relapsed or refractory AML. (2017). at <https://www.fda.gov/Drugs/InformationOnDrugs/ApprovedDrugs/ucm569482.htm>
 60. FDA approves ivosidenib for relapsed or refractory acute myeloid leukemia. (2018). at <https://www.fda.gov/Drugs/InformationOnDrugs/ApprovedDrugs/ucm614128.htm>
 61. Ding, L. *et al.* Clonal evolution in relapsed acute myeloid leukaemia revealed by whole-genome sequencing. *Nature* **481**, 506–10 (2012).
 62. Yeung, C. C. S. & Radich, J. Predicting Chemotherapy Resistance in AML. *Curr. Hematol.*

- Malig. Rep.* **12**, 530–536 (2017).
63. Godley, L. A. & Larson, R. A. Therapy-related myeloid leukemia. *Semin. Oncol.* **35**, 418–29 (2008).
 64. Wong, T. N. *et al.* Role of TP53 mutations in the origin and evolution of therapy-related acute myeloid leukaemia. *Nature* **518**, 552–555 (2015).
 65. Choi, S. *et al.* Relapse in children with acute lymphoblastic leukemia involving selection of a preexisting drug-resistant subclone. *Blood* **110**, 632–639 (2007).
 66. Parkin, B. *et al.* Clonal evolution and devolution after chemotherapy in adult acute myelogenous leukemia. *Blood* **121**, 369–77 (2013).
 67. Marin, J. J. G., Briz, O., Rodríguez-Macias, G., Díez-Martín, J. L. & Macias, R. I. R. Role of drug transport and metabolism in the chemoresistance of acute myeloid leukemia. *Blood Rev.* **30**, 55–64 (2016).
 68. Hu, X. F. *et al.* Altered multidrug resistance phenotype caused by anthracycline analogues and cytosine arabinoside in myeloid leukemia. *Blood* **93**, 4086–95 (1999).
 69. Hu, X. F. *et al.* Rapid up-regulation of *mdr1* expression by anthracyclines in a classical multidrug-resistant cell line. *Br. J. Cancer* **71**, 931–6 (1995).
 70. Pallis, M. & Russell, N. P-glycoprotein plays a drug-efflux-independent role in augmenting cell survival in acute myeloblastic leukemia and is associated with modulation of a sphingomyelin-ceramide apoptotic pathway. *Blood* **95**, 2897–904 (2000).
 71. Del Poeta, G. *et al.* Clinical relevance of P-glycoprotein expression in de novo acute myeloid leukemia. *Blood* **87**, 1997–2004 (1996).
 72. Senent, L. *et al.* P-glycoprotein expression and prognostic value in acute myeloid leukemia. *Haematologica* **83**, 783–7 (1998).
 73. Guerci, A. *et al.* Predictive value for treatment outcome in acute myeloid leukemia of cellular daunorubicin accumulation and P-glycoprotein expression simultaneously determined by flow cytometry. *Blood* **85**, 2147–53 (1995).
 74. Filipits, M. *et al.* Multidrug resistance-associated protein in acute myeloid leukemia: No impact on treatment outcome. *Clin. Cancer Res.* **3**, 1419–25 (1997).
 75. Wuchter, C. *et al.* Clinical significance of P-glycoprotein expression and function for response to induction chemotherapy, relapse rate and overall survival in acute leukemia. *Haematologica* **85**, 711–21 (2000).
 76. Kuwazuru, Y. *et al.* Expression of the multidrug transporter, P-glycoprotein, in acute leukemia cells and correlation to clinical drug resistance. *Cancer* **66**, 868–73 (1990).
 77. Tóthová, E. *et al.* P-glycoprotein expression in adult acute myeloid leukemia: correlation with induction treatment outcome. *Neoplasma* **48**, 393–7 (2001).
 78. Ino, T. *et al.* Expression of P-glycoprotein in de novo acute myelogenous leukemia at initial diagnosis: Results of molecular and functional assays, and correlation with treatment outcome. *Leukemia* **8**, (1994).
 79. Kasimir-Bauer, S. *et al.* Impact of the expression of P glycoprotein, the multidrug resistance-related protein, *bcl-2*, mutant *p53*, and heat shock protein 27 on response to induction therapy and long-term survival in patients with de novo acute myeloid leukemia. *Exp. Hematol.* **30**, 1302–8 (2002).
 80. Hopper-Borge, E. *et al.* Human Multidrug Resistance Protein 7 (ABCC10) Is a Resistance Factor for Nucleoside Analogues and Etoposide. *Cancer Res.* **69**, 178–184 (2009).
 81. Guo, Y. *et al.* Expression of ABCC-Type Nucleotide Exporters in Blasts of Adult Acute Myeloid Leukemia: Relation to Long-term Survival. *Clin. Cancer Res.* **15**, 1762–1769 (2009).
 82. Hubeek, I. *et al.* The human equilibrative nucleoside transporter 1 mediates in vitro

- cytarabine sensitivity in childhood acute myeloid leukaemia. *Br. J. Cancer* **93**, 1388–94 (2005).
83. Abraham, A. *et al.* RNA expression of genes involved in cytarabine metabolism and transport predicts cytarabine response in acute myeloid leukemia. *Pharmacogenomics* **16**, 877–890 (2015).
 84. Galmarini, C. M. *et al.* In vivo mechanisms of resistance to cytarabine in acute myeloid leukaemia. *Br. J. Haematol.* **117**, 860–8 (2002).
 85. Lamba, J. K. Genetic factors influencing cytarabine therapy. *Pharmacogenomics* **10**, 1657–74 (2009).
 86. McLornan, D. P., McMullin, M. F., Johnston, P. & Longley, D. B. Molecular mechanisms of drug resistance in acute myeloid leukaemia. *Expert Opin. Drug Metab. Toxicol.* **3**, 363–377 (2007).
 87. Song, J. H. *et al.* Defective expression of deoxycytidine kinase in cytarabine-resistant acute myeloid leukemia cells. *Int. J. Oncol.* **34**, 1165–71 (2009).
 88. Rathe, S. K. *et al.* Using RNA-seq and targeted nucleases to identify mechanisms of drug resistance in acute myeloid leukemia. *Sci. Rep.* **4**, 6048 (2014).
 89. Galmarini, C. M. *et al.* Deoxycytidine kinase and cN-II nucleotidase expression in blast cells predict survival in acute myeloid leukaemia patients treated with cytarabine. *Br. J. Haematol.* **122**, 53–60 (2003).
 90. Galmarini, C. M. *et al.* Expression of high Km 5'-nucleotidase in leukemic blasts is an independent prognostic factor in adults with acute myeloid leukemia. *Blood* **98**, 1922–6 (2001).
 91. Schneider, C. *et al.* SAMHD1 is a biomarker for cytarabine response and a therapeutic target in acute myeloid leukemia. *Nat. Med.* **23**, 250–255 (2017).
 92. Herold, N. *et al.* Targeting SAMHD1 with the Vpx protein to improve cytarabine therapy for hematological malignancies. *Nat. Med.* **23**, 256–263 (2017).
 93. Megias-Vericat, J. E. *et al.* Pharmacogenetics of Metabolic Genes of Anthracyclines in Acute Myeloid Leukemia. *Curr. Drug Metab.* **19**, 55–74 (2018).
 94. Megias-Vericat, J. E. *et al.* Influence of cytarabine metabolic pathway polymorphisms in acute myeloid leukemia induction treatment. *Leuk. Lymphoma* **58**, 2880–2894 (2017).
 95. Kim, J. H. *et al.* SLC29A1 (ENT1) polymorphisms and outcome of complete remission in acute myeloid leukemia. *Cancer Chemother. Pharmacol.* **78**, 533–540 (2016).
 96. Wan, H. *et al.* SLC29A1 single nucleotide polymorphisms as independent prognostic predictors for survival of patients with acute myeloid leukemia: an in vitro study. *J. Exp. Clin. Cancer Res.* **33**, 90 (2014).
 97. McKenna, S. L. Multidrug resistance in leukaemia. *Br. J. Haematol.* **96**, 659–674 (1997).
 98. Matsunaga, T. *et al.* Interaction between leukemic-cell VLA-4 and stromal fibronectin is a decisive factor for minimal residual disease of acute myelogenous leukemia. *Nat. Med.* **9**, 1158–65 (2003).
 99. Matsunaga, T. *et al.* Combination therapy of an anticancer drug with the FNIII14 peptide of fibronectin effectively overcomes cell adhesion-mediated drug resistance of acute myelogenous leukemia. *Leukemia* **22**, 353–360 (2008).
 100. Becker, P. S. *et al.* Very late antigen-4 function of myeloblasts correlates with improved overall survival for patients with acute myeloid leukemia. *Blood* **113**, 866–874 (2009).
 101. Hazlehurst, L. A. *et al.* Reduction in drug-induced DNA double-strand breaks associated with beta1 integrin-mediated adhesion correlates with drug resistance in U937 cells. *Blood* **98**, 1897–903 (2001).
 102. Hazlehurst, L. A. *et al.* Cell Adhesion to Fibronectin (CAM-DR) Influences Acquired

- Mitoxantrone Resistance in U937 Cells. *Cancer Res.* **66**, 2338–2345 (2006).
103. Berger, S., Kouzarides, T., Shiekhattar, R. & Shilatifard, A. An operational definition of epigenetics. *Genes Dev.* **23**, 781–783 (2009).
 104. Albert, M. & Helin, K. Histone methyltransferases in cancer. *Semin. Cell Dev. Biol.* **21**, 209–220 (2010).
 105. Kornberg, R. D. Chromatin structure: a repeating unit of histones and DNA. *Science (80-)*. **184**, 868–71 (1974).
 106. McGhee, J. D. & Felsenfeld, G. Nucleosome Structure. *Annu. Rev. Biochem.* **49**, 1115–1156 (1980).
 107. Luger, K., Mäder, A. W., Richmond, R. K., Sargent, D. F. & Richmond, T. J. Crystal structure of the nucleosome core particle at 2.8 Å resolution. *Nature* **389**, 251–260 (1997).
 108. Richmond, T. J. & Davey, C. A. The structure of DNA in the nucleosome core. *Nature* **423**, 145–150 (2003).
 109. Thoma, F., Koller, T. & Klug, A. Involvement of histone H1 in the organization of the nucleosome and of the salt-dependent superstructures of chromatin. *J. Cell Biol.* **83**, 403–27 (1979).
 110. Graziano, V., Gerchman, S. E., Schneider, D. K. & Ramakrishnan, V. Histone H1 is located in the interior of the chromatin 30-nm filament. *Nature* **368**, 351–354 (1994).
 111. Strahl, B. & Allis, C. The language of covalent histone modifications. *Nature* **403**, 41–45 (2000).
 112. Varier, R. A. & Timmers, H. T. M. Histone lysine methylation and demethylation pathways in cancer. *Biochim. Biophys. Acta - Rev. Cancer* **1815**, 75–89 (2011).
 113. Rojas, J. R. *et al.* Structure of Tetrahymena GCN5 bound to coenzyme A and a histone H3 peptide. *Nature* **401**, 93–98 (1999).
 114. Dong, K. B. *et al.* DNA methylation in ES cells requires the lysine methyltransferase G9a but not its catalytic activity. *EMBO J.* **27**, 2691–2701 (2008).
 115. Tachibana, M., Matsumura, Y., Fukuda, M., Kimura, H. & Shinkai, Y. G9a/GLP complexes independently mediate H3K9 and DNA methylation to silence transcription. *EMBO J.* **27**, 2681–2690 (2008).
 116. Shi, L., Wen, H. & Shi, X. The Histone Variant H3.3 in Transcriptional Regulation and Human Disease. *J. Mol. Biol.* **429**, 1934–1945 (2017).
 117. Bagot, R. C., Labonté, B., Pena, C. J. & Nestler, E. J. Epigenetic signaling in psychiatric disorders: stress and depression. *Dialogues Clin. Neurosci.* **3**, (2014).
 118. Chen, P. *et al.* H3.3 actively marks enhancers and primes gene transcription via opening higher-ordered chromatin. *Genes Dev.* **27**, 2109–2124 (2013).
 119. Barski, A. *et al.* High-Resolution Profiling of Histone Methylations in the Human Genome. *Cell* **129**, 823–837 (2007).
 120. Bernstein, B. E. *et al.* A Bivalent Chromatin Structure Marks Key Developmental Genes in Embryonic Stem Cells. *Cell* **125**, 315–326 (2006).
 121. Voigt, P., Tee, W.-W. & Reinberg, D. A double take on bivalent promoters. *Genes Dev.* **27**, 1318–38 (2013).
 122. McGrath, J. & Trojer, P. Targeting histone lysine methylation in cancer. *Pharmacol. Ther.* **150**, 1–22 (2015).
 123. Chittock, E. C., Latwiel, S., Miller, T. C. R. & Müller, C. W. Molecular architecture of polycomb repressive complexes. *Biochem. Soc. Trans.* **45**, 193–205 (2017).
 124. Hauri, S. *et al.* A High-Density Map for Navigating the Human Polycomb Complexome. *Cell Rep.* **17**, 583–595 (2016).
 125. Ciferri, C. *et al.* Molecular architecture of human polycomb repressive complex 2. *Elife* **1**,

- e00005 (2012).
126. Cao, R. & Zhang, Y. SUZ12 Is Required for Both the Histone Methyltransferase Activity and the Silencing Function of the EED-EZH2 Complex. *Mol. Cell* **15**, 57–67 (2004).
 127. Chase, A. & Cross, N. C. P. Aberrations of EZH2 in Cancer. *Clin. Cancer Res.* **17**, 2613–2618 (2011).
 128. Khan, S. N. *et al.* Multiple mechanisms deregulate EZH2 and histone H3 lysine 27 epigenetic changes in myeloid malignancies. *Leukemia* **27**, 1301–1309 (2013).
 129. Heard, E. Delving into the diversity of facultative heterochromatin: the epigenetics of the inactive X chromosome. *Curr. Opin. Genet. Dev.* **15**, 482–489 (2005).
 130. Martinez, A.-M. & Cavalli, G. The role of Polycomb Group Proteins in Cell Cycle Regulation During Development. *Cell Cycle* **5**, 1189–1197 (2006).
 131. Schwartzenuber, J. *et al.* Driver mutations in histone H3.3 and chromatin remodelling genes in paediatric glioblastoma. *Nature* **482**, 226–231 (2012).
 132. Lewis, P. W. *et al.* Inhibition of PRC2 Activity by a Gain-of-Function H3 Mutation Found in Pediatric Glioblastoma. *Science (80-)*. **340**, 857–861 (2013).
 133. Justin, N. *et al.* Structural basis of oncogenic histone H3K27M inhibition of human polycomb repressive complex 2. *Nat. Commun.* **7**, 11316 (2016).
 134. Shi, Y. *et al.* Histone demethylation mediated by the nuclear amine oxidase homolog LSD1. *Cell* **119**, 941–53 (2004).
 135. Janardhan, A. *et al.* Prominent role of histone lysine demethylases in cancer epigenetics and therapy. *Oncotarget* **9**, 34429–34448 (2018).
 136. Dimitrova, E., Turberfield, A. H. & Klose, R. J. Histone demethylases in chromatin biology and beyond. *EMBO Rep.* **16**, 1620–1639 (2015).
 137. Huang, J. *et al.* p53 is regulated by the lysine demethylase LSD1. *Nature* **449**, 105–8 (2007).
 138. Lu, T. *et al.* Regulation of NF-kappaB by NSD1/FBXL11-dependent reversible lysine methylation of p65. *Proc. Natl. Acad. Sci. U. S. A.* **107**, 46–51 (2010).
 139. Lu, L. *et al.* Kdm2a/b Lysine Demethylases Regulate Canonical Wnt Signaling by Modulating the Stability of Nuclear β -Catenin. *Dev. Cell* **33**, 660–74 (2015).
 140. Biggar, K. K. & Li, S. S.-C. Non-histone protein methylation as a regulator of cellular signalling and function. *Nat. Rev. Mol. Cell Biol.* **16**, 5–17 (2015).
 141. Yan, M., Yang, X., Wang, H. & Shao, Q. The critical role of histone lysine demethylase KDM2B in cancer. *Am. J. Transl. Res.* **10**, 2222–2233 (2018).
 142. Hosseini, A. & Minucci, S. A comprehensive review of lysine-specific demethylase 1 and its roles in cancer. *Epigenomics* **9**, 1123–1142 (2017).
 143. Shigekawa, Y. *et al.* Overexpression of KDM5B/JARID1B is associated with poor prognosis in hepatocellular carcinoma. *Oncotarget* **9**, 34320–34335 (2018).
 144. Lee, K.-H. *et al.* Histone demethylase KDM7A controls androgen receptor activity and tumor growth in prostate cancer. *Int. J. Cancer* (2018). doi:10.1002/ijc.31843
 145. van Haaften, G. *et al.* Somatic mutations of the histone H3K27 demethylase gene UTX in human cancer. *Nat. Genet.* **41**, 521–3 (2009).
 146. Hayami, S. *et al.* Overexpression of LSD1 contributes to human carcinogenesis through chromatin regulation in various cancers. *Int. J. Cancer* **128**, 574–586 (2011).
 147. Dang, L., Jin, S. & Su, S. M. IDH mutations in glioma and acute myeloid leukemia. *Trends Mol. Med.* **16**, 387–397 (2010).
 148. Agger, K. *et al.* UTX and JMJD3 are histone H3K27 demethylases involved in HOX gene regulation and development. *Nature* **449**, 731–734 (2007).
 149. Min, G. L. *et al.* Demethylation of H3K27 regulates polycomb recruitment and H2A

- ubiquitination. *Science (80-.)*. **318**, 447–450 (2007).
150. Hong, S. *et al.* Identification of JmjC domain-containing UTX and JMJD3 as histone H3 lysine 27 demethylases. *Proc. Natl. Acad. Sci.* **104**, 18439–18444 (2007).
 151. Lan, F. *et al.* A histone H3 lysine 27 demethylase regulates animal posterior development. *Nature* **449**, 689–694 (2007).
 152. Greenfield, A. *et al.* The UTX gene escapes X inactivation in mice and humans. *Hum. Mol. Genet.* **7**, 737–742 (1998).
 153. Van der Meulen, J. *et al.* The H3K27me3 demethylase UTX is a gender-specific tumor suppressor in T-cell acute lymphoblastic leukemia. *Blood* **125**, 13–22 (2015).
 154. Xu, J., Deng, X., Watkins, R. & Distèche, C. M. Sex-Specific Differences in Expression of Histone Demethylases Utx and Uty in Mouse Brain and Neurons. *J. Neurosci.* **28**, 4521–4527 (2008).
 155. Walport, L. J. *et al.* Human UTY(KDM6C) Is a Male-specific N^ε-Methyl Lysyl Demethylase. *J. Biol. Chem.* **289**, 18302–18313 (2014).
 156. Shpargel, K. B., Sengoku, T., Yokoyama, S. & Magnuson, T. UTX and UTY Demonstrate Histone Demethylase-Independent Function in Mouse Embryonic Development. *PLoS Genet.* **8**, e1002964 (2012).
 157. Liu, W. *et al.* IBS: an illustrator for the presentation and visualization of biological sequences. *Bioinformatics* **31**, 3359–3361 (2015).
 158. Froimchuk, E., Jang, Y. & Ge, K. Histone H3 lysine 4 methyltransferase KMT2D. *Gene* **627**, 337–342 (2017).
 159. Issaeva, I. *et al.* Knockdown of ALR (MLL2) reveals ALR target genes and leads to alterations in cell adhesion and growth. *Mol. Cell. Biol.* **27**, 1889–903 (2007).
 160. Lai, B. *et al.* MLL3/MLL4 are required for CBP/p300 binding on enhancers and super-enhancer formation in brown adipogenesis. *Nucleic Acids Res.* **45**, 6388–6403 (2017).
 161. Wang, C. *et al.* Enhancer priming by H3K4 methyltransferase MLL4 controls cell fate transition. *Proc. Natl. Acad. Sci. U. S. A.* **113**, 11871–11876 (2016).
 162. Calo, E. & Wysocka, J. Modification of Enhancer Chromatin: What, How, and Why? *Mol. Cell* **49**, 825–837 (2013).
 163. Kim, D.-H. *et al.* Histone H3K27 Trimethylation Inhibits H3 Binding and Function of SET1-Like H3K4 Methyltransferase Complexes. *Mol. Cell. Biol.* **33**, 4936–4946 (2013).
 164. Jang, Y., Wang, C., Zhuang, L., Liu, C. & Ge, K. H3K4 Methyltransferase Activity Is Required for MLL4 Protein Stability. *J. Mol. Biol.* **429**, 2046–2054 (2017).
 165. Lee, S., Lee, J. W. & Lee, S.-K. UTX, a histone H3-lysine 27 demethylase, acts as a critical switch to activate the cardiac developmental program. *Dev. Cell* **22**, 25–37 (2012).
 166. Welstead, G. G. *et al.* X-linked H3K27me3 demethylase Utx is required for embryonic development in a sex-specific manner. *Proc. Natl. Acad. Sci.* **109**, 13004–13009 (2012).
 167. Wang, C. *et al.* UTX regulates mesoderm differentiation of embryonic stem cells independent of H3K27 demethylase activity. *Proc. Natl. Acad. Sci.* **109**, 15324–15329 (2012).
 168. Thieme, S. *et al.* The histone demethylase UTX regulates stem cell migration and hematopoiesis. *Blood* **121**, 2462–2473 (2013).
 169. Liu, J. *et al.* A functional role for the histone demethylase UTX in normal and malignant hematopoietic cells. *Exp. Hematol.* **40**, 487–498.e3 (2012).
 170. Zheng, L. *et al.* Utx loss causes myeloid transformation. *Leukemia* **32**, 1458–1465 (2018).
 171. Copur, Ö. & Müller, J. The histone H3-K27 demethylase Utx regulates HOX gene expression in Drosophila in a temporally restricted manner. *Development* **140**, 3478–85 (2013).

172. Seenundun, S. *et al.* UTX mediates demethylation of H3K27me3 at muscle-specific genes during myogenesis. *EMBO J.* **29**, 1401–11 (2010).
173. Wang, J. K. *et al.* The histone demethylase UTX enables RB-dependent cell fate control. *Genes Dev.* **24**, 327–32 (2010).
174. Lederer, D. *et al.* Deletion of KDM6A, a histone demethylase interacting with MLL2, in three patients with Kabuki syndrome. *Am. J. Hum. Genet.* **90**, 119–24 (2012).
175. Miyake, N. *et al.* KDM6A Point Mutations Cause Kabuki Syndrome. *Hum. Mutat.* **34**, 108–110 (2013).
176. Miyake, N. *et al.* MLL2 and KDM6A mutations in patients with Kabuki syndrome. *Am. J. Med. Genet. Part A* **161**, 2234–2243 (2013).
177. Cheon, C. K. *et al.* Identification of KMT2D and KDM6A mutations by exome sequencing in Korean patients with Kabuki syndrome. *J. Hum. Genet.* **59**, 321–325 (2014).
178. Hannibal, M. C. *et al.* Spectrum of MLL2 (ALR) mutations in 110 cases of Kabuki syndrome. *Am. J. Med. Genet. Part A* **155**, 1511–1516 (2011).
179. Li, Y. *et al.* A mutation screen in patients with Kabuki syndrome. *Hum. Genet.* **130**, 715–724 (2011).
180. Ng, S. B. *et al.* Exome sequencing identifies MLL2 mutations as a cause of Kabuki syndrome. *Nat. Genet.* **42**, 790–793 (2010).
181. Cheon, C.-K. & Ko, J. M. Kabuki syndrome: clinical and molecular characteristics. *Korean J. Pediatr.* **58**, 317–24 (2015).
182. Van der Meulen, J., Speleman, F. & Van Vlierberghe, P. The H3K27me3 demethylase UTX in normal development and disease. *Epigenetics* **9**, 658–68 (2014).
183. Ross, J. S. *et al.* Genomic profiling of advanced-stage, metaplastic breast carcinoma by next-generation sequencing reveals frequent, targetable genomic abnormalities and potential new treatment options. *Arch. Pathol. Lab. Med.* **139**, 642–649 (2015).
184. Nickerson, M. L. *et al.* Concurrent alterations in TERT, KDM6A, and the BRCA pathway in bladder cancer. *Clin. Cancer Res.* **20**, 4935–4948 (2014).
185. Huether, R. *et al.* The landscape of somatic mutations in epigenetic regulators across 1,000 paediatric cancer genomes. *Nat. Commun.* **5**, 1–7 (2014).
186. Lawrence, M. S. *et al.* Discovery and saturation analysis of cancer genes across 21 tumour types. *Nature* **505**, 495–501 (2014).
187. Poon, S. L. *et al.* Genome-wide mutational signatures of aristolochic acid and its application as a screening tool. *Sci. Transl. Med.* **5**, 197–101 (2013).
188. Waddell, N. *et al.* Whole genomes redefine the mutational landscape of pancreatic cancer. *Nature* **518**, 495–501 (2015).
189. Ler, L. D. *et al.* Loss of tumor suppressor KDM6A amplifies PRC2-regulated transcriptional repression in bladder cancer and can be targeted through inhibition of EZH2. *Sci. Transl. Med.* **9**, 1–14 (2017).
190. Ho, A. S. *et al.* The mutational landscape of adenoid cystic carcinoma. *Nat. Genet.* **45**, 791–8 (2013).
191. Pawlyn, C. *et al.* The Spectrum and Clinical Impact of Epigenetic Modifier Mutations in Myeloma. *Clin. Cancer Res.* **22**, 5783–5794 (2016).
192. Bolli, N. *et al.* Characterization of gene mutations and copy number changes in acute myeloid leukemia using a rapid target enrichment protocol. *Haematologica* **100**, 214–222 (2015).
193. Spinella, J.-F. *et al.* Genomic characterization of pediatric T-cell acute lymphoblastic leukemia reveals novel recurrent driver mutations. *Oncotarget* **7**, (2016).
194. Mar, B. G. *et al.* Sequencing histone-modifying enzymes identifies UTX mutations in acute

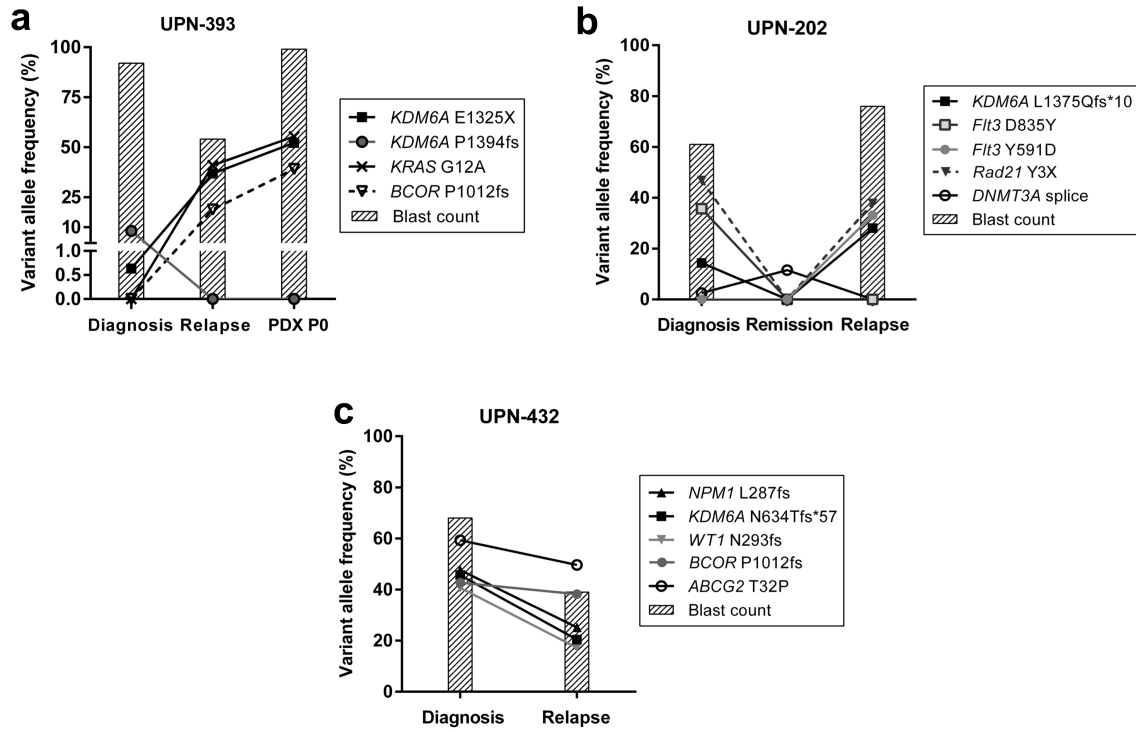
- lymphoblastic leukemia. *Leukemia* **26**, 1881–3 (2012).
195. Jankowska, A. M. *et al.* Mutational spectrum analysis of chronic myelomonocytic leukemia includes genes associated with epigenetic regulation: UTX, EZH2, and DNMT3A. *Blood* **118**, 3932–41 (2011).
 196. Andricovich, J. *et al.* Loss of KDM6A Activates Super-Enhancers to Induce Gender-Specific Squamous-like Pancreatic Cancer and Confers Sensitivity to BET Inhibitors. *Cancer Cell* **33**, 512–526.e8 (2018).
 197. Gozdecka, M. *et al.* UTX-mediated enhancer and chromatin remodeling suppresses myeloid leukemogenesis through noncatalytic inverse regulation of ETS and GATA programs. *Nat. Genet.* **50**, 883–894 (2018).
 198. Dobin, A. *et al.* STAR: ultrafast universal RNA-seq aligner. *Bioinformatics* **29**, 15–21 (2013).
 199. Soumillon, M., Cacchiarelli, D., Semrau, S., van Oudenaarden, A., Mikkelsen, T. . Characterization of directed differentiation by highthroughput single-cell RNA-seq. *bioRxiv* (2014).
 200. Parekh, S., Ziegenhain, C., Vieth, B., Enard, W. & Hellmann, I. zUMIs - A fast and flexible pipeline to process RNA sequencing data with UMIs. *Gigascience* **7**, (2018).
 201. Ritchie, M. E. *et al.* limma powers differential expression analyses for RNA-sequencing and microarray studies. *Nucleic Acids Res.* **43**, e47 (2015).
 202. Robinson, M. D., McCarthy, D. J. & Smyth, G. K. edgeR: a Bioconductor package for differential expression analysis of digital gene expression data. *Bioinformatics* **26**, 139–40 (2010).
 203. Wermke, M. *et al.* RNAi profiling of primary human AML cells identifies ROCK1 as a therapeutic target and nominates fasudil as an antileukemic drug. *Blood* **125**, 3760–3768 (2015).
 204. Bonnet, D. in *Current Protocols in Stem Cell Biology* **Chapter 3**, Unit 3.2 (John Wiley & Sons, Inc., 2008).
 205. Terziyska, N. *et al.* In vivo imaging enables high resolution preclinical trials on patients' leukemia cells growing in mice. *PLoS One* **7**, e52798 (2012).
 206. Ebinger, S. *et al.* Characterization of Rare, Dormant, and Therapy-Resistant Cells in Acute Lymphoblastic Leukemia. *Cancer Cell* **30**, 849–862 (2016).
 207. Mulholland, C. B. *et al.* A modular open platform for systematic functional studies under physiological conditions. *Nucleic Acids Res.* **43**, (2015).
 208. Bradford, M. M. A rapid and sensitive method for the quantitation of microgram quantities of protein utilizing the principle of protein-dye binding. *Anal. Biochem.* **72**, 248–54 (1976).
 209. Ziegler-Heitbrock, H. W. *et al.* Establishment of a human cell line (Mono Mac 6) with characteristics of mature monocytes. *Int. J. cancer* **41**, 456–61 (1988).
 210. Early, A. P., Preisler, H. D., Slocum, H. & Rustum, Y. M. A pilot study of high-dose 1-beta-D-arabinofuranosylcytosine for acute leukemia and refractory lymphoma: clinical response and pharmacology. *Cancer Res.* **42**, 1587–94 (1982).
 211. MacLeod, R. A., Voges, M. & Drexler, H. G. Mono Mac 6: a mature monoblastic leukemia cell line with t(9;11)(p21;q23). *Blood* **82**, 3221–2 (1993).
 212. Subramaniana, A. *et al.* Gene set enrichment analysis: A knowledge-based approach for interpreting genome-wide expression profiles. *Proc. Natl. Acad. Sci.* **102**, 15545–15550 (2005).
 213. Pastor-Anglada, M. & Perez-Torras, S. Nucleoside transporter proteins as biomarkers of drug responsiveness and drug targets. *Front. Pharmacol.* **6**, (2015).
 214. Sengoku, T. & Yokoyama, S. Structural basis for histone H3 Lys 27 demethylation by

- UTX/KDM6A. *Genes Dev.* **25**, 2266–2277 (2011).
215. Xiao, H. *et al.* Mutations in epigenetic regulators are involved in acute lymphoblastic leukemia relapse following allogeneic hematopoietic stem cell transplantation. *Oncotarget* **7**, 2696–708 (2016).
216. Mar, B. G. *et al.* Mutations in epigenetic regulators including SETD2 are gained during relapse in paediatric acute lymphoblastic leukaemia. *Nat. Commun.* **5**, 3469 (2014).
217. Ribera, J. *et al.* Copy number profiling of adult relapsed B-cell precursor acute lymphoblastic leukemia reveals potential leukemia progression mechanisms. *Genes, Chromosom. Cancer* **56**, 810–820 (2017).
218. Audenet, F. *et al.* Clonal relatedness and mutational differences between upper tract and bladder urothelial carcinoma. *Clin. Cancer Res.* (2018). doi:10.1158/1078-0432.CCR-18-2039
219. Li, X. *et al.* UTX is an escape from X-inactivation tumor-suppressor in B cell lymphoma. *Nat. Commun.* **9**, 2720 (2018).
220. Duijf, P. H. G., Schultz, N. & Benezra, R. Cancer cells preferentially lose small chromosomes. *Int. J. cancer* **132**, 2316–26 (2013).
221. Göllner, S. *et al.* Loss of the histone methyltransferase EZH2 induces resistance to multiple drugs in acute myeloid leukemia. *Nat. Med.* **23**, 69–78 (2017).
222. Levis, M. FLT3 mutations in acute myeloid leukemia: what is the best approach in 2013? *Hematology* **2013**, 220–226 (2013).
223. Rücker, F. G. *et al.* TP53 alterations in acute myeloid leukemia with complex karyotype correlate with specific copy number alterations, monosomal karyotype, and dismal outcome. *Blood* **119**, 2114–2121 (2012).
224. Schnittger, S. *et al.* RUNX1 mutations are frequent in de novo AML with noncomplex karyotype and confer an unfavorable prognosis. *Blood* **117**, 2348–2357 (2011).
225. Gaidzik, V. *et al.* RUNX1 mutations in acute myeloid leukemia are associated with distinct clinico-pathologic and genetic features. *Leukemia* **30**, 2160–2168 (2016).
226. Löwenberg, B. *et al.* Cytarabine Dose for Acute Myeloid Leukemia. *N. Engl. J. Med.* **364**, 1027–1036 (2011).
227. Hummel-Eisenbeiss, J. *et al.* The role of human equilibrative nucleoside transporter 1 on the cellular transport of the DNA methyltransferase inhibitors 5-azacytidine and CP-4200 in human leukemia cells. *Mol. Pharmacol.* **84**, 438–50 (2013).
228. Macanas-Pirard, P. *et al.* Resistance of leukemia cells to cytarabine chemotherapy is mediated by bone marrow stroma, involves cell-surface equilibrative nucleoside transporter-1 removal and correlates with patient outcome. *Oncotarget* **8**, 23073–23086 (2017).
229. Jez, J. M., Bennett, M. J., Schlegel, B. P., Lewis, M. & Penning, T. M. Comparative anatomy of the aldo-keto reductase superfamily. *Biochem. J.* **326**, 625–36 (1997).
230. Barski, O. A., Tipparaju, S. M. & Bhatnagar, A. The aldo-keto reductase superfamily and its role in drug metabolism and detoxification. *Drug Metab. Rev.* **40**, 553–624 (2008).
231. Zeng, C.-M. *et al.* Aldo-Keto Reductase AKR1C1-AKR1C4: Functions, Regulation, and Intervention for Anti-cancer Therapy. *Front. Pharmacol.* **8**, (2017).
232. Deng, H. B., Parekh, H. K., Chow, K.-C. & Simpkins, H. Increased Expression of Dihydrodiol Dehydrogenase Induces Resistance to Cisplatin in Human Ovarian Carcinoma Cells. *J. Biol. Chem.* **277**, 15035–15043 (2002).
233. Matsunaga, T. *et al.* Pathophysiological roles of aldo-keto reductases (AKR1C1 and AKR1C3) in development of cisplatin resistance in human colon cancers. *Chem. Biol. Interact.* **202**, 234–242 (2013).

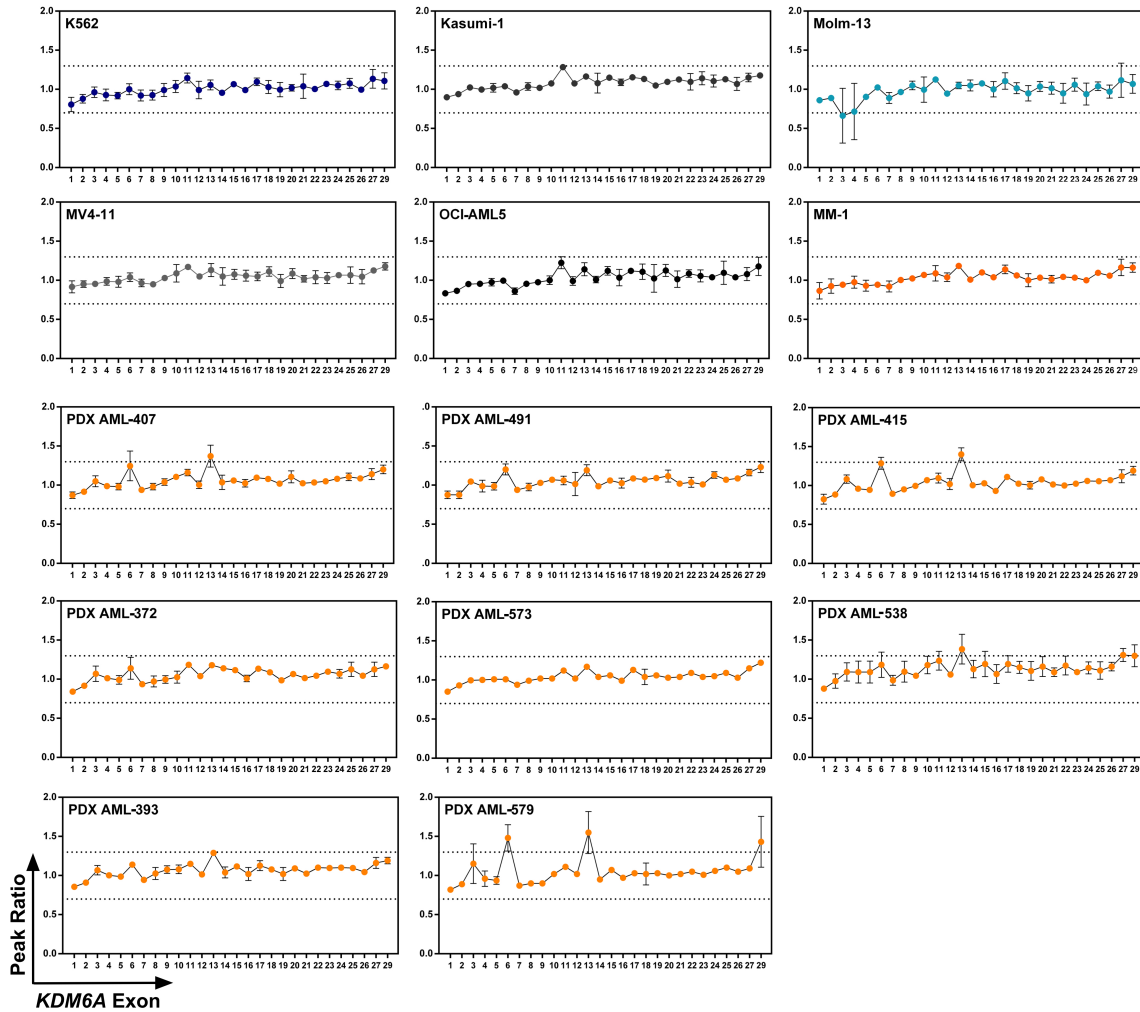
234. Matsunaga, T. *et al.* Induction of aldo-keto reductases (AKR1C1 and AKR1C3) abolishes the efficacy of daunorubicin chemotherapy for leukemic U937 cells. *Anticancer. Drugs* **25**, 868–877 (2014).
235. Bauman, D. R. *et al.* Development of Nonsteroidal Anti-Inflammatory Drug Analogs and Steroid Carboxylates Selective for Human Aldo-Keto Reductase Isoforms: Potential Antineoplastic Agents That Work Independently of Cyclooxygenase Isozymes. *Mol. Pharmacol.* **67**, 60–68 (2005).

8 Annex

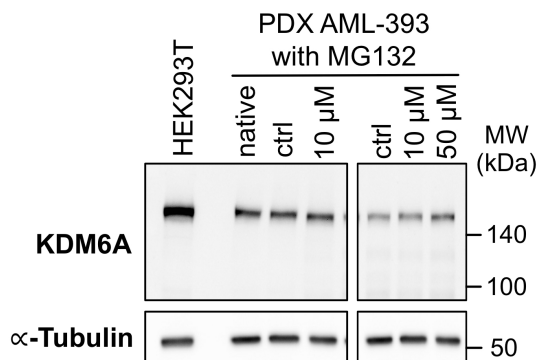
8.1 Supplementary Figures



Supplementary Figure 1 Evolutionary patterns during progression of AML. a,b,c, VAF plots for different evolutionary patterns observed from diagnosis to relapse in three AML patients. Bars represent the blast count and each line represents one mutation. In addition, for patient UPN-393 (a) VAFs of the PDX sample from passage 0 (P0) and for UPN-202 (b) VAFs of a remission sample are shown.



Supplementary Figure 2 *KDM6A* exon deletions in AML cell lines and AML PDX samples identified. The peak ratio for each *KDM6A* exon specific probe, detected by quantitative MLPA analysis, is shown. Results for 6/40 of the investigated myeloid cell lines (summarized in Table 8) and 8/8 PDX AML cells are shown. Additionally six cell lines are shown in Figure 15. The area of a normal peak ratio lies within the two dotted lines and ranges from 0.7 to 1.3. Mean \pm s.d. are given for at least two independent experiments.



Supplementary Figure 3 *In vitro* analysis of the *KDM6A* mutant E1325X in PDX AML-393 cells regarding proteasomal degradation. Immunoblot showing *KDM6A* expression in *KDM6A* mutant PDX AML-393 cells after treatment with the proteasomal inhibitor MG132 for 6 hours. MW, molecular weight; α -Tubulin, loading control.

8.2 Supplementary Table

Supplementary Table 1 Summary of 112 differential expressed genes in KDM6A silenced cells. The \log_2 fold changes and the respective \log_{10} P -values are listed for each of the 112 differentially expressed genes found in all three KDM6A silenced K562 cells compared to controls: shKDM6A #7_shGFP, KDM6A KO #1_WT #1 and KDM6A KO #2_WT #1 ($P < 0.05$).

Gene Name	shKDM6A #7_shGFP		KDM6A KO #1_WT #1		KDM6A KO #2_WT #1	
	\log_2 FC	\log_{10} P -value	\log_2 FC	\log_{10} P -value	\log_2 FC	\log_{10} P -value
AC004233.3	-0.77	-3.43	-1.10	-2.96	-1.22	-3.32
AC010327.1	-0.71	-3.13	-0.64	-5.06	-0.86	-7.37
AC090409.1	0.79	-4.26	0.71	-10.11	0.58	-7.31
ADAM8	-1.58	-3.05	-2.05	-5.43	-1.76	-4.68
ADTRP	-0.75	-3.97	-2.33	-9.44	-1.39	-6.38
AIF1	-2.73	-8.03	-2.09	-8.13	-2.23	-7.92
AIM2	2.34	-6.41	1.27	-3.95	1.28	-3.96
AKR1C1	1.13	-8.30	0.98	-9.03	1.50	-16.18
AKR1C2	0.97	-5.00	1.34	-8.89	1.38	-9.14
AMHR2	-0.86	-4.62	-1.13	-11.71	-1.30	-13.15
ANXA6	-0.64	-4.27	-1.36	-10.68	-0.87	-6.42
APOBR	-0.96	-3.41	-0.97	-3.89	-1.71	-6.96
AREG	1.20	-8.43	0.98	-5.89	0.97	-5.63
ARHGDI3	-0.46	-4.75	-1.16	-16.20	-1.28	-17.45
ARHGGEF6	-1.03	-6.39	-1.50	-6.67	-1.38	-6.08
B2M	-0.39	-5.65	-0.23	-2.81	-0.26	-3.43
C12orf75	1.49	-6.11	1.28	-7.95	0.86	-4.03
C1orf54	-0.72	-3.23	-1.19	-11.47	-1.18	-11.11
C1orf61	-1.01	-6.36	-0.96	-7.54	-1.47	-11.72
C9orf47	2.77	-6.06	2.26	-3.83	3.02	-6.40
CALB1	2.32	-6.11	3.47	-30.62	3.13	-27.47
CAPG	-1.35	-6.74	-0.87	-6.52	-0.82	-5.92
CAVI	1.63	-3.76	2.78	-15.61	2.31	-11.91
CCDC74A	2.18	-3.06	1.14	-4.42	2.50	-15.75
CCND1	0.88	-4.05	0.85	-6.67	0.97	-8.06
CCND2	-0.57	-4.82	-0.88	-9.37	-1.67	-16.77
CD36	2.05	-4.33	4.91	-15.14	3.35	-8.55
CD37	-1.71	-6.79	-2.01	-6.87	-2.32	-7.23
CD3D	-0.83	-3.76	-0.77	-4.36	-1.46	-9.62
CD52	-0.95	-7.28	-0.89	-7.13	-1.18	-9.89
CD53	-1.24	-12.54	-2.21	-10.15	-2.77	-10.99
CNN3	1.55	-3.09	1.37	-2.57	1.71	-3.74
COA1	-0.33	-4.90	-0.44	-5.65	-0.33	-3.45
COL4A2	-2.45	-3.92	-1.59	-3.55	-3.15	-6.56
CREB3L2	-0.82	-7.77	-0.60	-3.64	-0.61	-3.70

Annex

<i>CTSS</i>	-0.72	-4.69	-1.75	-10.48	-1.47	-8.99
<i>CXCL1</i>	2.65	-6.96	2.04	-5.01	2.74	-8.30
<i>CXCL3</i>	1.29	-4.19	1.43	-9.77	1.61	-11.71
<i>DLC1</i>	-3.14	-5.07	-2.57	-4.49	-2.72	-4.28
<i>DOCK2</i>	-1.09	-8.85	-1.26	-9.48	-1.77	-12.61
<i>DUSP3</i>	0.55	-3.56	0.33	-2.71	0.49	-5.02
<i>DUT</i>	-0.34	-5.43	-0.23	-4.32	-0.21	-3.76
<i>ENC1</i>	1.18	-5.98	1.64	-11.70	2.02	-15.55
<i>EPCAM</i>	-0.44	-5.24	-0.66	-6.12	-0.96	-9.77
<i>ERRF1</i>	1.81	-3.35	2.30	-6.77	1.59	-3.43
<i>FAM213A</i>	-0.44	-3.89	-0.71	-12.59	-0.74	-13.06
<i>FAM49A</i>	-2.57	-5.69	-4.28	-10.59	-3.62	-9.34
<i>FEZ1</i>	-1.20	-6.18	-1.88	-17.67	-1.72	-16.07
<i>FNI</i>	1.61	-4.96	1.89	-8.14	1.91	-8.15
<i>FYB1</i>	-2.42	-5.80	-1.77	-2.54	-2.24	-3.08
<i>FYN</i>	-0.74	-4.93	-0.64	-4.44	-0.80	-5.83
<i>GBE1</i>	0.74	-4.55	0.70	-4.72	0.66	-4.22
<i>GFOD1</i>	1.11	-4.57	1.01	-7.01	0.88	-5.51
<i>GMPPA</i>	-0.46	-3.33	-0.22	-2.22	-0.28	-3.01
<i>GPRC5C</i>	-0.63	-2.97	-1.25	-6.42	-1.77	-8.56
<i>GYPE</i>	-0.71	-11.71	-0.55	-8.92	-0.64	-10.60
<i>HBA2</i>	0.89	-3.29	1.40	-7.39	1.41	-7.21
<i>HBBP1</i>	1.14	-5.70	2.14	-11.08	1.54	-6.29
<i>HPGD</i>	1.67	-3.62	2.48	-9.39	2.14	-7.30
<i>IFT57</i>	0.63	-3.53	0.37	-3.48	0.58	-6.82
<i>KCNN4</i>	-1.07	-3.19	-1.24	-8.36	-1.19	-7.58
<i>KRT18</i>	0.35	-3.09	1.12	-14.15	1.06	-12.61
<i>KRT18P55</i>	0.52	-4.04	1.26	-5.46	1.10	-4.27
<i>KRT8</i>	0.40	-3.22	1.09	-13.86	0.90	-10.24
<i>KYNU</i>	1.34	-7.95	1.38	-11.27	1.64	-14.25
<i>LPCAT2</i>	-1.29	-8.24	-3.50	-10.91	-1.91	-8.61
<i>MAGEB2</i>	0.35	-3.82	0.67	-12.20	0.66	-11.71
<i>ME1</i>	0.81	-4.80	0.54	-3.26	0.70	-4.89
<i>MEIS1</i>	-0.75	-3.60	-1.69	-5.68	-1.79	-5.68
<i>MT1A</i>	1.25	-6.26	1.43	-6.92	1.02	-3.79
<i>MT2A</i>	1.26	-5.56	1.54	-10.00	1.05	-5.20
<i>MUC19</i>	1.40	-4.87	1.81	-7.68	0.94	-2.34
<i>MYO1F</i>	-0.67	-4.01	-0.84	-3.40	-0.75	-2.82
<i>MYO3B</i>	0.61	-3.06	1.35	-9.49	1.20	-7.66
<i>OAT</i>	-0.80	-3.73	-1.11	-11.75	-1.06	-10.80
<i>OSBP2</i>	-1.44	-3.59	-1.17	-4.14	-1.53	-4.98
<i>PASD1</i>	-1.44	-4.30	-0.91	-2.42	-1.33	-3.48
<i>PCDH11Y</i>	0.49	-3.03	1.32	-4.33	1.15	-3.32
<i>PDLIM1</i>	-0.50	-5.55	-0.74	-9.63	-0.61	-7.16
<i>PEAR1</i>	-1.44	-3.78	-2.41	-8.89	-2.52	-9.16

Annex

<i>PHLDA1</i>	1.73	-9.73	1.01	-6.38	0.86	-4.87
<i>PIR</i>	0.62	-4.61	1.50	-15.88	1.07	-9.50
<i>PLK2</i>	0.94	-4.95	1.76	-15.19	1.32	-9.80
<i>PPOX</i>	-1.05	-6.09	-0.56	-4.37	-0.52	-3.85
<i>PRG2</i>	-1.41	-7.56	-0.62	-3.11	-0.61	-2.94
<i>PRICKLE1</i>	2.33	-7.06	1.32	-7.36	1.35	-7.58
<i>PRSS23</i>	1.49	-4.45	1.86	-7.65	2.51	-12.26
<i>RAB20</i>	-1.25	-3.02	-1.72	-3.47	-2.04	-3.94
<i>RASSF5</i>	-0.43	-4.04	-0.50	-2.35	-0.71	-3.78
<i>RFLNB</i>	1.39	-3.16	1.77	-2.91	1.63	-2.47
<i>RNASE1</i>	-1.13	-7.71	-1.29	-10.32	-2.02	-14.92
<i>SI00A16</i>	0.80	-4.68	0.91	-10.49	0.45	-3.30
<i>SIPR3</i>	2.24	-6.79	1.31	-7.85	1.58	-10.54
<i>SERPINB9</i>	1.38	-5.66	0.67	-3.47	1.12	-7.87
<i>SERPINF1</i>	-0.57	-3.02	-2.37	-15.35	-2.61	-16.12
<i>SLC29A1</i>	-0.75	-3.89	-0.29	-2.24	-0.36	-3.05
<i>SNCA</i>	-1.06	-3.41	-3.38	-22.16	-0.64	-5.43
<i>SPARC</i>	-1.30	-12.15	-1.69	-19.40	-1.50	-16.94
<i>STAP1</i>	-1.30	-9.71	-1.05	-3.35	-1.67	-5.29
<i>STAR</i>	-0.79	-6.19	-0.92	-9.73	-1.32	-13.82
<i>SUGCT</i>	0.73	-5.74	0.66	-4.90	0.92	-8.18
<i>TESPA1</i>	-2.94	-5.94	-3.39	-9.08	-3.19	-8.26
<i>TEX9</i>	0.91	-5.07	1.09	-9.42	1.17	-10.20
<i>TGM2</i>	-0.92	-5.26	-1.12	-11.36	-0.82	-7.72
<i>TIMP1</i>	0.78	-5.46	1.04	-11.74	0.87	-8.81
<i>TMEM158</i>	1.38	-6.80	0.98	-4.78	1.28	-7.41
<i>TMEM173</i>	-0.69	-4.61	-0.74	-3.91	-0.84	-4.49
<i>TMEM98</i>	-0.40	-4.59	-0.57	-11.39	-0.39	-6.57
<i>TMSB4X</i>	-1.13	-15.95	-0.63	-4.86	-0.97	-8.50
<i>TNNT1</i>	-0.43	-4.67	-0.42	-6.24	-0.52	-7.96
<i>TRPV2</i>	0.52	-6.95	0.26	-2.61	0.39	-4.82
<i>TSPAN5</i>	1.55	-3.81	1.87	-6.95	1.61	-5.36

FC, fold change.

8.3 Abbreviations

6-TG	6-Thioguanine
α	Anti, Alpha
A	Ampère
ad	fill up to
Adv	Adverse
ADP	Adenosine diphosphate
ALL	Acute Lymphoblastic Leukemia
allo-HCT	allogeneic hematopoietic-cell transplantation
AML	Acute Myeloid Leukemia
AraC	Cytarabine
ATP	Adenosine triphosphate
β	Beta
B-ALL	B-cell ALL
bp	base pair(s)
BET	bromodomain and extra-terminal
BSA	Bovine serum albumin
CDA	cytidine deaminase
CDP	cytidine diphosphate
CLL	Chronic Lymphocytic Leukemia
CML	Chronic Myeloid Leukemia
CMML	Chronic Myelomonocytic Leukemia
CN	cytogenetically normal
CNA	copy number alterations
COMPASS	Complex of Proteins Associated with Set1
CR	complete remission
DCK	Deoxycytidine kinase
dCTP	deoxycytidine triphosphate
DCTD	Deoxycytidylate deaminase
del	deletion
dest	distilled
DFS	disease-free survival
DMEM	Dulbecco's Modified Eagle Medium
DMSO	Dimethyl Sulfoxide
DNA	Deoxyribonucleic acid
DNMT	DNA methyltransferase
DNMT3A	DNA methyltransferase 3 alpha
DNR	Daunorubicin
dNTP	deoxynucleotide triphosphate
DSMZ	German Collection of ^[1] _{SEP} Microorganisms and Cell Cultures
ECL	enhanced chemoluminescence
EDTA	ethylene diamine tetraacetic acid
e.g.	for example

ELN	European LeukemiaNet
ENT1	equilibrative nucleoside transporter 1
ESC	embryonic stem cell
ETS	E26 transformation-specific or E-twenty-six
EZH2	enhancer of zeste homolog 2
F	female
FAB	French-American-British classification system
FAD	flavin adenine dinucleotide
FACS	fluorescence activated cell sorter
FC	fold change
FITC	Fluorescein isothiocyanate
FBS	Fetal bovine serum
FLT3	fms-like tyrosine kinase 3
FOR	forward
g	gram, genomic, gravity acceleration
GFP	green fluorescent protein
h	hour(s)
H	histone
HAT	histone acetyltransferase
HBS	Hepes-buffered saline
HDAC	histone deacetylases
HMT	histone methyltransferase
Hox	homeobox
HRP	horseradish peroxidase
HSC	Hematopoietic Stem Cell
HSPC	Hematopoietic Stem and Progenitor Cell
IC ₅₀	half-inhibitory concentration
IC ₇₅	inhibitory concentration that leads to a response of 25%
IDH1/2	isocitrate dehydrogenase (NADP(+)) 1/2, cytosolic
Int	Intermediate
inv	inversion
IL-3	Interleukin-3
IL-6	Interleukin-6
i.p.	intraperitoneal
IRES	Internal ribosomal entry site
ITD	Internal tandem duplication
i.v.	intravenous
JmjC	Jumonji C
kb	Kilo base pairs
KD	knockdown
kDa	kilodalton(s)
KDM	Lysine demethylase
kg	kilogram
KMT	Lysine methyltransferase

KO	knockout
KS	Kabuki syndrome
l	liter
LSC	leukemic stem cell
M	molar (mol/l), male
m	milli (1×10^{-3})
MDR	multidrug-resistance
min	minute(s)
miRNA	microRNA
MLL	Mixed Lineage Leukemia
MLPA	Multiplex Ligation-dependent Probe Amplification
MM-1	MONO-MAC-1
MM-6	MONO-MAC-6
mRNA	messenger RNA
n	nano (1×10^{-9})
NADPH	Nicotinamide Adenine Dinucleotide Phosphate Hydrogen
NGS	Next-generation sequencing
NPM1	nucleophosmin-1
n.s.	not significant
NT5C2	5' nucleotidase
OS	Overall Survival
PAGE	Polyacrylamide gel electrophoresis
PBS	phosphate buffered saline
PCR	polymerase chain reaction
PCR1	polycomb repressive complex 1
PCR2	polycomb repressive complex 2
PDX	patient-derived xenograft
PI	Propidium Iodide
preL	Pre-leukemic
REV	reverse
RFS	relapse-free survival
rh	recombinant human
RNA	ribonucleic acid
rpm	rounds per minute
RPMI	Roswell Park Memorial Institute
RT	room temperature, real time
s	second
SAM	S-adenosyl-L-methionine
sAML	secondary AML
SC	single cell
SCF	stem cell factor
SCT	stem cell transplantation
s.d.	standard deviation
SDS	sodium dodecyl sulfate

SET	Su(var)3-9, Enhancer-of-zeste and Trithorax
S-HAM	sequential high dose AraC with mitoxantrone
shRNA	short hairpin RNA
siRNA	small interfering RNA
ss-DNA	single stranded DNA
t	Translocation
TAD	Treatment regime including 6-TG, AraC and DNR
T-ALL	T-cell ALL
t-AML	therapy-related AML
TE	Tris-EDTA
TET2	tet methylcytosine dioxygenase 2
Topo-II	Topoisomerase II
Tp53	tumor protein p53
TPR	tetratricopeptide repeat
UPN	Unique Patient Number
UTX	ubiquitously transcribed tetratricopeptide repeat, X chromosome
UTY	ubiquitously transcribed tetratricopeptide repeat, Y-linked
V	Volt
VAF	variant allele frequency
WB	Western Blot
WES	Whole exome sequencing
WGS	Whole genome sequencing
WHO	World Health Organization
WT	wild type
μ	micro (1×10^{-6})
°C	degree Celsius
%	percentage

Single letter codes for amino acids**nonpolar**

A	Alanine (Ala)
V	Valine (Val)
L	Leucine (Leu)
I	Isoleucine (Ile)
M	Methionine (Met)
P	Proline (Pro)
G	Glycine (Gly)

polar hydrophilic

S	Serine (Ser)
T	Threonine (Thr)
C	Cysteine (Cys)
N	Asparagine (Asn)
E	Glutamic acid (Glu)

positively charged

K	Lysine (Lys)
R	Arginine (Arg)
H	Histidine (His)

negatively charged

Q	Glutamine (Gln)
D	Aspartic acid (Asp)

aromatic

F	Phenylalanine (Phe)
Y	Tyrosine (Tyr)
W	Tryptophan (Trp)

8.4 Table of Figures

Figure 1 Overview of recurrently mutated genes in AML.	3
Figure 2 Process of clonal evolution with linear and branching architecture.	5
Figure 3 Patterns of tumor evolution at relapse in AML.	8
Figure 4 Schematic representation of common mechanisms of resistance to chemotherapeutic agents.	10
Figure 5 Metabolic pathway of DNR and AraC.	11
Figure 6 Chromatin organization and histone modifications at N-terminal histone tails. .	14
Figure 7 Schematic overview of the KDM6 protein family.	17
Figure 8 The KMT2D protein complex.	18
Figure 9 <i>KDM6A</i> mutations at diagnosis.	50
Figure 10 Gain of recurrent <i>KDM6A</i> mutations at relapse.	51
Figure 11 Recurrent <i>KDM6A</i> mutants are degraded by the proteasome.	53
Figure 12 <i>KDM6A</i> protein expression patterns in diagnosed and relapsed AML.	54
Figure 13 Heterogeneous <i>KDM6A</i> expression patterns in PDX cells of relapsed AML patients.	55
Figure 14 <i>KDM6B</i> and <i>EZH2</i> mRNA levels in PDX relapsed AML cells.	56
Figure 16 Identification of <i>KDM6A</i> exon deletions in AML cell lines.	58
Figure 17 Identification of <i>KDM6A</i> aberrations in AML cell lines.	59
Figure 18 Loss of <i>KDM6A</i> protein expression in <i>KDM6A</i> mutant AML cell lines.	60
Figure 19 High H3K27 tri-methylation in <i>KDM6A</i> mutant cells.	61
Figure 20 <i>KDM6B</i> and <i>EZH2</i> mRNA expression in <i>KDM6A</i> WT and mutant cell lines. .	62
Figure 22 <i>KDM6A</i> expression and H3K27 tri-methylation in <i>KDM6A</i> KD K562 cells. .	63
Figure 23 Knockdown of <i>KDM6A</i> confers decreased AraC resistance in K562 cells.	65
Figure 24 <i>KDM6A</i> KD confers a proliferative advantage during multiple treatments with AraC and DNR but not 6-TG.	66
Figure 25 Knockdown of <i>KDM6A</i> in K562 cells leads to a competitive growth advantage in the presence of AraC.	67
Figure 26 Generation of <i>KDM6A</i> KO K562 single cell clones.	68
Figure 27 Analysis of H3K27 tri-methylation in <i>KDM6A</i> WT and KO cells.	69
Figure 28 Loss of <i>KDM6A</i> results in decreased sensitivity towards AraC but not DNR and 6-TG treatment.	70
Figure 29 Generation of <i>KDM6A</i> KO and WT MM-1 single cell clones.	71
Figure 30 <i>KDM6A</i> loss in MM-1 recapitulates the drug phenotype of the <i>KDM6A</i> mutant sister cell line MM-6.	72
Figure 31 Time course of siRNA-mediated silencing of <i>KDM6A</i> in HEK293T cells.	74
Figure 32 Identification of differentially expressed genes in K562 cells treated with siRNA targeting <i>KDM6A</i>	74
Figure 34 Identification of differentially expressed genes in <i>KDM6A</i> KO K562 cells.	76
Figure 35 Identification of transcriptional deregulated genes in both <i>KDM6A</i> silencing systems.	78
Figure 36 Differential expression of <i>SLC29A1</i> in <i>KDM6A</i> silenced cells.	79
Figure 37 Differential expression of <i>AKR1C1</i> and <i>AKR1C2</i> in <i>KDM6A</i> silenced cells. ..	80
Figure 38 Proposed model for <i>KDM6A</i> -controlled AraC resistance in AML cells.	90

8.5 Table of Supplementary Figures

Supplementary Figure 1 Evolutionary patterns during progression of AML.....	109
Supplementary Figure 2 <i>KDM6A</i> exon deletions in AML cell lines and AML PDX samples identified.....	110
Supplementary Figure 3 <i>In vitro</i> analysis of the <i>KDM6A</i> mutant E1325X in PDX AML- 393 cells regarding proteasomal degradation..	111

8.6 Table of Tables

Table 1 List of used reagents and chemicals.....	22
Table 2 List of used buffers.....	24
Table 3 List of used kits.....	25
Table 4 List of used primary and secondary antibodies.....	26
Table 5 List of used primers.....	26
Table 6 List of used siRNA's, shRNA's and gRNA.....	28
Table 7 List of used plasmids.....	28
Table 8 List of used cell lines. All cell lines were obtained from the DSMZ.....	29
Table 9 List of used PDX AML cells.....	30
Table 10 List of used equipment.....	31
Table 11 List of used consumables.....	32
Table 12 List of used software and programs.....	33
Table 13 Patients characteristics.....	52
Table 14 Patients characteristics of samples analyzed by immunoblotting.....	54
Table 15 Summary of top 20 differentially expressed genes found in both <i>KDM6A</i> KO K562 single cell clones.....	77
Table 16 Summary of top 20 differentially expressed genes in both <i>KDM6A</i> silencing approaches.....	78
Supplementary Table 1 Summary of 112 differential expressed genes in <i>KDM6A</i> silenced cells.....	112

8.7 Publications

Most of the results presented in this work are part of the study “Loss of KDM6A confers drug resistance in acute myeloid leukemia”, Stief *et al.*, Leukemia 2019.

- **Stief S. M.**, Hanneforth A.-L., Weser S., Mattes R., Carlet M., Liu W.-H., Bartoschek M. D., Domínguez Moreno H., Oettle M., Kempf J., Vick B., Ksienzyk B., Tizazu B., Rothenberg-Thurley M., Quentmeier H., Hiddemann W., Vosberg S., Greif P. A., Metzeler K. H., Schotta G., Bultmann S., Jeremias I., Leonhardt H., and Spiekermann K., Loss of KDM6A confers drug resistance in acute myeloid leukemia, Leukemia, 2019. DOI:10.1038/s41375-019-0497-6
- Greif P. A., Hartmann L., Vosberg S., **Stief S. M.**, Mattes R., Hellmann I., Metzeler K. H., Herold T., Bamopoulos S., Kerbs P., Jurinovic V., Schumacher D., Pastore F., Bräundl K., Zellmeier E., Ksienzyk B., Konstandin N. P., Schneider S., Graf A., Krebs S., Blum H., Neumann M., Baldus C. D., Bohlander S. K., Wolf S., Görlich D., Berdel W., Wörmann B. J., Hiddemann W., Spiekermann K., Evolution of Cytogenetically Normal Acute Myeloid Leukemia During Therapy and Relapse: An Exome Sequencing Study of 50 Patients, Clinical Cancer Research, 2018. DOI: 10.1158/1078-0432.CCR-17-2344
- *Drzymala-Czyż S., ***Janich S.**, Klingler M., Demmelmair J., Walkowiak J., Koletzko B., Whole blood glycerophospholipids in dried blood spots - a reliable marker for the fatty acid status, Chemistry and Physics of Lipids, 2017. DOI:10.1016/j.chemphyslip.2017.06.003 ***First author**
- Wang Y., Gratzke C., Tamalunas A., Rutz B., Ciotkowska A., Strittmatter F., Herlemann A., **Janich S.**, Waidelich R., Liu C., Stief CG., Hennenberg M., Smooth muscle contraction and growth of stromal cells in the human prostate are both inhibited by the Src family kinase inhibitors, AZM475271 and PP2, British Journal of Pharmacology, 2016. DOI: 10.1111/bph.13623

8.8 Acknowledgment

First of all, I would like to show my deepest gratitude to Prof. Dr. Karsten Spiekermann for giving me the opportunity to carry out my research work under his supervision. Thank you for your continuous support and guidance.

Furthermore, I would like to thank Prof. Dr. Heinrich Leonhardt for our collaboration, fruitful discussions during my thesis advisory committee (TAC) meetings and for reviewing my doctoral thesis as first examiner.

I am thankful to Prof. Dr. Bettina Kempkes for agreeing to be the second reviewer of this work.

In addition, my thanks go to Prof. Dr. Irmela Jeremias for helpful discussions and scientific advices during my TAC meetings. I would like to thank Dr. Binje Vick for help with PDX work and Dr. Wen-Shin Liu and Dr. Michela Carlet for help with lentiviral designs.

I would like to thank the German Cancer Research Center (DKFZ), the German Research Council (DFG) within the SFB 1243 “Cancer Evolution”, the Life Science Munich (LSM) Graduate School, and the Department of Internal Medicine III at the LMU University Hospital for providing scientific and financial support.

My sincere thanks go to colleagues and friends for scientific advice, continuous support and a fantastic working atmosphere: Anna Vetter, Belay Tizazu, Bianka Ksienzyk, Harald Polzer, Julia Kempf, Katrin Reiter, Maïke Roas, Matthias Oettle, Michael Bartoschek, Nadine Sandhöfer, Sabrina Weser, Sayantanee Dutta, and Georg Leubolt. Particularly, I am grateful to Raphael Mattes, Anna-Li Hanneforth, and Michael Bartoschek. Thank you for your help and dedication.

Furthermore, I would like to thank my family for their tremendous support. I am deeply grateful to my husband Philipp for his unremitting support and encouragement.

